EVALUATION OF LANDSAT-D
THEMATIC MAPPER PERFORMANCE
AS APPLIED TO HYDROCARBON EXPLORATION

J. Dykstra, J. Everett, R. Livaccarri,
R. Michael, G. Richardson, S. Prucha,
O. Russell, M. Ruth, C. Sheffield,
R. Staskowski, L. Wynn, L. Zall
Earth Satellite Corporation (EarthSat)
7222 47th Street
Chevy Chase, Maryland 20815

FINAL REPORT
June 1984

Prepared for

GODDARD SPACE FLIGHT CENTER
Greenbelt, Maryland 20771

1. Report No.	2. Government Accession No.	3. Recipient's Catalog No.
4. Title and Subtitle		5. Report Date **Feb. 1984**
		6. Performing Organization Code
7. Author(s) J. Dykstra, J. Everett, C. Sheffield		8. Performing Organization Report No. 1459
9. Performing Organization Name and Address Goddard Space Flight Center Greenbelt, Maryland 20771		10. Work Unit No.
		11. Contract or Grant No. NA55-27384
12. Sponsoring Agency Name and Address		13. Type of Report and Period Covered Type III Final Report
		14. Sponsoring Agency Code

15. Supplementary Notes

16. Abstract

Work with digital data of Oklahoma, Colorado, Wyoming, Utah and California demonstrate that the increased spectral refinement and spatial resolution of TM over MSS data greatly increase the value of the data to petroleum exploration in roles ranging from logistic planning to direct detection of phenomena related to microseepage of hydrocarbons. In arid areas with careful digital processing TM images differentiate a wide variety of lithologic and soil materials and mimic conventional geologic maps. The value of the spatial content versus the spectral content of the data increases as soil and vegetation cover increase. In all areas examined the structural detail visible in the imagery can contribute to exploration at the prospect level.

Examination of the variance-covariance matrix suggests that a combination of bands 1, 4, and 5 displays the most information for most areas. However, in some areas bands 4, 5, and 7 appear to be better for geology.. P tapes are preferred to A tapes for petroleum exploration.

17. Key Words (Selected by Author(s)) Thematic Mapper, Digital Enhancement, Hydrocarbon, Exploration, Surface Alteration	18. Distribution Statement	
19. Security Classif. (of this report)	20. Security Classif. (of this page)	21. No. of Pages 239	22. Price*

TABLE OF CONTENTS

Table of Contents (Continued)

LIST OF FIGURES

LIST OF TABLES

1.0 INTRODUCTION

The purpose of this research project is to evaluate the characteristics of Landsat-4 Thematic Mapper (TM) data in terms of their applicability to hydrocarbon exploration. As originally conceived, this involved examining the engineering performance characteristics of the data acquisition, transmission and processing systems, as well as the spectral and spatial characteristics of the data. The general approach was to not only examine the technical performance characteristics of the various systems but to also assess the amount and types of geologic data that could be extracted over various known hydrocarbon exploration provinces.

Very early in the project, particularly after the first Landsat-4 Workshop, it became clear that several other very capable investigators were examining the performance of the technical and engineering aspects of each system in far more detail and with more sophistication than we would to be able to bring to bear, given our rather limited resources and time. This indicated that our most useful contribution to the overall Landsat-D Image Data Quality Analysis program (LIDQA) would be to focus on evaluating the applicability of the data to hydrocarbon exploration in the context of the data's technical characteristics.

Our original plan had called for examining data acquired during two different seasons for each of several test sites. Because of the limited amount of data to be collected and processed, the National Aeronautics and Space Administration (NASA) modified the plan to include two test sites (Anadarko Basin, Oklahoma and Williston Basin, Montana). Our original 14-16 sites would serve as alternates, if it were impossible to cover the primary sites. Most

-1-

of our candidate sites lay near or west of the 100th meridian, that is, near the edge or beyond the "footprint" of the Goddard receiving station. Limitations on the amount of data acquired and processed, the location of our sites, other high priority requirements on the systems, and the deteriorating health of Landsat-4 made it clear early in the project that we were not likely to receive all of the data to execute our initial plan. Consequently, we decided to examine any relatively cloud-free data over any of several geologically interesting areas that our alternate sites represented.

In retrospect, the breadth of applicability and value of our results probably increased as a result of these changes, despite problems of weather and season. As luck would have it, most of our eastern test sites were cloud covered and several of our western sites were snow covered at the time of data acquisition. The small amount of cloud cover over the Oklahoma site did not interfere with evaluation, but vegetation was in senescence, which essentially precluded work on geobotany. These problems underscore the value of having a spacecraft in orbit that can acquire data over a long period of time, with a high likelihood of acquiring data under near optimal climatic and seasonal conditions. Hopefully, Landsat-D' will enjoy a long, healthy life.

Despite the vicissitudes of weather, timing, etc., we acquired and examined imagery over five areas that represent a diversity of climates, vegetation conditions and geology. Our final group of test sites, as shown in Figure 1, include:

Landsat 4 Test Sites:
1. Owl Creek, Wyoming
2. Greeley, Colorado
3. Velma, Oklahoma
4. Cement, Oklahoma
5. Bluff, Utah, Colorado, Arizona, New Mexico
6. Death Valley, California, Nevada
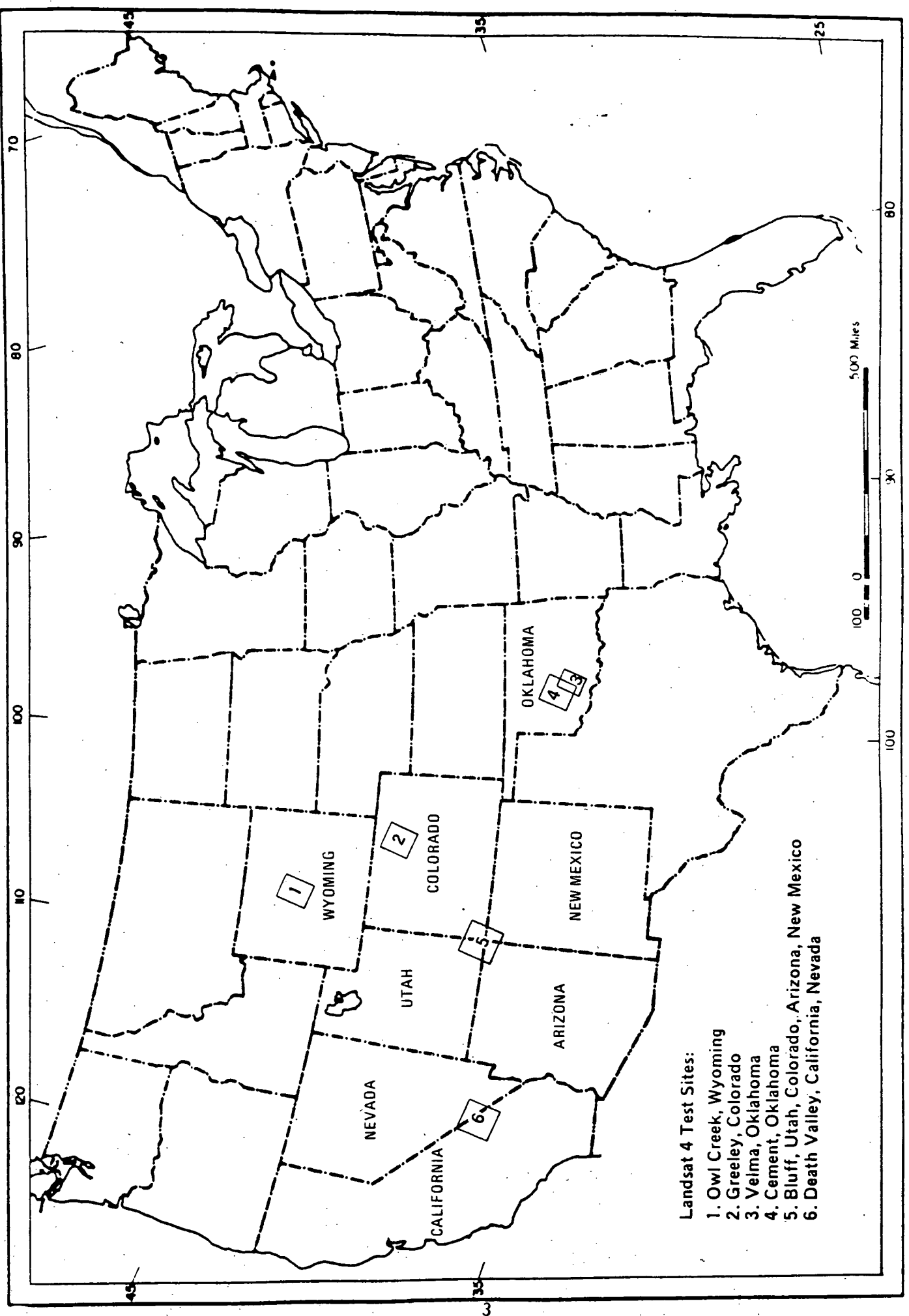
Figure 1. Location of the Landsat 4 Test Sites.

Cement-Velma, Oklahoma in the Anadarko Basin, a thoroughly cultivated, relatively humid and well-vegetated intracratonic Paleozoic basin.

Greeley, Colorado in the Laramide age Denver-Julesberg Basin, a highly cultivated, semi-arid, high plains area.

Big Horn Basin-Owl Creek Range-Wind River Basin, Wyoming, semi-arid Laramide basins and mountains of primarily grazing agriculture.

Blanding Basin, Utah, on the arid Colorado Plateau, an area with little cultivation.

Death Valley, California, a hard desert with virtually no cultivation and little vegetation except at high altitudes, and abundant evidence of recent geologic deformation.

Our work in these five areas made it clear that the increased number of bands, broader band spread, and better spectral and spatial resolution of the new bands all expand the application of Landsat TM data to geologic exploration over previously available satellite acquired data. The greater spectral and spatial resolution of the data permit their enlargement to scales commonly used in the petroleum industry (e.g., 1" = 4000') and will contribute greatly to their acceptance and routine usage in geologic exploration.

The new data are extraordinarily powerful in themselves. However, their true power is realized when they are imaginatively combined with careful field work and other geological, geochemical, and geophysical data in the context of an innovative exploration program held together with perceptive, creative geologic thinking.

If the past is any indication of the future, we will not completely understand how to exploit these new data for several years. We are still increasing our understanding and ability to apply Landsat Multispectral Scanner (MSS) data more than a decade after the launch of Landsat-1.

A secondary purpose served by this project is that it has familiarized many scientists actively engaged in petroleum exploration with this excellent new source of geologic information. This is partly the result of presentation and publication of papers resulting from the project. At least equally important is the participation of several of our colleagues from the companies that funded this research. We are deeply indebted to our associates in Natural Resources Corporation, Eason Oil Company, Japan Petroleum Exploration Company, Ltd., and British Petroleum, Ltd. for their encouragement, assistance, insight and support in this work.

2.0 SUMMARY AND CONCLUSIONS

It would be difficult to overstate the potential value of TM data to hydrocarbon exploration. Realization of this potential will require many man-years of use and experimentation with data over areas of interest acquired at several different times of year. This underlines the requirement for a satellite or satellites with greater life expectancy than Landsat-4 and an increased capability for receiving and processing data that the satellite acquires.

The increased spectral refinement and spatial resolution of TM data over Multispectral Scanner (MSS) data greatly increases the applicability of the data to hydrocarbon exploration in roles ranging from planning logistical support to detection of phenomena related to microseepage of hydrocarbons. TM data do not replace or supplant MSS data, but are a valuable adjunct and act as an important bridge between the resolution of MSS and that of aerial photography. TM data reveal many more details of structural and lithologic features than MSS data; the degree of identification (versus detection) of features is much higher and consequently the degree of confidence in the interpretation is much greater than with MSS data.

Nonetheless, there seem to be several classes of regional features that are best seen with the coarser resolution of MSS imagery. It appears that the vastly increased amount of detail in TM imagery can distract one from perceiving the continuity of some features. However, examination of these features in TM data almost always reveals details that lead to a greater understanding of the regional geology. Examples is the evidence of left-lateral thrust movement on features of Cement, Chickasha and Velma Fields in

Oklahoma and the right-lateral movement on the northwest-trending fractures that extend from the mountain front into the Denver Basin.

The value of the spectral information in the TM data is much greater than in the MSS data. This was the intent of the selection and placement of the TM bands and is demonstrable in a very practical sense. It is also true that the value of the spectral content relative to the spatial content of data tends to decrease as vegetation and soil cover increase. In the hard desert of Death Valley, it is possible, with minimal reference to ancillary information and some shrewd spectral processing, to do a very credible job of imitating a conventional geologic map with well differentiated (if not identified) lithologic units. Lithologic differences are somewhat less distinct but still well expressed in TM imagery of southeastern Utah. Spectral differentiation contributes some important insights in Wyoming, Colorado, and Oklahoma, but the spatial aspect of the data is clearly paramount. Part of the problem may be our current lack of knowledge and experience in being able to extract and understand spectral information but the major portion of the problem is that the breadth and placement of the spectral bands, and the environment, conspire to confound this effort.

Just as with MSS data, different environments require different types of processing for optimum extraction of geologic information from TM data. Considerations of the variance-covariance matrix suggest that a TM 1,4,5 band composite contains the greatest amount of information in most environments of any three band combination. However, experience suggests that in some environments, other three-

band combinations are more useful for geologic purposes. For instance, in Wyoming, 1,4,5 was good but the decorrelated 1,3,4 combination was better for recognizing geologic features. In Colorado, the 1,4,5 combination was discarded during interactive review of two dozen or more possible combinations and a 4,5,7 combination was found to be much better. The 1,4,5 combination appears to be the best three band combination in Utah and Oklahoma. More exotic processes such as Intensity-Hue-Saturation (IHS) images (California) and principal component (eigen) 1,2,3 images (Utah) were the best of all images tried in these areas. (It is interesting that the principal component image did poorly in California and the IHS was of little help in Utah.) This suggests that if one goes to the trouble and expense to produce and interpret one version of an image, they are well advised to produce and interpret several versions.

Regardless of how well any single process reveals the geology, we found that there was always unique information available in other processes. It is crucial to have an easily understandable reference image (such as a 1,2,3 natural color or 1,3,4 or 2,3,4 false-color infrared) in all environments. These reference images assist in the interpretation of other images, particularly the more exotic varieties, and greatly assist in recognizing cultural features and artifacts.

For each area, we tested between twenty and fifty digital processing techniques and variations on an I^2S interactive display system before selecting a limited number of processes to convert to images for further evaluation. In all instances, we produced natural color (bands 1,2,3) and false-color infrared images (either

2,3,4 or 1,3,4) as standards of comparison for more exotic image

types. In all areas, natural color and false-color infrared images

are available as standards of comparison but, in most areas, the

band 1,4,5 combination is more useful. The exceptions to this were

in Wyoming where a decorrelated 1,3,4 false-color infrared was

deemed best for overall mapping (1,4,5 was useful but not as good in

the flats or the mountains) and Colorado, where 4,5,7 composites in

two versions were the most useful product.

A major focus of the project was searching for indications,

either geochemical, geobotanical, or geomorphic, of microseepage of

hydrocarbon. Results of this project were somewhat discouraging.

The season of acquisition (late fall/winter) of most imagery

frustrated much of the geobotanical effort. There appears to be a

general correlation of hydrocarbon production and "blackjack" oak in

Oklahoma. The association is weak and flawed and there is no

indication that the association has a causal relationship.

There are several areas where there appears to be a brightening

of otherwise dark units in the Blanding Basin. One bright area is a

known bleached area of the Cutler Formation in the Mexican Hat

Field. A general lightening of the unit extends throughout the

field and some distance to the north (best seen in the principal

component and the 1,4,5 composite). Rocks within the Ismay and

Aneth Fields are light and have very ragged geomorphic expression

but are not demonstrably different from the same units in

nonproductive areas. A known area of bleaching and anomalous

cementation in the Peter's Nipple area near Ismay does not stand out

on any of the imagery as particularly anomalous.

In Oklahoma there were no recognizable spectral anomalies at known altered areas in either Cement or Velma Fields. There was a high correlation between production and a curious yellowish-brown tone in the 1,4,5 image, but we have no data to suggest this is more than coincidental.

What is very clear in all areas is that there is an abundance of structural information in the data that will contribute greatly to petroleum exploration. Subtle low relief and productive surface structures are easy to map on the Utah imagery. Even the subtle low relief subsurface faults that controlled the algae buildups responsible for the production at Aneth and Ismay stand out well. In Oklahoma and Colorado, the abundant structural detail visible can contribute to exploration at the prospect level. In Oklahoma, the thermal (band 6) data contributes a great deal to the recognition of through-going fracture systems.

We concentrated our engineering evaluation on what benefit, if any, there might be in processing an "A" tape rather than a "P" tape for hydrocarbon exploration purposes. This included evaluating spectral fidelity, intra-detector banding, forward versus reverse sweep banding, geometry, etc. The geometric corrections necessary are complicated and nonlinear and NASA does an excellent job of recreating accurate geometry. There appears to be very little difference in spectral fidelity between "A" and "P" tapes. By beginning with an "A" tape, it is possible to reduce the various types of striping present and slightly improve the clarity of the image (an "A" tape product without edge enhancement has about the same sharpness as an edge enhanced "P" tape product). On balance, it is not worth the time, effort and expense to begin with an "A"

tape for petroleum exploration purposes. The "P" tape is an excellent product.

In short, TM data provides petroleum explorationists with a powerful new tool. The increase in quantity, quality and reliability of the information available in TM versus MSS imagery is much greater than increases in spectral and spatial resolution of the data would at first suggest. The task now is to discover how best to manipulate and incorporate these new data into exploration efforts.

3.0 BACKGROUND

Geologically, Landsat-4 has appeared on the scene at a very interesting time, both in terms of the development of new ideas and the acceptance and absorption of new technology. This "geologic" context influenced our approach to various aspects of this project. For instance, we focused considerable effort on developing image products that advantageously display regional relationships, important in plate tectonic thinking, and formats that are easy to incorporate with conventional types of geologic data. We also spent considerable time searching for evidence of hydrocarbon micro-seepage.

Since the early 1960's, the science of geology has been under-going a major revolution. The new paradigm of plate tectonics and seafloor spreading is replacing the older paradigm of a rigid, stable earth. Inherent in the development of plate tectonic theory is a growing appreciation of the role of plate motion in determining the location of mineral deposits and hydrocarbon accumulations. Developments in spaceborne remote sensing which parallel these developments in geologic thinking have given us remote sensing tools that view the earth with appropriate scale and scope to enable mapping the regional structures that reflect the motions of continent-sized segments of the earth's crust. We received our first glimpses of the earth from space with photos from the Apollo and Gemini flights at about the same time interest in seafloor spreading and plate tectonics began to develop. The first three Landsat satellites gave us nearly complete high-resolution (80-metre) coverage of the earth in four spectral bands. These data have had and continue to have enormous impact on tectonics, global

geologic thinking, and on all facets of the perception and management of renewable and non-renewable natural resources and the environment.

In addition to plate tectonics, there is a second revolution going on in petroleum exploration thinking. The old paradigm of tightly sealed hydrocarbon traps which retain for long periods of time petroleum that was generated and migrated in the distant past is giving way to a more dynamic model in which most, if not all, traps leak, and the generation and migration of hydrocarbons is a continuing process. This implies that there is very little, if any, really old oil or gas; rather, there are new hydrocarbons generated from old rocks or retained in old traps. The hydrocarbon leaked from these imperfect traps moves essentially vertically through the overlying rocks to the surface and, in the course of its movement, produces a host of chemical changes. The near surface environment manifests this leakage in a variety of geochemical, biological, geobotanical, or geomorphological anomalies and by the simple presence of hydrocarbon itself.

This new paradigm also has significance for mineral exploration. The chemical environment created by leaking hydrocarbon has caused the emplacement of a vast amount of lead, zinc, uranium, and silver, and has potentially played a role in localizing some deposits of gold, copper, and barite.

In a general sense, data from the first three Landsat satellites have made their major contribution to hydrocarbon exploration in the spatial domain. In mineral exploration, Landsat has revealed some spectral information, but again, the major contribution is spatial. The synoptic view of over 34,000 square kilometres of the

earth's surface on a single Landsat image permits the detection and mapping of major regional structures crucial to the understanding of entire geologic provinces. It is also possible, through special digital enhancements, to map some of the more subtle surface expressions of fracturing, folding and alteration associated with hydrocarbon accumulations and the emplacement of mineral deposits. These data make it possible to interrelate widely separated geologic features and detect subtle changes that occur over tens of kilometres and hence, which have gone unnoticed on the ground or with conventional types of data. Perhaps most important of all, the new perspective that the view from space provides stimulates us, even forces us, to think of geology in new ways and perceive new possibilities. It is an extremely powerful tool. It has not by itself "found" an oil field or a mine, but it has made significant contributions to the exploration thinking that has led to the discovery or millions of barrels of oil and millions of tons of ore. In all this the contribution has been primarily spatial.

The two major advantages of TM data over that of the MSS system are the increased spatial resolution and the greater number of narrow, strategically placed spectral bands. The 30-metre pixel size will permit finer definition of ground features and thereby improve the reliability of photo-geologic interpretation of geologic structure. Of equal importance is the increased homogeneity of the type of surface material included in a given pixel. The less mixed the pixel, the greater the potential of extracting useful spectral information. The increased spectral resolution is allowing geologists to map altered zones associated with mineralization based not only on iron oxides, but on the basis of recognizing rocks and

soils rich in hydroxyl groups, such as many of the clays formed as a product of the mineralization process.

The increased spectral sensitivity also promises the ability to detect some types of vegetation changes that are associated with anomalous mineralization. This will be particularly helpful where soil and plants obscure the bedrock. This capability is not definitely proven, but there are hints that it is possible.

All of the above implies that digital processing techniques will play a much greater role in the application of TM data to exploration than it has in the application of MSS data. One of the lessons we relearned many times while using MSS data is that there is no single process that is appropriate to all areas or to all applications. Processing must suit the application and the area studied. Processing of TM data must be even more carefully tailored to purpose and environment than processing of MSS data.

In general, the value of the spatial data increases relative to the value of the spectral data as soil and vegetation cover increase. However, even in covered areas, the increased spectral sensitivity contributes to interpretation by making the spatial elements of terrain fractures, geomorphology, etc., more easily recognizable. One factor that aids interpretation immensely is 30-metre resolution, so that the digitally processed images easily stand enlargement to scales of 1:48,000 or larger - a capability that greatly reduces uncertainty, ambiguity and error in interpretations and allows images to be matched to standard petroleum industry base maps.

This is the final report associated with this project. However, in a very real sense, it is an interim report on develop-

ment of methods and techniques for exploiting TM data for the purpose of hydrocarbon exploration.

3.1 Imagery Acquisition

The evaluation of TM imagery for geobotanical indications of hydrocarbon microseepage is best done on imagery acquired during the "leaf-on" or growing season of the vegetation, when both vegetation vigor and difference in vegetation communities are best assessed. The majority of TM imagery acquired in petroleum provinces of interest was obtained in the fall and winter seasons. This was particularly so in the western United States, where the only TM data acquired were from the Canadian Ground Station at Prince Albert, Saskatchawan, which commenced recording on 7 November 1982. The failure of the TM transmission capability in February 1983 terminated further imagery acquisition. These circumstances have frustrated our "geobotanical" efforts.

Another minor frustration was that image processing was rather slow during the research and development phase of the project. During the "Scrounge" period of the research and development phase of TM operations, only one scene per day was processed (the term "Scrounge" was applied because a variety of data processing and control elements located at both Goddard Space Flight Center (GSFC) and EROS Data Center (EDC) were used in processing the early TM data). Several scenes of potential interest to petroleum exploration were acquired from NASA as they became available, beginning with the Detroit, Michigan image (four bands only) which was made available shortly after

launch to provide experimenters with an image to aid in developing the necessary software for image processing.

The Death Valley, California image became available in October 1982 and was acquired independent of the project, as it does not cover a petroleum province. The data were of such interest in demonstrating the potential value of TM imagery that several different types of processed imagery were distributed to all co-investigators.

The Lawton, Oklahoma image (subscenes identified as Cement and Velma) was released in April 1983. This image, acquired on 29 November 1982, was designated as a primary study area in our NASA agreement. The Cement oil field area continues to be of substantial interest as a site where surface alteration has occurred as a result of microseepage of hydrocarbons.

In March 1983, the Owl Creek Mountain, Wyoming Computer Compatible Tape (CCT) was obtained because it is an area of considerable interest in petroleum exploration, and because there was some potential for the detection of surface alteration. The date of data acquisition, 21 November 1982, precluded any potential for geobotanical studies. Actually, there proved to be a considerable "dusting" of snow over large portions of the image area that "clouded" the validity of results from the spectral evaluation.

NASA originally committed to cover only two test areas with CCT's from two seasons in support of the petroleum exploration phase of the investigation. However, as NASA was unable to provide imagery of the designated test areas in seasons suitable for all of the objectives of the study, they

provided additional CCT's. In June 1983 the image of Greeley, Colorado was obtained for evaluation. This image, acquired on 16 November 1982, had extensive portions covered with snow and clouds, but a quadrant in the west central portion of the scene was largely snow and cloud free. Various processes were performed on the data, and several proved to be useful for structural interpretation.

Because the TM Simulator (TMS) studies conducted by Jet Propulsion Laboratory over the Lost Creek, West Virginia area indicated a geobotanical anomaly associated with an oil field, a TM CCT of West Virginia was selected for evaluation when it became available in April 1983. The TM overpass was in early September when leaf condition of vegetation was still good, but thin, wispy clouds cover much of the image and make all spectral analysis suspect.

In October 1983, the Bluff, Utah CCT was obtained because at least one example of known surface alteration associated with the presence of hydrocarbons fell within the area. This image was acquired from an overpass on 16 November 1982. The areas of higher elevation were snow covered. The San Juan River Valley was snow free, but much of the image was streaked by high, thin, cirrus clouds. Although this cloud cover may have degraded the potential for significant spectral discrimination, it did not affect the utility of the imagery for structural interpretation.

3.2 Landsat-4 System Description

Landsat-4 was successfully launched on July 16, 1982, and orbital maneuvers were completed on July 29, 1982, to place the spacecraft on the Landsat-4 Worldwide Reference System (WRS) orbital path profile. Landsat-4 is a second generation earth observation platform in the 11-year old Landsat program. In contrast to the first three experimental Landsats, launched in 1972, 1975, and 1978, Landsat-4 is intended to provide an operational earth-sensing capability. The key differences between Landsat-4 and the three previous satellites are: an upgraded instrument package that includes the new TM and no Return Beam Vidicon (RBV); a new Tracking and Data Relay Satellite system (TDRS); and a transfer of program management from NASA to the National Oceanic and Atmospheric Administration (NOAA), with a corresponding change in program status from experimental to operational. The primary objectives of the Landsat-4 program are:

o   To assess the capability of the new TM sensor to provide improved information for earth resource management;

o   To provide continued availability of MSS data;

o   To provide a transition from MSS data to the higher resolution and data rate of TM;

o   To provide for system-level feasibility demonstrations to define the characteristics of an operational system, including transfer of Landsat-4 management from NASA to NOAA;

o   To encourage continued foreign participation in the program.

Landsat-4 is in a sun-synchronous, repetitive, near-polar orbit at an altitude of 705 kilometres. The satellite repeats coverage between 81.8°N and 81.8°S every 16 days, making just over 14.5 orbits per day that last about 99 minutes each. The orbit crosses the equator on its descending orbit at approximately 9:45 a.m., and each consecutive orbit is spaced 2,752 kilometres apart. Adjacent ground traces are 172 kilometres apart at the equator, and occur seven days apart. Ground coverage for each orbit is fixed at 185 kilometres (115 miles), the same as for the previous Landsats (see Figures 2, 3, and 4). However, the change in the repeat ground coverage cycle to 16 days, from 18 days for Landsats-1, -2, and -3, make the Path/Row grid for Landsat-4 incompatible with the earlier WRS. The new reference system includes 233 paths rather than the 251 which were present in the previous grid.

The Landsat-4 payload includes two scanning sensors. An MSS similar to the MSS on Landsats-1, -2, and -3 provides continuity of data between the first and second generation satellites. The TM is designed to achieve higher image resolution, sharper spectral separation, improved geometric fidelity, and greater radiometric accuracy than its MSS predecessor. These enhanced sensor capabilities result primarily from design modifications in the MSS that allow the TM to record or sense data in both scan directions rather than one, and to record that data in seven spectral bands rather than four. Figure 5 is a diagram showing the Landsat-4 system. Table 1 summarizes information covering Landsats-1, -2, -3, and -4.
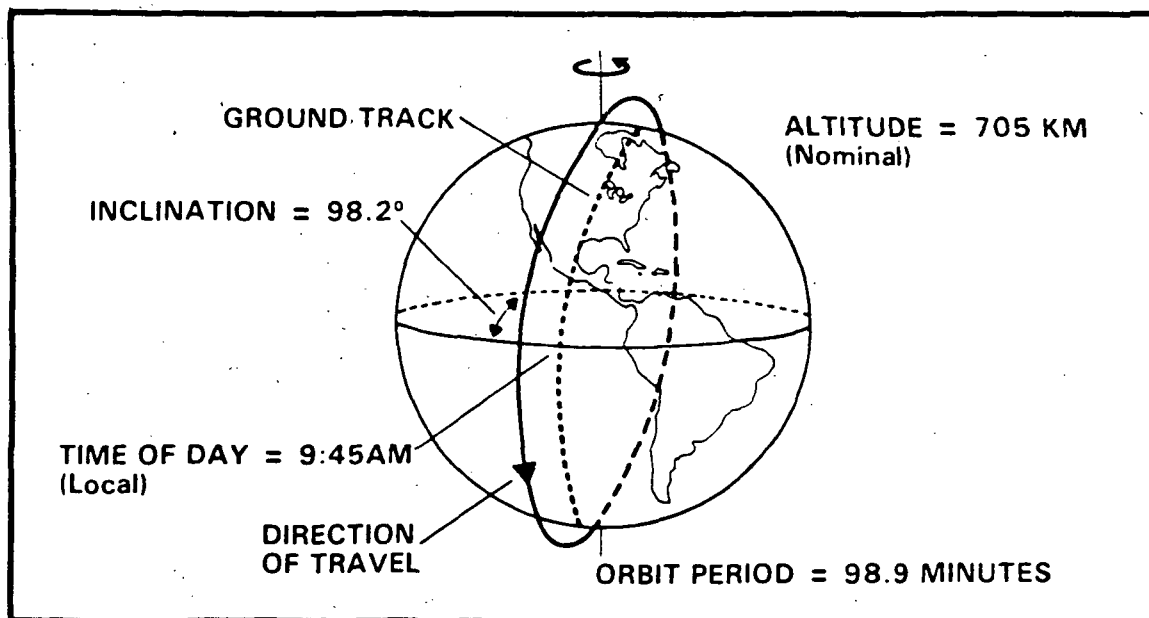
Figure 2   Landsat 4 orbit characteristics (from NASA, 1982a)
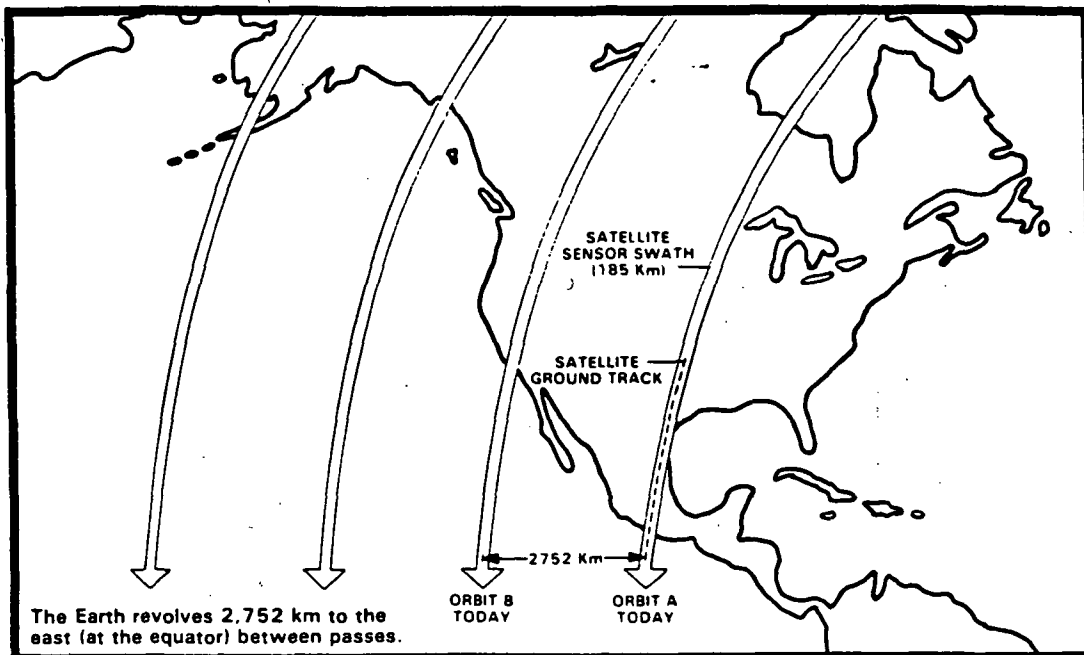
Figure 3   Landsat 4 consecutive orbit passes (from NASA, 1982a)
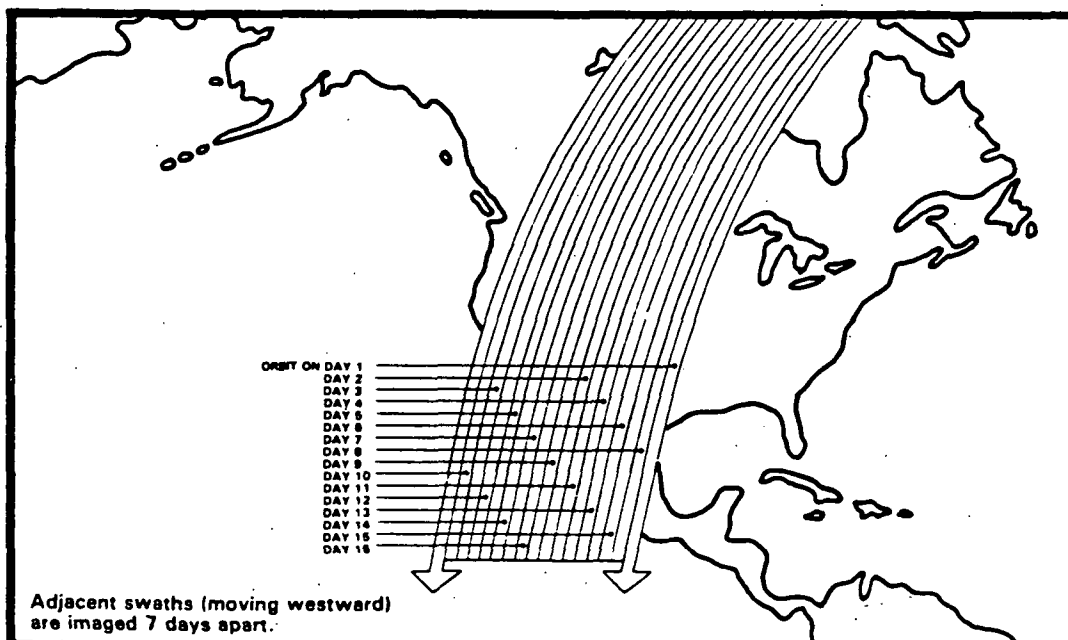
Figure 4   Landsat 4 adjacent ground swaths (from NASA, 1982a)
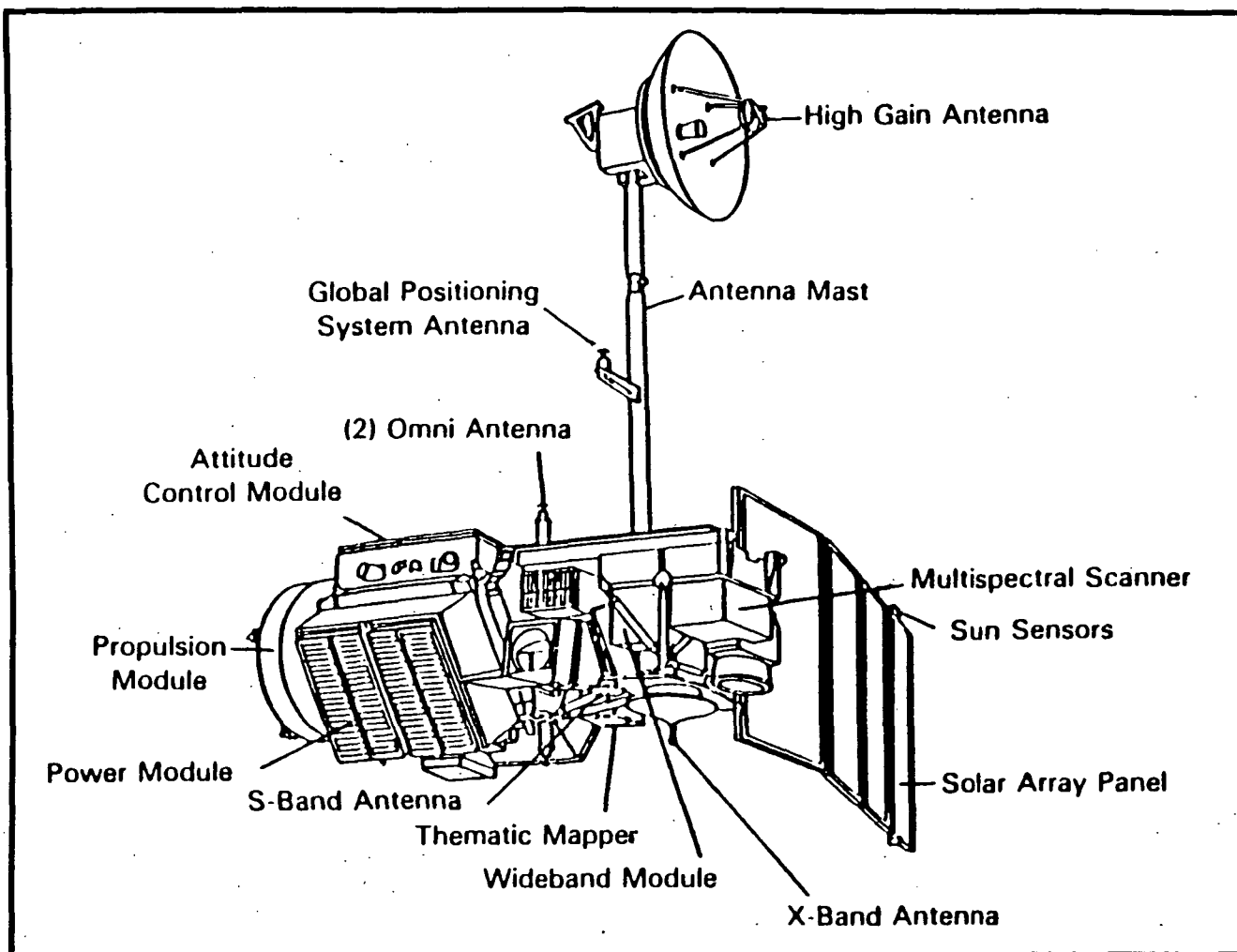
Figure 5   Landsat 4 Flight Segment (from NOAA, 1983)

TABLE 1

DESCRIPTION OF LANDSATS-1, -2, -3, and -4

Launch Date: Landsat-1 - July 23, 1972; terminated January 6, 1978.
Landsat-2 - January 22, 1975; inoperational since February 25, 1982. Shutdown July 83.
Landsat-3 - March 5, 1978; of limited use by March 1982. Shutdown Sept. 83.
Landsat-4 - July 16, 1982; Transmitter loss Feb. 1983.

Ground Coverage: Between latitudes 81°N and 81°S
Repetitive Coverage: Landsat-1, -2, and -3 - 18 days; Landsat-4 - 16 days
Satellite Altitude: Landsat-1, -2, and -3 - Approximately 900 km
Landsat-4 - Approximately 700 km

Sensors:

A. Multispectral Scanner (MSS), Landsat-1, -2, -3, and (4):

Spectral Band	Wavelength (micrometres)	Spectrum
4 (1)	0.5 - 0.6	Green, Yellow, Orange
5 (2)	0.6 - 0.7	Red
6 (3)	0.7 - 0.8	Reflective Infrared
7 (4)	0.8 - 1.1	Reflective Infrared
8	10.4 - 12.6	Thermal Infrared (Landsat-3 only)

o Spatial Resolution: 79 metres
o Image Format: 185 kilometres by 185 kilometres
o Thermal Infrared (band 8) failed to function properly.

B. Return Beam Vidicon (RBV), Landsat-3:

o Panchromatic: 0.505 - 0.750 micrometres
o Spatial Resolution: 38 metres
o Image Format: Two cameras aligned to view an across track pair of 98 square km ground scenes with 14 km of sidelap. Two pairs view the same area as an MSS scene.

C. Thematic Mapper, Landsat-4:

Spectral Band	Wavelength (micrometres)	Spectrum
1	0.45 - 0.52	Blue
2	0.52 - 0.60	Green/Yellow
3	0.63 - 0.69	Red
4	0.76 - 0.90	Reflective (near) Infrared
5	1.55 - 1.75	Reflective (middle) Infrared
6	10.40 - 12.50	Thermal (far) Infrared
7	2.08 - 2.35	Reflective (middle) Infrared

o Spatial Resolution: 30 metres (Band 6, 120 metres)
o Image Format: 185 kilometres by 185 kilometres

Most significant, perhaps, is the telemetry system of

Landsat-4. When the system becomes fully operational, data

will not only be sent to ground receiving stations, they will

be sent from Landsat-4 to two Tracking and Data Relay

Satellites (TDRS) in geostationary orbits. One or the other of

these TDRS spacecrafts will be in line-of-sight communications

with Landsat-4 at all times except for the period when the

satellite is over part of the Indian sub-continent and the USSR

area immediately to its north. Data from TDRS will be

transmitted in turn to a central ground receiving station

situated at White Sands, New Mexico. With this system, the

need for other ground receiving stations will be much

diminished and there will be no need for on-board tape

recorders (Sheffield, 1982).

3.2.1 Landsat-4 Current Status and Future Plans

The original plans developed for Landsat-4 are subject

to change. The TM capability of Landsat-4 was largely lost in

March 1983 due to failure of two of the four solar panels, and

for practical purposes, TM data acquisition ceased at that

time. Approximately 6,300 TM scenes were acquired prior to

this problem, providing a supply of data for resource managers

until Landsat-D' is launched. The launch is scheduled for

March 1, 1984. The orbit of Landsat-5 will be phased to that

of Landsat-4, passing over a specific point exactly eight days

later. Both Landsats-4 and -5 will be kept operational as long

as useful data are obtained. Before complete failure of

Landsat-4 occurs, it is planned to bring the satellite to a

lower orbit and "park" it in an orbit accessible to the Shuttle for possible future recovery and repair.

The experimental TM is scheduled to become operational on January 31, 1985, following a period during which NASA will qualify this new instrument and install a new TM ground processing system (NASA, 1982c).

The TDRS system may have potential problems due to degradation of one of the two high-data-rate forward Ku band single access systems, which has necessitated the switch to a second, redundant antenna. As yet, no impairment of the TDRS-1 mission has occurred or is expected. It will probably be late 1984 before the second TDRS is launched.

3.2.2 Multispectral Scanner

The MSS has been the principal recording instrument on Landsats-1, -2, and -3. The MSS records radiant energy from the earth in four spectral bands, two in the visible portion of the electromagnetic spectrum at 0.5 to 0.6 micrometres (green) and 0.6 to 0.7 micrometres (red), and two in the reflected (not thermal) infrared at 0.7 to 0.8 micrometres and 0.8 to 1.1 micrometres. These bands had been designated as bands 4, 5, 6, and 7, respectively, for Landsats-1, -2, and -3. Although spectrally unchanged, MSS bands 4, 5, 6 and 7 have been redesignated on Landsat-4 as bands 1, 2, 3, and 4, respectively.

The MSS on Landsat-4 is essentially the same as those on the previous Landsats. The optics have been modified, however, to maintain a pixel size of approximately 80 metres because of

the lower altitude of Landsat-4 (705 km) versus that of

Landsats-1 through 3 (920 km).

The MSS continuously scans the terrain line-by-line,

with every line of data representing a strip on the earth's

surface approximately 185 kilometres long by 79 metres wide.

The continuous swath of Landsat data is partitioned into scenes

that represent approximately 185 kilometres by 185 kilometres

on the ground. Each individual scan line is sampled to give

3,240 reflectance values in each of the four bands. A single

band Landsat MSS scene consists of 2,340 scan lines, each scan

line containing approximately 3,240, 57 metre by 79 metre

minimum resolution cells called pixels (abbreviation for

picture element). Therefore, for each Landsat spectral band,

there are approximately 7,500,000 pixels. Within each pixel,

the intensity of reflected sunlight for each spectral band is

recorded and stored as integers. Because there are four

spectral bands, there are four integers per pixel, one for each

band recorded on CCT's.

3.2.3 <u>Thematic Mapper</u>

The TM uses significantly narrower bands in the green,

red and near infrared compared to the MSS system. These

narrower bands allow the increased reflectance of vegetation in

the green (0.52-0.6 micron in the TM vs. 0.5-0.6 micron in the

MSS) and near infrared (0.76-0.9 micron in the TM vs. 0.7-1.1

micron in the MSS) to be measured more precisely (NASA 1982b).

Figure 6 graphically represents and compares the band widths

detected by the MSS and TM sensors for all four Landsat satel-
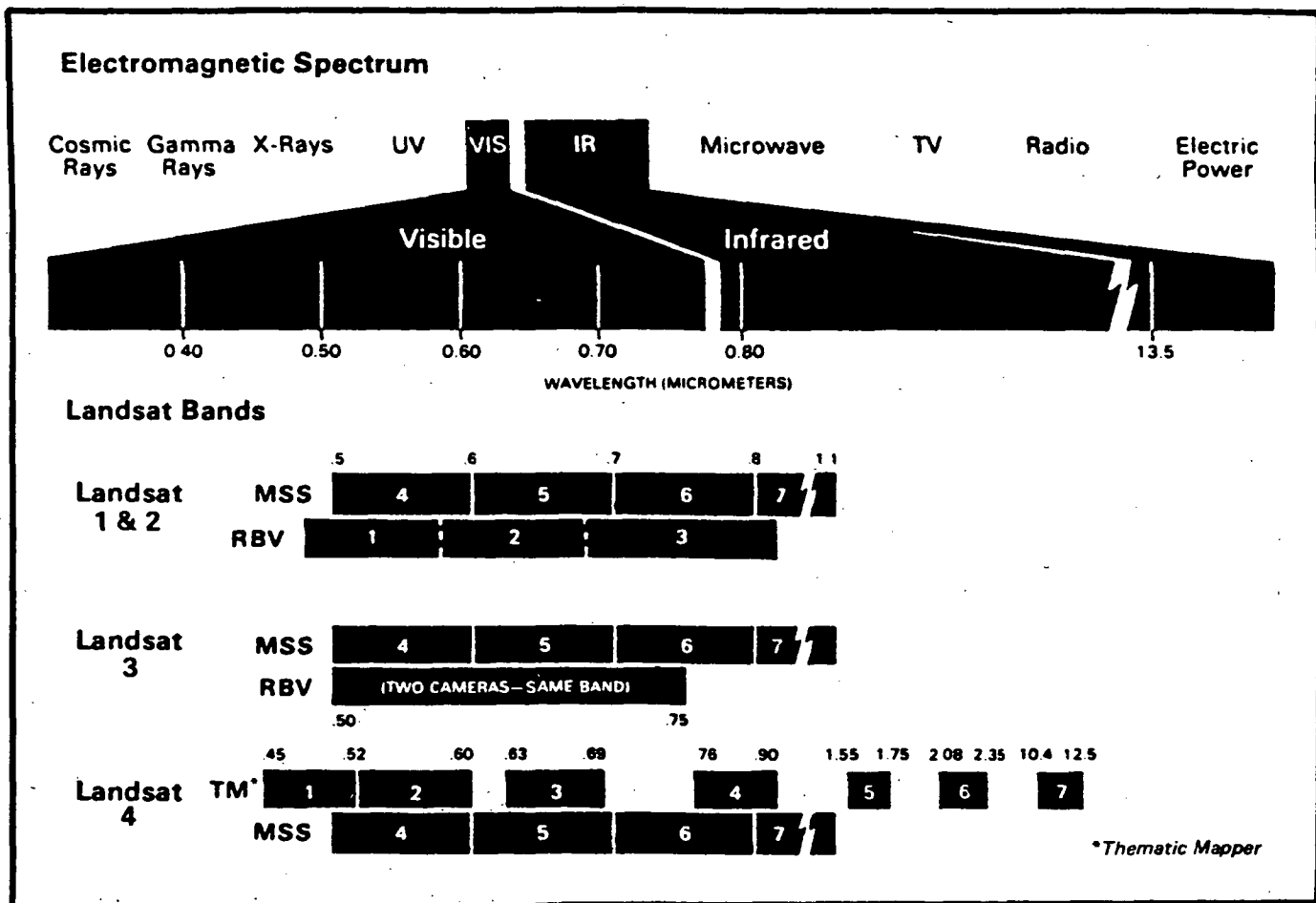
Figure 6   Comparison of spectral sensitivity of the instrumentation on
Landsats 1, 2, 3, and 4 (from NASA, 1982b)

lites. The RBV camera is not part of the Landsat-4 payload.
Natural color images of the Earth's surface features are now
possible for the first time from Landsat because of the blue-
green band on TM.

The TM has a 30 by 30 metre instantaneous-field-of-view
(IFOV) as compared to an 82 by 82 metre IFOV in the Landsat-4
MSS or a 79 by 79 metre IFOV for the Landsats-1, 2, and 3. The
TM IFOV covers an area one-seventh the area of the MSS and
allows much smaller features on the surface to be identified
and measured (NASA, 1982b).

The pixel of a TM scene covers an area approximately 30
x 30 metres for bands 1 through 5 and 7, and 120 x 120 metres
for band 6. Each 185 x 185 kilometre scene is composed of a
6167 x 6167 array of 30 metre pixels for the 6 bands, and a
1542 x 1542 array of 120 metre pixels in band 6, for a combined
total of over 230.5 million pixels. The increased resolution
of the TM over the MSS is achieved in part through larger
optics that better the signal to noise ratio. Improvement is
also realized by using 16 smaller detectors per band (compared
with six for each MSS band). Unlike the previous Landsat
scanners, in which radiation is admitted to the detector only
during the counterclockwise (west to east) oscillation of the
scan mirror, the mirror on TM obtains data in both directions
of a scan as it oscillates back and forth. This allows for
more dwell time on the smaller IFOV targets.

Incoming radiation is assigned to one of 256 gray levels
in each spectral channel by the TM. In comparison, the MSS is
less sensitive with an overall range of 64 gray levels in each

band. In summary, the TM possesses approximately twice the
spectral resolution, three times the spatial resolution, and
four times the sensitivity of the earlier MSS sensors.
Considered together, the TM represents an order of magnitude
increase in our Earth observation capabilities from space.

The seven spectral bands on TM were chosen primarily for
vegetation monitoring, with the addition of a single band that
offers geologic mapping applications (TM band 7). These band
designations, spectral ranges and principal applications are
summarized below.

o   Band 1   (0.45-0.52 μm)

     Designed for water body penetration, it is useful

     for coastal water mapping. Also useful for

     differentiation of soil from vegetation and

     deciduous from coniferous flora, differentiation of

     rock types, and when viewed in conjunction with

     other bands in the visible portion of spectrum, it

     allows definition of the presence or absence of

     limonite.

o   Band 2   (0.52-0.60 μm)

     Designed to measure visible green reflectance peak

     of vegetation for vigor assessment. Also useful

     for differentiation of rock types and the presence

     or absence of limonite.

o   Band 3   (0.63-0.69 μm)

     Chlorophyll absorption band important for vege-

     tation discrimination. One of the best bands for

     crop classification, vegetation cover, and density.

-30-

Also useful for differentiation of rock types and presence or absence of limonite.

o   Band 4   (0.76-0.90 μm)

Useful for determining biomass content, delineation of water bodies, differentiation of rock types and presence or absence of limonite.

o   Band 5   (1.55-1.75 μm)

Indicative of vegetation moisture content and soil moisture. Highest rock reflectance values occur in this band making it very useful as a standard band with which other bands can be compared when used in a ratio. Also useful for differentiation of snow from clouds (snow appears as very dark while clouds remain quite bright).

o   Band 6   (10.40-12.50 μm)

Thermal infrared band useful in vegetation stress analysis, soil moisture discrimination and surface temperature mapping.

o   Band 7   (2.08-2.35 μm)

Selected for its potential for discriminating rock types and for hydrothermal mapping. It is useful for hydroxyl and water absorption measurements. Band 5 and Band 7 are useful for detecting variations in the type and abundance of clay minerals exposed at the Earth's surface.

3.3 Image Processing

All of the Landsat imagery analyzed as part of this project have been produced from the seven channel NASA processed (P-tape) CCT's made available to EarthSat through the EDC in Sioux Falls, South Dakota. The data were first inter- actively analyzed using EarthSat's GEOMAS image processing system, during which time selections were made as to which image types, band combinations, color permutations and contrast adjustments would be used for the GEOPIC image production (the GEOMAS/GEOPIC trade names refer to the collection of image processing software and complementary photographic techniques which were developed by EarthSat for the production of digitally enhanced satellite imagery).

Digitally enhanced satellite imagery can be loosely grouped into three categories: Spatial, Spectral and Spatial/- Spectral (see Table 2). Those which present principally the spatial or principally the spectral information achieve the enhancements of one largely at the expense of the other. That is to say, algorithms which enhance spatial information suppress spectral information and vice versa. There are several image types which simultaneously enhance both the spatial and spectral properties of the data. These are the most important for geologic interpretation and will be discussed at length in the following sections.

TABLE 2: IMAGERY TYPES FOR GEOLOGIC APPLICATIONS

Spatial/Spectral	Spectral	Spatial
Band Combinations	Principal Component or Eigen	Single Band
Decorrelated (Decor) Intensity, Hue, Saturation (IHS)	Ratios	Convolutions

The following will discuss each of the above image types
and will present some observations as to their application to
geologic interpretation of TM imagery.

3.3.1 Spatial/Spectral Imagery

By far the most useful of the image types for geologic
analysis are those which present a good portion of both the
spatial and spectral information. These imagery represent the
vast majority of the image products generated in support of
geologic interpretations. Most of the algorithms are structured
to emphasize the spatial or spectral enhancements, discussed
below in the next two sections. Imagery processed by several of
these algorithms are usually generated and interpreted only on
the interactive system. The complement of GEOPIC imagery
examined for this project are image types which fall into the
spatial/spectral category.

3.3.1.1 Band Combinations

The natural and false-color composite imagery are
straightforward color composites of three TM spectral bands.
The only additional computer processing applied by EarthSat,
over that performed by NASA in the generation of the P-tape

CCT's, has been a "hybrid stretch" contrast enhancement. The hybrid stretch algorithm differs from a standard linear or histogram equalization (ramp distribution) stretch in that the data are distributed across the dynamic range of the film writer to differentially maximize the contrast within the most populated portions of the histograms while preventing condensation of data at the histogram tails. The resulting image displays an optimum degree of contrast without sacrificing information at the high and low extremes of the brightness range.

The natural color TM image is a composite of TM bands 1, 2, and 3 displayed in the blue, green, and red emulsions of the color film, respectively[1]. The emulsion sensitivities of the color film are nearly the same as the wavelength ranges of the respective bands, therefore, the resulting image is very similar to the true colors that one might see from a high-altitude aircraft on a very clear day.

A false-color TM image is a composite of any TM bands other than 1, 2 and 3 in blue, green, and red light, respectively. By definition, the spectral sensitivities of these bands will be different from the emulsion sensitivities with which they are composited, therefore, the resulting image is of "false" color.

_____

[1] In all discussions of color compositing of spectral bands, the compositing order is blue, green, and red. Thus, a composite expressed as 2, 3, 4 will have color assignments as follows: band 2 (blue), band 3 (green), and band 4 (red). The production of a color print from a color negative is a subtractive process so the band numbers printed in the upper image margin will be in complementary colors, i.e., band 2 will appear in yellow, band 3 in magenta, and band 4 in cyan.

With the MSS system, the selection of which combination of three spectral bands to use in generating false-color composites was a moot question. The high degree of spectal similarity between MSS6 and MSS7 made a traditional selection of MSS4, MSS5, and MSS7 a rather straightforward and logical choice. However, with the TM system we are faced with the task of selecting the best three from an available total of seven spectral bands.

A total of 35 unique sets of three can be drawn from the 7 TM bands. In order to generate an objective assessment of the potential "information" content, we have developed a computer program which ranks the 35 possible combinations according to the determinant calculated from their respective 3x3 variance-covariance matrices. The definition of "information" is one of a statistical nature. The combinations with the larger individual variances and the smaller cross-correlation (covariances) will have the larger determinant values and will therefore be ranked as having the higher information content. One question is whether or not high determinant base information means high geologic information or, more appropriately, are the high determinant base selections the best for geologic interpretation? In general, the answer is affirmative. For the Death Valley subscene the 35 possible combinations are listed according to their determinant size in Table 3. The band combinations in the upper portion of the list displayed considerably more spectral and spatial information than those in the bottom portion. However, with closer inspection the combinations in the upper portions of the list were found, because of the high

TABLE 3: DETERMINANT RANKING OF THREE BAND COMBINATIONS OF TM SPECTRAL DATA; DEATH VALLEY, CALIFORNIA

RANK	DETERMINANT	TM BAND COMBINATIONS
1	1272497	145
2	1143280	157
3	605756	135
4	544953	147
5	465850	357
6	370533	457
7	299501	257
8	298694	156
9	267809	345
10	265281	245
11	240642	137
12	236136	125
13	121905	356
14	111947	347
15	111714	247
16	105650	167
17	103271	235
18	94622	456
19	94215	127
20	78063	256
21	45354	367
22	39842	237
23	38382	134
24	36956	467
25	34010	146
26	28529	267
27	22276	567
28	20520	124
29	18148	136
30	8815	123
31	6113	246
32	5547	346
33	4910	234
34	4831	126
35	2171	236

correlation between the visible bands (see Table 5), to have

several combinations with clearly redundant spectral infor-

mation. The top 17 combinations could be reduced to six, which

show substantial differences in useful and interpretable

information. Table 4 lists the top 17 band combinations of

Death Valley scene and notes those which are significantly

similar to others within the list.

TABLE 4: COMPARISON OF THE BEST BAND COMBINATIONS
FOR THE DEATH VALLEY SCENE

Combo	Comment
145	- Unique-
156	- Unique-
135	- Unique-
146	Same as 145
356	Similar to 156
456	- Unique-
256	Same as 156
157	- Unique-
345	Same as 245
245	- Unique-
136	Same as 135
125	Similar to 135
357	Same as 157
346	Similar to 345
246	Similar to 145
167	Same as 157
235	Same as 135

Those six combinations which are listed above as "unique"

were found to have areas of distinctly different presentation of

spectral and/or spactial information. False-color composites of

these six are shown in Plate 2b for the Cotton subscene of the

Death Valley image. These subscenes have been sampled at a two

pixel spacing, to present an approximately 9 km area at a scale

of 1:250,000. Along with these six, Plate 2a contains the

natural color (1,2,3) and standard false-color (1,3,4) composites of the same subscene. These composites are number 30 and 23, respectively, on the determinant ranking; the obvious lack of spectral contrast compared to the other six subscenes leaves little question as to why they were ranked so low.

By virtue of their spectral similarity to the MSS bands, the 2,3,4 or 1,3,4 TM false-color composites were traditionally chosen as the "standard" false-color composites. The familiarity of the interpreter with the spectral response of surface material within these spectral bands made this an obvious choice. We have found that with the new near-infrared bands available to the TM system, a universally good band combination is the 1,4,5, as it offers some of the best spectral and spatial information. However, experience in this project has shown that there is some scene dependence as to utility of a specific band combination. For example, in the Greeley, Colorado area, combinations 4,5,7 and 7,5,4 were chosen as the better band combinations over 1,4,5. In the Bluff, Utah area the 1,2,3; 1,4,5; and 1,5,7 were all equally good. The color renditions of several of the possible combinations are new to interpreters and are often disorienting. For this reason, we suggest that they be accompanied by the natural color 1,2,3 composite. The natural color composite provides an excellent base for data compilation and is extremely easy to relate to, both in the shop and in the field.

From the comparisons of the Cotton false-color composite subscene, several conclusions can be drawn;

1. The determinant ranking approach is useful as a first-cut ordering of information content.

2. Tight correlations among bands will create redundancies; imagery must be inspected interactively to eliminate redundancies or, alternatively, the 7 band variance-covariance matrix can be used to determine crossband correlations.

3. Suggested new "standard" false-color composite for the TM system is 1,4,5; 3,4,5 in heavily vegetated areas.

4. The natural color of (1,2,3) composite is suggested as the most suitable base image for data compilation and field navigation.

3.3.1.2 Decorrelated (decor) Imagery

The main advantage of the decor algorithm is that it maximizes the contrast between the highly correlated bands, which allows the maximum utilization of spectral information in a color composite. The decorrelation algorithm involves a contrast enhancement to achieve the maximum dynamic range of brightness (i.e., spatial information) available within each TM band, plus a decorrelation of the TM bands to allow the maximum utilization of the spectral information available within a multi-channel image.

In order to optimize the correlated data sets for "n" dimensions (or bands), a transformation must be applied to convert the elliptically distributed data to the non-correlated symmetrical distribution in "n" dimensions. The algorithm which performs this transformation is an "inverted principal

components" or "decorrelation" algorithm. The transformation requires three steps as follows:

First, a Karunen-Loeve or "principal components" transformation must be performed. In this transformation, each of the "n" dimensions of the ellipsoid count distribution is assigned a new axis. The first principal component is assigned to the longest dimension of the ellipsoid, and the second axis is assigned to the second longest dimension of the ellipsoid, and so on until all "n" dimensions are assigned. The resulting distribution is oriented around a new set of orthogonal axes which have been rotated from the raw TM coordinate system. The rotation matrix is saved for the third step of the decorrelation transformation.

The second step of the decorrelation transformation requires the use of a contrast stretch applied to the component axes. The purpose of a linear contrast stretch is to set off all the diagonal elements in a correlation matrix to zero. The effect of a contrast stretch applied to the components is to change the ellipsoidally distributed data to a spherical distribution.

The third step in the decorrelation transformation is to inversely rotate the contrast enhanced principal components back to the original (raw TM) axes of distribution. In the contrast enhancement step, the histogram normalization creates a circular distribution of the values around the principal component axes. However, in a spherical distribution, all axis systems are equivalent, allowing rotation back to the original axes without reintroducing correlation from the now decorrelated data sets.

In the inverse transformation, the original principal component transformation matrix is inverted, the original axes are approximately reproduced, and the band means are maintained so that the inherent color relationships of the original TM color composite are preserved.

3.3.1.3   Intensity-Hue-Saturation (IHS) Imagery

The photographic process of creating a color image from three black-and-white bands involves color compositing the three spatially registered images with blue, green, and red light using a separate color for each of the three input bands. This method is Red-Green-Blue (RGB) color compositing. The spectral information of the three input bands is individually presented in the three emulsions of color film. An alternative method of combining three input bands is to apply a computer algorithm which allows them to individually control the intensity, hue, and saturation of the final color image. This method is the Intensity-Hue-Saturation (IHS), also known as Hue, Saturation and Value (HSV), method of band combinations. The following will first discuss the conventional red-green-blue color composite method and then the IHS approach.

RGB

The RGB method of color compositing involves combining three spatially registered input bands with red, green, and blue light, respectively. The resulting color image displays the spectral information of the data using what is known as the RGB color model. The RGB model is a Cartesian coordinate system

defining a unit color cube (Figure 7). The RGB primaries (red, green, and blue) are additive, i.e., the individual contributions of each are added to the absence of light to form the resulting color. The cyan, magenta, and yellow are subtractive, i.e., individual contributions of each are subtracted from white light to form the resulting color. The primary colors are used when generating imagery on the CRT screen; the subtractive (complementary) colors are used in color printing. Referring back to Figure 7, all possible colors can be plotted within the volume of the color cube. Each color can be represented as a combination of the three primary colors or of the three complementary colors.

IHS

The IHS model, compared to the RGB model, represents a much more "user oriented" approach to color image production. Rather than a cube, the color space is defined as a six-sided cone, or hexcone (Figure 8). The top of the hexcone corresponds to maximum intensity (I = 1), which contains the maximum intensity colors. The angle H around the vertical axis is the hue (where H = 0 is defined as red). Note that each complementary color is 180 degrees opposite its respective primary color. The saturation (S) is an approximate measure of color purity. Along the vertical axis of the hexcone there is zero saturation (S = 0). When S = 0, the intensity (I) will determine the resulting shade of gray between black (I = 0) and white (I = 1). Along the perimeter of the hexcone there is full saturation (S = 1) and

-42-
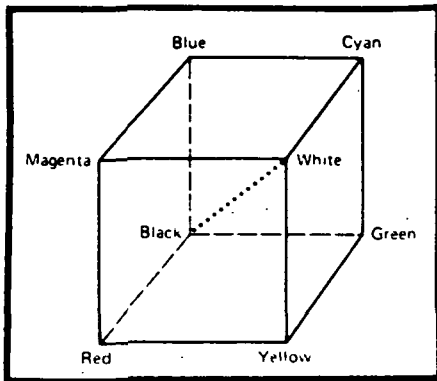
Figure 7   RGB color cube. Grays are on the dotted main diagonal.
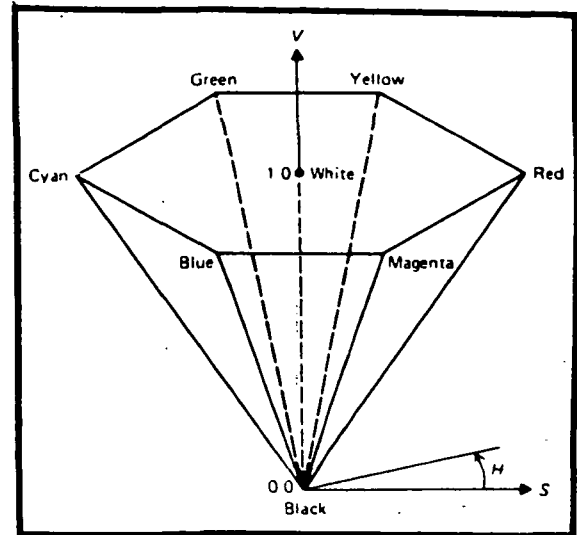
Figure 8   Single hexcone IHS color model.
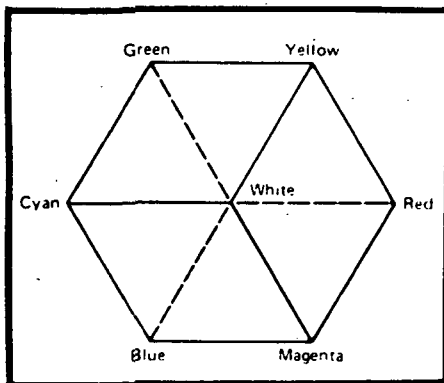
Figure 9   RGB color cube viewed along principal diagonal. Visible edges of cube are solid, while the invisible ones are dashed.
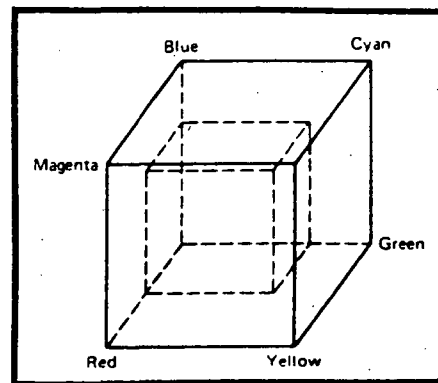
Figure 10   RGB cube and a subcube.

43

the intensity value will determine the brightness of the pure color defined by the hue (H).

The IHS model corresponds closely to concepts from the artist's color system of tint, shade and tone. For example, any color (H) with I = 1 and S = 1 is akin to an artist's pure pigment used as a starting point in mixing colors. Adding white pigment corresponds to decreasing S (without changing I). Adding black pigment corresponds to decreasing I (without changing S). Tones are created by decreasing both S and I. Of course, changing H corresponds to selecting a different pure pigment with which to start.

The top of the IHS hexcone corresponds to a surface seen by looking along the principal diagonal of the RGB color cube from white toward black (Figure 9). The RGB cube has sub-cubes, as illustrated in Figure 10. Each sub-cube, when viewed along its main diagonal, appears like the hexagon in Figure 9, except smaller. Each plain of constant I in IHS space corresponds to such a view of a sub-cube in RGB space. The main diagonal of the sub-cube space becomes the I axis of the IHS space.

In order to display an image on the CRT screen, or on photographic film, the data must conform to the RGB model. Using the correspondence between RGB and IHS established above, computer algorithms have been developed which enable the conversion from IHS to RGB, thus permitting conventional color compositing of the final print.

3.3.2 Spectral Imagery

The following image types are processed principally for the enhancement of spectral information.

3.3.2.1 Principal Component Imagery

Using the seven spectral bands of the TM data as an orthogonal seven-dimension space (color space), a given TM pixel has a unique position within the color space. The principal component transformation, also known as the an eigen or Karhunen-Loeve transformation, represents a rotation and translation of the normal color space coordinate system to a new, mutually orthogonal, seven-dimension "eigen" space. In the new eigen space each TM pixel has a new projected value on eigenband 1 through eigenband 7.

The eigenstructure calculation is a function of the variance-covariance matrix. An example of a variance-covariance matrix, calculated from the Death Valley TM seven band spectral data, is shown as Table 5. Note that the covariances have been converted to correlation coefficients to facilitate comparisons.

The orientations of the eigenvectors are such that the first eigenvector has the largest percentage of the total scene variance, with the second through last each containing a decreasing percentage of the scene variance. The seven eigenvectors are listed in Table 6 along with their respective percentages of the total scene variance. The tabulated values are the coefficients defining the unit vector direction of each eigenvector. The eigenband value of a given pixel would be

Table 5

Variance/Correlation matrix of the seven channel TM data of Death Valley, California (Scene ID No. 40124-17495; 17 November 1982)

	TM 1	TM 2	TM 3	TM 4	TM 5	TM 7	TM 6
TM 1	256.84	0.97	0.94	0.89	0.62	0.58	0.17
TM 2	—	90.44	0.98	0.95	0.74	0.70	0.24
TM 3	—	—	182.41	0.98	0.81	0.78	0.29
TM 4	—	—	—	168.39	0.83	0.80	0.27
TM 5	—	—	—	—	586.90	0.97	0.44
TM 7	—	—	—	—	—	205.26	0.48
TM 6	—	—	—	—	—	—	64.99

Table 6

Eigenvector statistics for the seven
channel TM data of Death Valley, California
(Scene ID No. 40124-17495; 17 November 1982)

Unit vector coefficients for each respective TM channel

	TM 1	TM 2	TM 3	TM 4	TM 5	TM 7	TM 6
1.	0.3694	0.2403	0.3572	0.3447	0.6434	0.3707	0.0897
2.	0.6211	0.2733	0.2877	0.2080	- 0.5075	- 0.3356	- 0.2080
3.	0.1282	0.4020	0.0613	- 0.0820	- 0.2130	- 0.0011	0.9623
4.	- 0.5290	- 0.0496	0.2452	0.7730	- 0.1366	- 0.1810	0.0925
5.	- 0.0594	- 0.0025	0.0945	0.0485	- 0.5140	0.8424	- 0.1067
6.	- 0.3991	0.4493	0.6461	- 0.4616	0.0013	- 0.0779	- 0.0468
7.	- 0.1365	0.8133	- 0.5472	0.1348	- 0.0191	0.0378	0.0248

Eigenvectors (Principal Components)

Percent of Total Scene Variance contained
in the Projections on each eigenvector

Eigenvector	% Total Variance
1.	82.3805
2.	12.9513
3.	3.1777
4.	0.7083
5.	0.5544
6.	0.1494
7.	0.0786

obtained by forming the scalar product of the seven-channel pixels with the appropriate eigenvector. These eigenbands may then be color composited to produce a principal component image, or be used as input bands for the IHS image algorithm.

The eigen transformation, which controls the information content of the final principal component image, is explicitly controlled by the spatial distibution of the raw TM data. Therefore, the second, third and other lower order eigen bands contain the most useful representation of the spectral information contained in the TM data. However, the first eigenband, which characteristically contains well over 90% of the total scene variance, totally homogenizes the spectral information. Therefore, care must be taken in interpreting principal component imagery.

Another clear consequence of the fact that the eigen transformation is a function of the raw data distribution is the frustrating problem that the principal component imagery from any given TM scene is unique to that scene. Therefore, what worked well with one principal component image in one scene may be different or impossible to achieve on another.

3.3.2.2 Ratio Imagery

Ratio imagery has long been the major supporting pillar of the geologic image interpretation process. The principal of band ratioing is to minimize the effects of varying incident illuminations, thereby achieving a better measure of the color balance, or spectral signature, of the surface material. The conventional method of presenting ratio data is as a Color Ratio

Composite (CRC). By their design, ratios reduce the effect of topography, thereby masking much of the geomorphology or structural information. This creates an image which is usually geographically disorienting. A more serious drawback of the CRC is the vastly increased noise level generated by the ratio process. This is particularly true in tightly correlated bands where the differences in the between-band system noise is almost as great or greater than the true spectral signal.

For these reasons, we have chosen to use the ratio data, not as components of a CRC, but rather as inputs to the IHS image algorithm. Within the IHS algorithm, the final appearance of the enhanced noise is greatly suppressed and the added geomorphological information contributed by the first eigenband greatly improves the interpretability of the final imagery.

3.3.3 Spatial Imagery

Image types which are principally used for spatial analysis of the TM data include single band black-and-white prints, and black-and-white prints of pixel convolutions.

3.3.3.1 Single Bands

The single band TM images are an important, and often overlooked, source of structural information. The seven black-and-white single band prints of the 1:250,000 scale Cotton subscene of the Death Valley image are presented in Plate 1a. Although each band has inherent spectral information (compare the vegetation at the Furnace Creek Ranch on TM 3 and TM 4), the

most useful application of this imagery is in structural inter-
pretations. The single band prints are free of resolution
losses caused by even the slightest misregistration during color
compositing. We therefore recommend that the individual black-
and-white bands be used to augment any structural interpretation
of color imagery.

3.3.3.2 Pixel Convolutions

We are defining pixel convolutions here to mean any
mathematical combination of one or two dimensional distributions
of pixels within a single band so as to create a new pixel
value. Pixel convolutions are not combining different bands,
but rather pixels from within the same spectral band. There-
fore, only spatial information is being enhanced. The most
common pixel convolution algorithms include edge enhancements,
lineament detectors and pixel smoothers. All of these were
employed to one degree or another during our interactive
analysis of the TM data. However, only the edge enhancements
were applied to the TM imagery delivered for this project. The
application of the edge enhancements took the form of a
Laplacian filter on the individual spectral bands of all the
natural and false-color composites, and on the first eigenband
used as the input band for the IHS imagery.

4.0 RESULTS OF CASE STUDIES

There are a wide variety of ways space acquired data can contribute to hydrocarbon exploration, ranging from logistic support to detecting indications of the presence of hydrocarbons themselves. In remote areas, Landsat-4 TM data provide a geometrically accurate map of substantial detail that in many ways is far more valuable than a standard planimetric map (e.g., it indicates land cover type, wet areas, etc.). This aspect of the data alone makes it valuable in an exploration program. It is also a valuable basis for planning geophysical surveys, field activities, and routing roads and pipelines in support of exploration.

Although exploration support and logistic uses of the data are important, it is the more direct contributions of TM data to exploration that are the primary focus of this project. Contributions of TM data include:

o   Lithologic mapping based on clear, accurate differentiation (if not identification) of rock types.

o   Structural mapping based on direct observation of structural relationships.

o   Mapping subsurface structural or depositional features beneath unconformable cover inferred from patterns of surface features.

o   Interrelationship of geographically separated features or recognition of regional structural patterns that imply tectonic processes and guide exploration thinking.

o   Under particular sets of conditions, recognition of geochemical (and possibly geobotanical) anomalies that imply

alternation associated with the emplacement or presence of minerals or hydrocarbons.

All of these petroleum exploration applications serve to high-light areas that deserve further exploration attention. That is, they assist in focusing exploration effort and resources. None lead directly to the discovery of hydrocarbons. The performance of the sensor, data transmission, and processing systems has been generally excellent. With the exception of a few data drops and glitches, the quality of the data (ignoring climatological problems) is high.

Beyond the performance of the sensor or the quality of the data, much of the "exploration" value of information derived from the TM data depends on inference. Thus, the background, training and experience of the interpreters and the quality and quantity of geologic, geophysical, and geochemical data integrated with the TM data are critically important. This does not detract from the immense exploration value of the data itself, but serves to emphasize that the value of the TM data interpretation increases with the quality of the collateral data used with it. The more that explorationists work with the TM data, the better they will under-stand how best to apply the data to the challenge of finding hydro-carbons.

The role that TM data play in any given exploration program is a function of several factors, including:

o   Geologic characteristics of the area;

o   Environment, including vegetation, topography, and climate;

o   Exploration maturity of the area;

o   Quantity and quality of available supporting data; and

o   The stage of development of the exploration program.

Because the purpose of this project is assessment or evaluation of the contribution of TM data to exploration, the case studies deal primarily with the first two factors, with passing reference to the others.

Integration of TM data into an exploration program is an iterative process. In a rank frontier area, TM data may be the best, most complete set of information available. It can provide regional structural fabric, general lithologic mapping (under proper conditions), a planning base for field work, logistics and additional survey work, and a basis for integrating and evaluating available data. In better known areas, or as work progresses in a frontier area, interpretations of TM data can be integrated with surface geology and regional geophysical data (especially aeromagnetic and gravity) to provide a regional tectonic and depositional model of the area and a basis to begin formulation of exploration models. The addition of subsurface data and seismic data add detail and refinement to three-dimensional models of the area and further the development of specific exploration targets. If known accumulations exist in an area or if drilling is successful, it is important to re-examine the TM data for "lookalike" areas which appear similar on TM imagery to the TM appearance of known producing areas.

As specific areas of interest are identified on the TM data, based either on similarity to known producing areas or the theoretical models developed, they become the focus for further exploration attention. In some situations, the TM data may play an

important role in selecting a drilling location (e.g., avoiding dikes in the San Juan or Raton Basins).

In the fortuitous situation where there are detectable geochemical or geobotanical anomalies related to the seepage of hydrocarbons, TM data can be used to rapidly focus the application of much more expensive geochemical and geophysical tools. Unfortunately, most areas do not have the appropriate rock type at the surface, the surface is too heavily vegetated or, most importantly, it is not yet known what constitutes an anomaly in some areas or how to detect an anomaly in TM data. Nevertheless, even though MSS data will continue to be used, it is clear that the improved spatial resolution and spectral sensitivity of TM data will greatly expand their role in, and contribution to, hydrocarbon exploration over that of previously available satellite data. Our work on this project and related exploration projects, together with data from the literature, demonstrates that greater spectral resolution would greatly improve our ability to detect and recognize geochemical and geobotanical anomalies.

The discussions of case studies below indicate some of the types of information that can be derived from TM data. The examples also suggest some of the types of processing and formats that are most useful for interpretation. One of the studies includes a comparison of the TM and MSS data.

4.1 Owl Creek, Wyoming

4.1.1 Regional Structure of the Owl Creek Area

The Owl Creek area is located in Central Wyoming (Figure 11). The Owl Creek uplift is a prominent east-west-trending
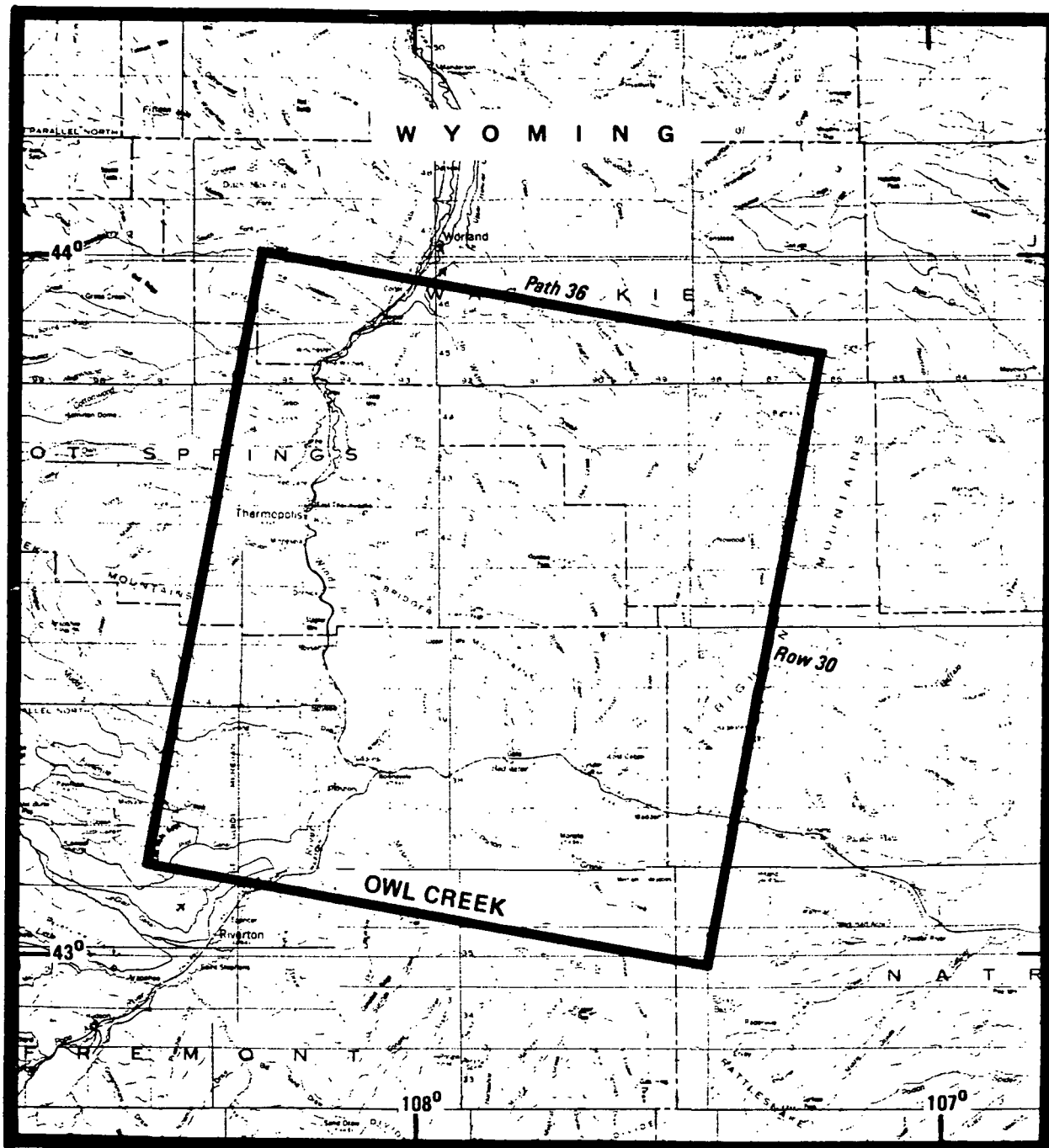
Figure 11 Owl Creek, Wyoming, location map

Region delineated is the area covered by Landsat 4 frame 40128-17232, 21 November 1982, Path 36/Row 30. A Geologic Interpretation was performed on this Landsat scene.

structural feature that is one structural element of the extremely complex and widespread Laramide foreland (Figures 12 and 13). The Laramide orogeny is a Late Cretaceous-early Tertiary compressive orogenic event that effected the craton or foreland of much of the western United States from southern Arizona to northern Montana. The Laramide orogeny is considered the most widespread and profound compressive event in the entire Phanerozoic history of the western United States Cordillera (Coney, 1978). The Laramide orogeny was characterized by development of basement-core overthrusts and adjacent synkinematic depositional basins. Faults that bound ranges are generally low-angle thrusts that flatten with depth indicating that horizontal compression was responsible for development of Laramide structures (Coney, 1976; Brewer and others, 1980; Bally, 1981; Hamilton, 1978). The Laramide orogeny occurred mainly from the latest Cretaceous (Middle Campanian) through about the middle or late Eocene (from about 75 to 37 m.y.B.P.). The amount of compression recorded on Laramide structures increases northward along the Laramide foreland (Hamilton, 1981). Foreland deformation is more intense in the Wyoming-northern Colorado area than in the southern Colorado-New Mexico area. As much as 100 km of intracratonic crustal shortening occurred along Laramide structures north of the Colorado Plateau in Colorado and Wyoming (Brewer and others, 1980; Gries, 1981, 1983). This is a great amount of shortening considering that it was all intracratonic shortening of continental crust.
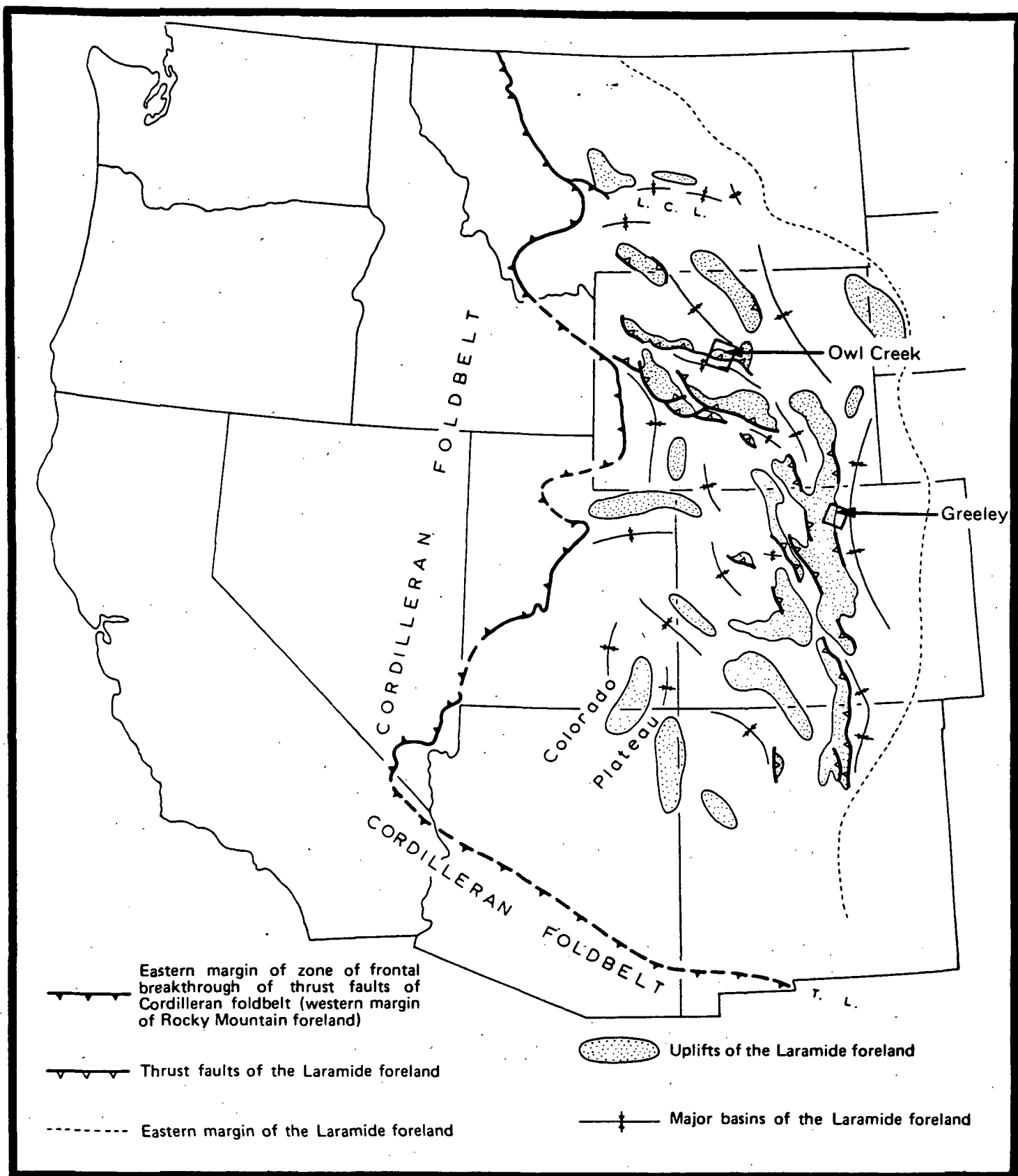
Figure 12 Generalized tectonic map of the Laramide foreland showing major overthrust structures: T.L. = Texas lineament, and L.C.L. = Lewis and Clark lineament (from Woodward, 1976). The approximate locations of the Owl Creek and Greeley Landsat 4 scenes are also shown.
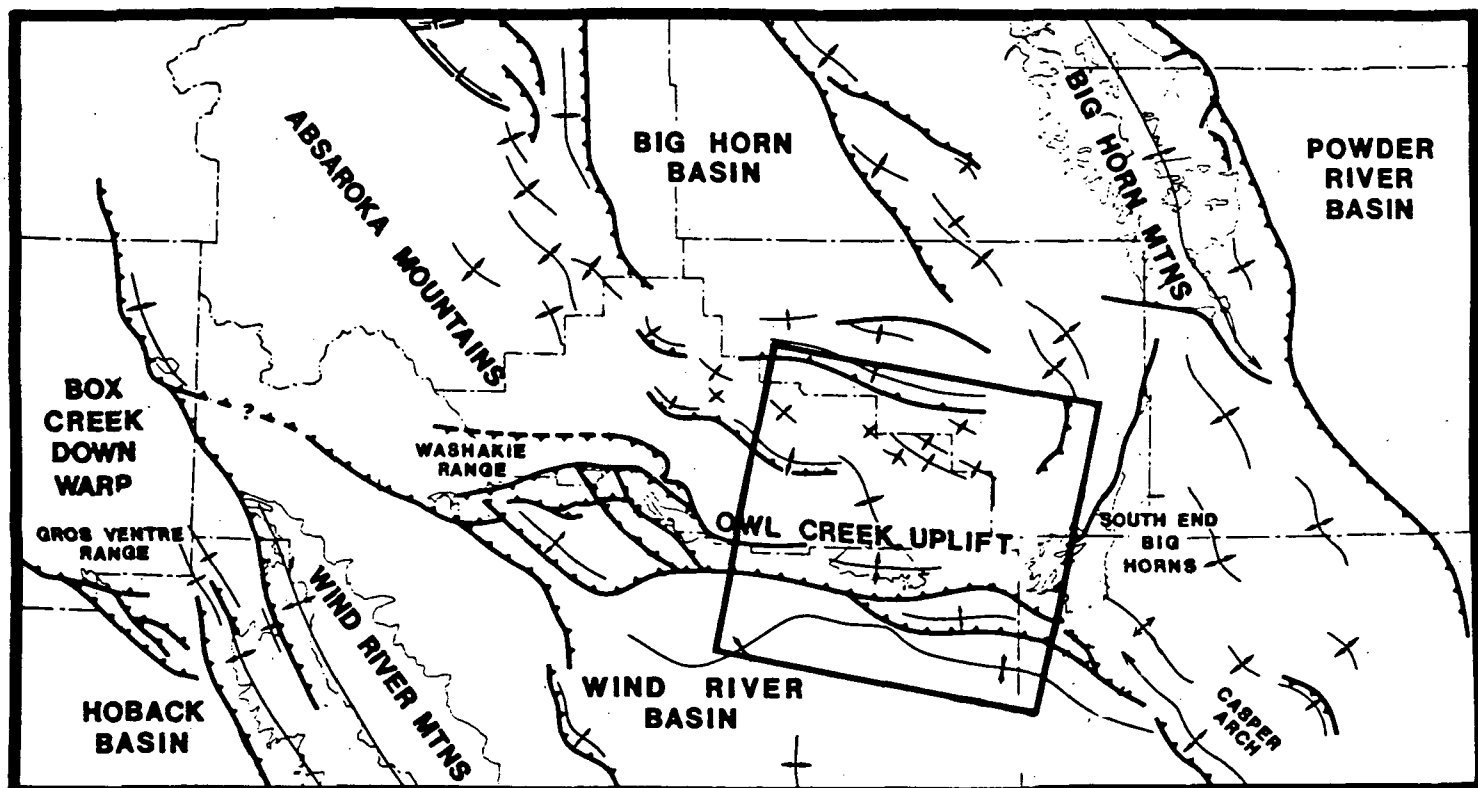
Figure 13 The Owl Creek uplift trends east-west and is bounded on the east by the south end of the Big Horn Mountains and on the west by the Washakie Range (from Gries, 1983). The Owl Creek Landsat 4 study area is outlined in the central part of the diagram.

Numerous models have been presented to explain the Late Cretaceous-early Tertiary Laramide orogeny that affected the foreland region of the western United States Cordillera (see Woodward, 1976, for a list of all models presented for the Laramide orogeny). The most attractive models invoke low-angle or flat plate subduction as a cause for the orogeny (Coney, 1972; Burchfiel and Davis, 1975; Coney and Reynolds, 1977; Dickinson and Snyder, 1978).

The amount of compressional stress that can be transmitted into the crust of the overriding plate adjacent to a subduction zone is directly related to both the area of interface between the overriding and subducting plates and the degree of coupling between these plates (Barazangi and Isacks 1976; Dickinson and Snyder, 1978). Subduction angle regulates both these features and, therefore, controls how much stress can be transmitted into a foreland region adjacent to a subduction zone (Cross and Pilger, 1982).

Throughout most of the late Mesozoic and early Tertiary, the Farallon plate was being subducted beneath the western edge of the North American plate (Coney, 1978). Convergence rate and the direction of subduction between the Farallon and North American plates varied during this time (Livaccari and Engbretson, 1983). The convergence rate between the Farallon and North American plates continually increased from the middle part of the Mesozoic until the end of the Laramide orogeny in the Eocene. Convergence rate between the North American and Farallon plates peaked during the latter part of the Laramide orogeny in the Eocene. At that time, subduction rates reached

their maximum of about 15 to 17 cm/yr (Engbretson, 1983; Keith, 1982). Rapid rates of relative convergence caused flattening of the subduction angle of the underriding Farallon plate. The Laramide orogeny is a response to this flattening of the sub-duction angle (Coney and Reynolds, 1977). Flattening of the subduction angle was perhaps assisted by subduction of more buoyant oceanic crust during this time (Livaccari et al., 1981). In summary, low-angle or flat plate subduction lead to enhanced viscous coupling between the overriding North American and underriding Farallon plates during the Late Cretaceous and early Tertiary. This increased regional compression which in turn, generated deformation in the Laramide foreland (Coney and Reynolds, 1977; Dickinson and Snyder, 1978; Cross and Pilger, 1978; 1982).

Two major episodes of the Laramide orogeny have been identified by Chapin and Cather (1981) and Gries (1983; Figure 14). This subdivision was earlier hinted at by the excellent field work of Murphy et al. (1956); Keefer (1965); and Love (1978) in the Wyoming area. The early phase in the Laramide orogeny occurred in the latest Cretaceous and Paleocene (75-56 m.y.B.P.). During this time the relative convergence rate between the North American and Farallon plates was east-northeast directed (Livaccari and Engbretson, 1983). This resulted in the Colorado Plateau block being moved eastward against the cratonic interior of North America along left-lateral strike-slip faults in Wyoming. Mainly north-south to northwest-southeast-trending Laramide uplifts were formed in the foreland at this time (Figure 14; Gries, 1981; 1983).
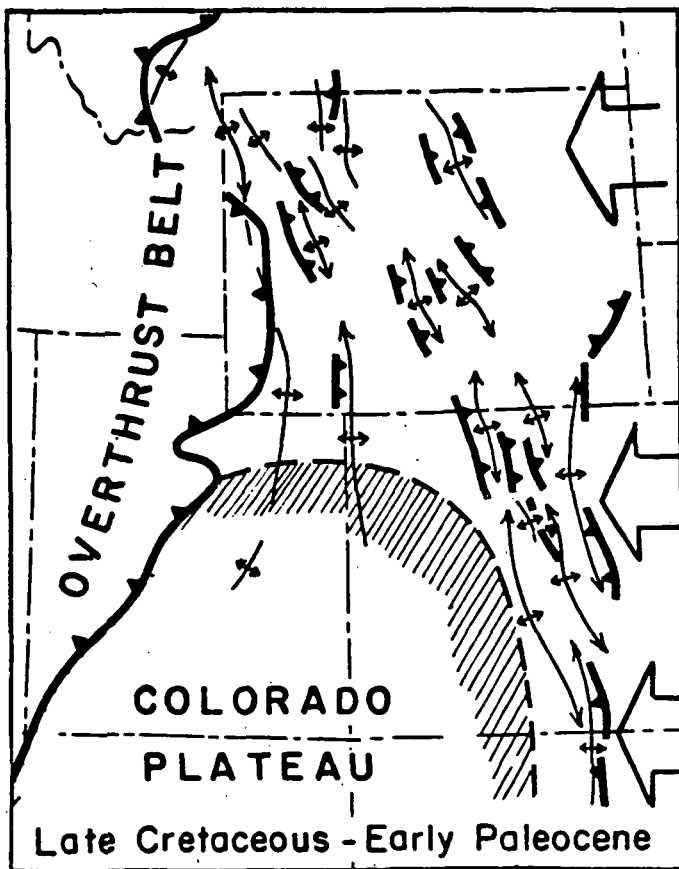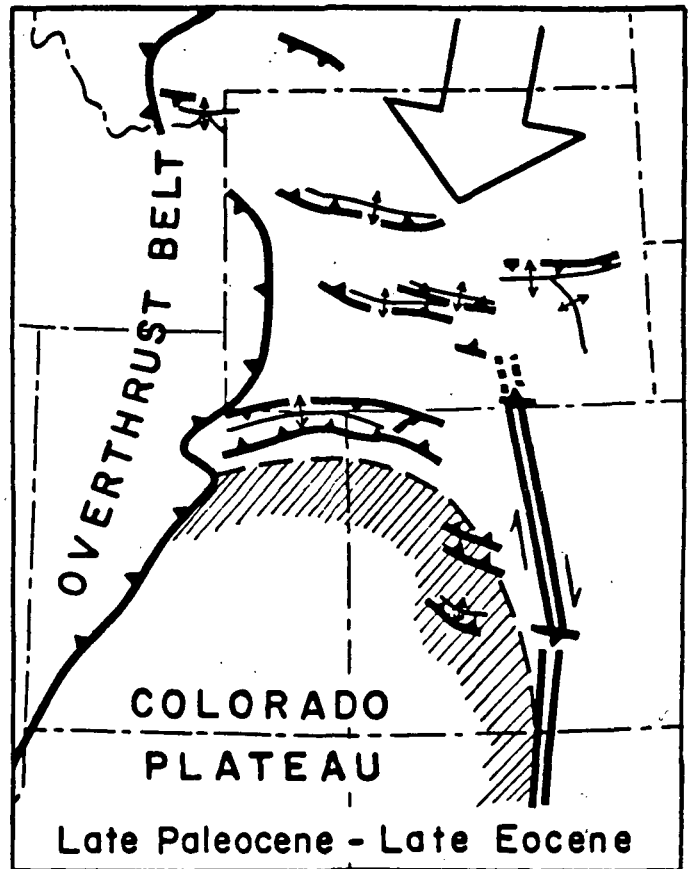
Figure 14 Timing and direction of compressional force related to the Colorado Plateau (from Gries, 1983b):
 a. During early Laramide movement, uplifts and thrusts appear to be stacked along the east flank of the Colorado Plateau with broad arches plunging off to the north.
 b. Late Laramide north-south compression caused formation of east-west-trending uplifts and basins from Montana to southern Colorado.

61

Major early Laramide structures include the Sangre de Cristos Mountains, Front Range, the Wind River Mountains, the Big Horn Mountains, and the Black Hills. This is essentially the classic model of Sales (1968) in which horizontal compressive stress drives the Colorado Plateau eastward along left-lateral strike-slip faults in Wyoming (Wyoming couple) resulting in north-south-trending overthrust structures in Colorado and New Mexico. An important aspect of this Laramide model is the inherent rigidity of the Colorado Plateau. The Colorado Plateau is bounded on three sides by large basement over-thrusts. Monoclinal flexures formed along the internal parts of the Colorado Plateau during the Laramide orogeny. These flexures are controlled at depth by low to moderate angle thrusts. These structures are the lesser extreme of the better developed overthrusts found throughout the rest of the Laramide foreland. Deformation along the edges of the Colorado Plateau is far more intense than within the plateau proper, suggesting that the entire Colorado Plateau acted as an intact block and stress guide to transfer compressive stress far eastward into the foreland during the Laramide orogeny. Therefore, it is reasonable to assume that the Colorado Plateau acted as an intact block during most of the Laramide orogeny.

The late Laramide orogeny occurred in the Eocene about 56 to 37 m.y.B.P. During this time the convergence rate between the North American and Farallon plates peaked at 15 to 17 cm/yr. The convergence direction between the North American and Farallon plates has also changed at this time to a more north-northeast direction (Livaccari and Engbretson, 1983).

This resulted in forcing the entire Colorado Plateau northward creating east-west-trending, north to south directed over-thrusting in the northern Laramide foreland of Wyoming and Montana (Gries, 1983b), and north-south-trending right-slip deformation along the eastern margin of the Colorado Plateau (Figure 14; Chapin and Cather, 1981). Major Eocene age east-west-trending structures of the northern Laramide foreland include the Unita Mountains, Owl Creek Range, south flank of the Wind River Range, Granite Mountains and north flank of the Laramie Mountains in Wyoming (Gries, 1981; 1983). The late Laramide phase is considered the most intense part of the Laramide orogeny. Sediment thickness of synkinematic Eocene units in nearby basins is much thicker than Maastrichtian Paleocene units. Also, most basement-cored uplifts were eroded down to their Precambrian core in the Eocene.

The east-west-trending Owl Creek uplift overthrusts the northern flank of the Wind River Basin (refer to Figure 13). The eastern end of the Owl Creek Range adjoins with the southern end of the Big Horn Mountains and the northern end of the Casper Arch. The west end of the Owl Creek uplift abutts with the Washakie Uplift. There are two sets of major structural features in the Owl Creek Range that were generated during the two major phases of the Laramide orogeny: (1) a latest Cretaceous-Paleocene set of northwest-trending fold thrust structures, and (2) an early and middle Eocene set of east-west-trending fold-thrust structures that truncated the older northwestern trends (Murphy and others, 1956; Keefer, 1965; Bown, 1982; Winterfeld and Conard, 1983). In the

Sheldon-Little dome area of the Owl Creeks, Murphy and others (1956) described northwest-trending folds that formed during the Paleocene and were later crosscut by Eocene age east-west-trending folds. Love (1978) described a similar sequence of events at the junction of the Owl Creek Range and southern Big Horn Mountains. The overprinting relationships between older northwest-trending structures and younger east-west-trending structures are clearly displayed on the high-resolution Landsat-4 imagery. Interpretation of Landsat-4 imagery clearly shows that the structural trends and style of smaller scale features mimics the larger scale structures in the Owl Creek Range. Northwest-trending structures of the Owl Creeks clearly seen on Landsat-4 imagery include folds 10 to 16 km long and a large overthrust with 150 to 600 m of vertical displacement. Major movement on the east-west-trending Owl Creek thrust occurred in the early Eocene and continued episodically through the late Eocene (see Gries, 1983). The Owl Creek Range was uplifted and thrusted southward over the adjacent subsiding Wind River Basin in a major tectonic event during the Eocene (Figures 13 and 14). This event truncated previously existing northwest-trending structures. Major east-west-trending Eocene age thrusts and folds are 85 to 100 km long and have 600 to 915 m of vertical displacement (Gries, 1983). These features are well displayed on the Landsat-4 imagery.

Seismic data along the southern flank of the Owl Creek Range indicate that asymmetrically folded sediments continue for more than 17 km in the subsurface beneath the leading edge of the Owl Creek thrust (Gries, 1983). Immediately west of the

Owl Creek Range along the southern flank of the Washakie Range,
Shell Oil drilled a well through more than 2,150 m of crystal-
line Precambrian rocks. The well was drilled on seismic
evidence that indicated sedimentary rocks should be present
five miles north of the leading edge of the thrust beneath
Precambrian rocks. Unfortunately, the well was not drilled
deep enough to test this concept.

The northern Owl Creek thrust fault on the north flank
of the Owl Creek Range trends roughly east-west for a distance
of 40 km. It is a south dipping thrust that has moved the
northern edge of the Owl Creek Range northward over sediments
of the Big Horn Basin. Thus, thrust faults occur along both
north and south flanks of the Owl Creek uplift (Gries, 1983).
Bounding thrusts of the Owl Creek Range dip towards each other
and probably converge at depth. Similar east-west-trending
Laramide uplifts bounded on both sides by opposing thrust
faults include the Granite Mountains and the Unita Mountains
(Gries, 1983). This type of structural style is interpreted as
evidence for the compressive origin of these uplifts (Hamilton,
1978; Gries, 1983).

4.1.2 Laramide Depositional History of the Wind River Basin

During the latest Cretaceous (early Laramide) the Wind
River Basin was downwarped into a large synclinal fold into
which the Lance Formation was deposited (Keefer, 1965; Keefer
and Love, 1963). Uplift occurred along the west end of the
Wind River Basin at the site of the northern end of the Wind
River Range and the southern end of the Washakie Range (Keefer,

1965). The Owl Creek Range and Casper Arch were not active during the deposition of latest Cretaceous Lance Formation.

During the Paleocene, continued basin subsidence of the Wind River Basin is reflected in deposition of the Fort Union Formation in the northeast part of the basin. Uplift continued along the Washakies and the western part of the Granite Mountains in the Paleocene (Keefer, 1965; Reynolds, 1978). The north end of the Wind River and Washakie Ranges may have furnished clastics fragments to the Paleocene Fort Union Formation that was being deposited in the northwestern part of the Wind River Basin (Keefer, 1957).

In the earliest Eocene, erosional detritus from Paleozoic and Precambrian units was being deposited into the Indian Meadows Formation. This marked the beginning of substantial Eocene age uplift and erosion of uplifts that surround the Wind River Basin. Large masses of Paleozoic rocks were incorporated into the Indian Meadows Formation (Keefer, 1965). The Casper arch also became more active in the earliest Eocene (Love, 1978). In the earliest Eocene, northwest-trending structures were further uplifted but there is no evidence that east-west-trending faults were active at this time.

Early Eocene deposition of the Wind River Formation in the Wind River Basin not only implies massive erosion of uplifts bounding the basin but also heralds development of east-west-trending uplifts bounded by east-west-trending thrusts such as the Owl Creek Range (Gries, 1983). The Wind River Formation is the most widespread unit in the Wind River

Basin. Clasts of Paleozoic and Precambrian rocks in the Wind River Formation are evidence of extreme denudation of adjacent uplifts at this time (Keefer, 1965). Lower Eocene rocks are more than 2,750 m thick in the northern part of the basin adjacent to the Owl Creek thrust. Clastic units adjacent to the Owl Creek uplift are composed of large boulder facies implying rapid uplift (Keefer, 1965). In summary, stratigraphic evidence suggests that major uplift of the Owl Creek Uplift occurred in the early and middle part of the Eocene along eastwest-trending faults.

4.1.3 Hydrocarbon Potential of the Owl Creek Uplift

The main advantage of Landsat-4 imagery in this area is the enhanced resolution which aids in the mapping of bedding and therefore, of structures apparent along the Owl Creek uplift. Truncation of early Laramide northwest-trending structures by late Laramide east-west structures can readily be documented by interpretation of Landsat-4 imagery. This has important aspects for delineating geologic structure along oil and gas fields adjacent to the Owl Creek Range.

Just south of the main Owl Creek uplift and east of Boysen Lake, is the Madden Deep. The Madden Deep is an important oil and gas field that is one of the more significant oil and gas fields in Wyoming. The Madden Deep is located on a large subsurface Madden anticline of the northern Wind River Basin. The Madden structure is an east-west-trending anticline with 600 m of closure on the top of the lower member of the Paleocene Fort Union Formation (Reid, 1978). The anticline is

17 km wide and over 35 km long. Fracturing is a significant factor in the reservoir development at the Madden Deep Field. Lineations identified on Landsat-4 imagery that cut across the Madden Deep reflect important fracture patterns controlling reservoir development. Gas, condensate, and oil are produced from the Tertiary Fort Union Formation and Cretaceous Lance, Mesaverde, and Cody Formations.

The fact that the Madden anticline is an east-west-trending structure implies that it is an early to middle Eocene structure that developed simultaneously with main development of the Owl Creek uplift.

4.1.4 <u>Qualitative Assessment of Thematic Mapper Imagery,</u>
<u>Owl Creek, Wyoming</u>

Landsat-4 TM data for the Owl Creek area were processed in several different band combinations. Processing of image #40128-17232-D0322 includes Decorrelated (Decor) band combinations 1,3,4; 1,2,3; and 1,4,5 and standard processing of bands 1,4,5 and 2,3,4. These images were enlarged to a scale of 1:100,000 for interpretation.

The Decor 1,3,4 image proved to be the best overall image for geologic interpretation in both the mountains and plains areas. In mountainous areas Decor 1,3,4 provides the excellent definition of bedding attitude which is a prime indicator of geologic structure. Extensive areas of homoclinal dip are well displayed, as are subtle but important changes in bedding attitude which reflect structures such as thrusts and folds. Color definition between various sedimentary units is

also well-defined. Structure in some of the mountainous areas
is unfortunately obscured by snow, however, lineaments
expressed by topographic differences can still be defined in
snow covered areas. Major structural features are clearly
defined and can be mapped with confidence on this image.
Numerous subsidiary splays from the main thrust can also be
inferred. In general, lineaments of all sizes are well-defined
on Decor 1,3,4. Mapping of the numerous short lineaments
visible on the image tend to obscure the regional linear
trends. This seems to be an inherent problem in the interpre-
tation of TM imagery.

The Decor 1,2,3 image is not as useful as the Decor
1,3,4 image for geologic interpretation. The Decor 1,2,3 image
displays more uniform colors with an overall grayish appearance
that trends to obscure many of the finer details of geologic
structures and lineaments. However, shadows seem to be subtly
enhanced, making some lineaments and slope breaks slightly
better defined. However, most of the stratigraphic units in
the area appear approximately the same color which somewhat
obscures the definition of bedding. The Decor 1,4,5 image
provides a good overall image for color definition of bedding
and lineaments. However, considering all factors, the Decor
1,3,4 image is better than the Decor 1,4,5 image.

In general, the 1,4,5 (non-Decor) image is not as useful
as the Decor 1,3,4 image. The 1,4,5 image does, however,
provide much better definition of linear features in snow
covered mountainous areas. Plains areas on this image are also
sharp and additional structural data are mappable.

Unfortunately, poor color definition of bedding on the 1,4,5 image obscures many of the major structural features.

Differentiation of bedding by color on the 2,3,4 image is quite poor. A brownish-yellowish tone predominates in this image. However, details of stream beds and small valleys and bedding slopes appear to be somewhat more crisp on the 2,3,4 image than on the other color composites. This makes the 2,3,4 image a valuable tool for analysis of lineaments defined by topographic differences.

In summary, the Decor 1,3,4 image and the 2,3,4 image provide the most useful combination of imagery for general geologic and lineament interpretation in the Owl Creek area.

4.2 Greeley, Colorado

4.2.1 Introduction

The Greeley, Colorado Landsat-4 quarter scene is located in central Colorado north of Denver (Figure 15). The image covers portions of the north-south-trending Front Range Mountains including, to the east, the plains area of the Denver Basin. The Front Range and adjacent Denver Basin are the major structural elements found within the Greeley Landsat-4 scene (Figure 12). The Colorado Front Range is a north-trending, Laramide age structure. It is bounded to the east by a major west-dipping low-angle thrust that juxtaposes Precambrian basement against Paleozoic and Mesozoic sediments. The adjacent Denver Basin is an asymmetrical basin with its axial deep parallel with, and adjacent to, the Front Range of Colorado. The deepest part of the Denver Basin is located
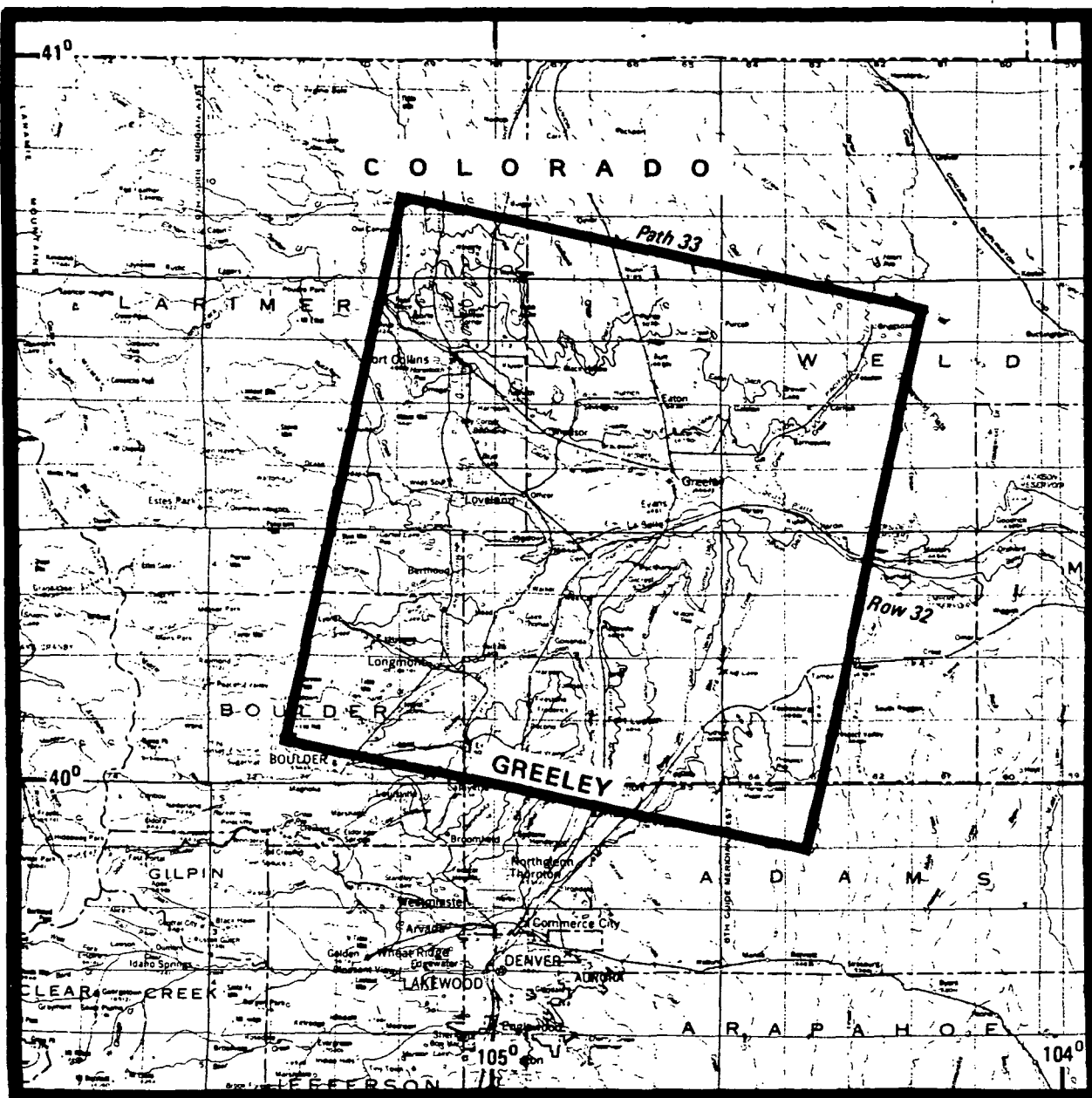
Figure 15 Greeley, Colorado, location map

Region delineated is the area covered by Landsat 4 frame 40123-17052, 16 November, 1982, Path 33/Row 32. A Geologic Interpretation was performed on this Landsat scene.

between Denver, Colorado and Cheyenne, Wyoming, where more than 4000 m of sedimentary rocks are found. The western edge of the Denver Basin is extensively deformed adjacent to the Front Range, while the eastern flank of the basin dips gently westward and is mildly deformed by relatively minor folds and faults.

4.2.2 Depositional History of Hydrocarbon-Bearing Units in the Denver Basin

The present-day Front Range-Denver Basin area was predominantly a marine shelf during the early Paleozoic. Uplift during the middle Paleozoic exposed these older rocks to erosional denudation. Mississippian and Pennsylvanian rocks, consisting of marine limestones and shales with rare alluvial deposits, overlie this middle Paleozoic unconformity (Martin, 1965). The Mississippian section of the Denver Basin consists of predominantly transgressive sediments that range in thickness from 0-120 m. These strata are absent from large areas of the basin. The lower part of the Mississippian contains sandstone interbedded with limestone, whereas the remainder consists of predominantly limestone with variable amounts of chert. The Pennsylvanian section of the Denver Basin includes rocks of the Morrowan, Atokan, Desmoinesian, and Missourian Series that consist of cyclic deposits of sandstone, shale, carbonate and minor evaporites. Both the Morrowan and Atokan Series consist of shale interbedded with sandstone and limestone lenses that unconformably rest on either Mississippian limestone or Precambrian basement. The

Desmoinesian Series consists of a basal sandstone overlain by carbonate deposits which are cyclically intercalated with black organic-rich shale. Both the Missourian and Virgilian Series consist of interbedded limestone, dolomite, shale and minor evaporites. Wilson (1978) reports that pockets of skelmoldic porosity and sucrosic dolomite with effective intracrystalline porosity are found within the Missourian and Virgilian sections. Wilson suggests that sabkha diagenesis (dolomitization) operated on a cyclic basis during deposition of both the Missourian and Virgilian Series.

Morrowan and Atokan shales with intercalated sandstone lenses produce gas in the southeastern portion of the Denver Basin (Martin, 1965). The Desmoinesian basal sands (Leo Sands) and Virgilian and Missourian carbonates produce hydrocarbon in the northern and eastern reaches of the Denver Basin.

The overlying Permian section includes rocks of Wolfcampian, Leonardian, and Guadalupian Series that consist of cyclic deposits of fluvial hypersaline to normal marine sediments. The Wolfcampian Series consists of variable amounts of red and gray shale, dolomite, anhydrite, salt and local sandstone. A regionally extensive anhydrite unit marks the top of the Wolfcampian section. The Leonardian Series is gradational with the underlying Wolfcampian and consists of silty sandstones. These sandstones (Lyons Formation) represent ancient littoral deposits that accumulated in near-shore fluvial and eolian environments (Levandowski and others, 1973). The Guadalupian Series consists of thick evaporite and shale deposits. Wolfcampian sandstones produce in the northern

Denver Basin. The Lyons Sandstone (Leonardian) is known to produce oil in numerous localities within the basin (Figure 16).

Overlying the Paleozoic section are thick Cretaceous sediments. Lower Cretaceous rocks include the Dakota Sandstone, Mowry Shale, Graneros Shale and the Greenhorn Limestone. These units collectively comprise a transgressive marine sequence interrupted by several major periods of marine regressions. The Dakota Sandstone and Graneros Shale are regressive deposits consisting of deltaic to fluvial sediments. The J Sandstone Member of the Dakota Formation is a deltaic sand deposited by a large west-northwest prograding delta and a smaller northeast prograding delta. The D Sandstone Member of the Graneros Shale is thought to be both fluvial and deltaic in origin. The D sands were deposited as marine barrier bars and distributary channels and are interbedded with shale deposited in swamps and tidal flats and lagoons. The Mowry Shale and Greenhorn Limestone represent transgressive marine cycles and consist of petroliferous shale and chalk, respectively. Several bentonite beds are found within the Mowry Shale.

Upper Cretaceous rocks consist of the Carlile Shale, Niobrara Formation, Pierre Shale, Foxhills Formation and Laramie Formation, which constitute a regressive sequence interrupted by several marine transgressions. The Carlile Shale consists of a basal chalk unit overlain by shales and an upper sandstone unit. The Niobrara Formation consists of chalk and shaley chalk deposited during a major marine transgression. The Pierre Shale is a thick shale with lesser amounts of

AGE	FORMATIONS		THICKNESS	
TERTIARY	DENVER-ARAPAHOE FORMATION		500' (152m)	
LATE CRETACEOUS		LARAMIE FORMATION	60' (18m)	
		FOX HILLS FORMATION		
	PIERRE SHALE	TERRY SANDSTONE	8000± (2439m)	●
		HYGIENE SANDSTONE		●
		MITTEN MEMBER		
		SHARON SPRINGS MEMBER		●
	NIOBRARA FORMATION	SMOKY HILL MEMBER	350' (107m)	
		FORT HAYS LIMESTONE (TIMPAS Ls.)		●
	CARLILE SHALE	CODELL SANDSTONE MEMBER	420' (128m)	●
				●
EARLY CRETACEOUS	GRANEROS SHALE	GREENHORN LIMESTONE	370' (112m)	●
		"D" SANDSTONE OF DRILLERS		●
		HUNTSMAN OF DRILLERS		
		MOWRY SHALE		
	DAKOTA SANDSTONE	"J" SANDSTONE OF DRILLERS		●
		SKULL CREEK EQUIVALENT		
		PLAINVIEW EQUIVALENT		
		LYTLE EQUIVALENT		
JURASSIC		MORRISON FORMATION	475' (145m)	
		RALSTON CREEK FORMATION		
TRIASSIC		LYKINS FORMATION	400' (122m)	
PERMIAN		LYONS FORMATION	120' (37m)	●
PENNSYLVANIAN		FOUNTAIN FORMATION	1000' (305m)	

Figure 16 Generalized stratigraphic column, Front Range area. Dots indicate units which have oil production (from Clayton and Swetland, 1977).

siltstone and sandstone, all of which were deposited in shallow marine to near-shore marine environments. Several sandstone members such as the Hygiene and Terry Members are present within the marine shale. These members are believed to represent sublittoral sand sheets and bars formed by longshore currents (Kiteley, 1977). The upper part of the Pierre Shale, the Foxhill Sandstone and the Laramie Formation all represent a regressive deltaic sequence that prograded eastward to southeastward into a shallow marine sea (Davis and Weimer, 1976). The Foxhill Sandstone is a fine-grained shallow marine sandstone believed to represent the beach and shoreface sequence. The Laramie Formation consists of sandstone, siltstone, shale and coal deposited as a delta plain, primarily in fresh waters (Davis and Weimer, 1976).

Production from both the Upper Cretaceous D and J sands accounts for approximately 90% of all oil and gas produced in the Denver Basin (Clayton and Swetland, 1977). Much of the remaining production is from the Mowry shale, Greenhorn Limestone, Carlile Shale, Pierre Shale (Terry and Hygiene Members) and the Niobrara Formation.

4.2.3 Regional Tectonics and Structural Geology of the
       Greeley Area

The Front Range and Denver Basin are products of the Laramide orogeny (Figure 12). Laramide deformation produced numerous high-angle reverse faults, as well as folds, with a diversity of strike directions along the flanks of the Front Range. Basement blocks along the Front Range were

differentially uplifted and rotated along a complex system of
faults. The Laramide orogeny may be divided into two phases -
an early phase of general east-northeast directed horizontal
compression and a late phase of regional north-northeast
directed horizontal compression (see the Owl Creek section of
this report for more detailed discussion of the regional
tectonics of the Laramide orogeny). During the early Laramide
orogeny, the Front Range was thrust toward the east. During
the late phase of the Laramide orogeny, north-northeast-
trending horizontal compressive stress resulted in northward
motion of the Colorado Plateau block with respect to the stable
midcontinent area of the United States. This resulted in
development of a series of right-lateral, strike-slip
structures on the eastern edge of the Front Range. The north-
northwest-trending folds found along the Front Range may be
related to right-lateral wrenching during the late Laramide
orogeny. Along the Front Range, Paleozoic and Mesozoic
sedimentary strata are folded into a variety of Laramide
structures, including monoclines, symmetrical and asymmetrical
anticlines and synclines, as well as domes and basinal areas.
Basement rocks and folded sedimentary rocks are well-exposed on
Landsat-4 imagery. The Precambrian basement is brittlely
faulted along with the overlying sedimentary rocks. These
structures formed by both horizontal compression and right
lateral drag along a wide dextral shear zone along the edge of
the Colorado Plateau.

A well-developed series of north-northwest-trending
folds and faults along the Front Range is very distinctive on

Landsat-4 imagery. The northwest-trending folds extend into

the Precambrian core of the Front Range and eventually die out

to the northwest. There is also a multitude of northeast-

trending faults within the Front Range that are interconnected

with the northwestern faults (see Matthews and Work, 1978).

Both these fault systems combine to "chop-up" basement of the

Front Range into a complex series of generally east-tilted

blocks.

Many structural features along the Front Range within

the Denver Basin are ancient Precambrian structures that were

recurrently reactivated during the Paleozoic and Mesozoic.

These important features include:

1. A northeast-trending Precambrian wrench fault

    system described by Warner (1978) that passes

    through the northern portion of the Denver Basin.

    According to Warner, this wrench system is

    2,500-3,500 km long and 170-250 km wide. The

    presence of such a pervasive fault system should

    facilitate basement block deformation during

    subsequent orogenic events.

2. Numerous workers have described the influence of a

    northeast-trending Transcontinental Arch (extending

    from Minnesota to Arizona and passing through the

    Denver Basin) based on the thickness and facies

    distribution of Paleozoic units. Weimer (1978)

    reported that regional isopach data show that a

    thinning of the Niobrara Formation and upper

    Carlile Formation exists along the trend of the

Transcontinental Arch. The isopach data suggest
that Cretaceous sedimentary patterns were deflected
by recurrent vertical movement along this
structure.

3. Weimer (1973) described north and east-trending
faults in the east-central Front Range area, which
probably originated in the Precambrian and were
later reactivated during Late Paleozoic and again
during Late Mesozoic deformation. He noted that
facies and thickness changes on the Fountain, Lyon
and Lykins Formations correlate with known
Precambrian fault zones. Thus, recurrent movement
along these fault zones probably influenced
sedimentation patterns in the Late Paleozoic. In
addition, he suggests that recurrent movement of
these basement faults may have indirectly
controlled growth faulting associated with deltaic
sedimentation during the early part of the Laramide
orogeny.

The extensive system of northwest and northeast-trending
fracture zones is very well expressed on Landsat-4 imagery.
Major northwest-southeast-trending lineaments appear to have
influenced both the depositional and structural evolution of
the Denver Basin. Some of the major folds and many of the
minor folds of the Denver Basin appear to be related to these
fracture zones.

The major fracture zones are areas of persistent crustal
weakness that have been intermittently active throughout the

Phanerozoic. During periods of deformation, stresses and resulting strains may have concentrated along these crustal inhomogeneities. The relative displacement on a given fracture zone is dependent on its orientation with respect to the governing regional stress field during the time of movement. During most of the later part of the Paleozoic, when a weak to moderate stress field existed, movement along the fractures was moderate and subject to regional variation in relative displacement. However, during periods of major deformation such as during the Laramide orogeny, movement along the preexisting crustal anisotropies varied depending on orientation with respect to the regional principal horizontal compressive direction. In the Denver Basin during the Laramide orogeny, it appears that movement along most faults had a vertical component with small but important components of strike-slip. Some geologists (Thomas, 1974, 1976; and Sales, 1968) suggest that movement along these zones was primarily strike-slip in nature, and that the system of regional lineaments represents a wrench fault system which, in turn, controlled the development of major and minor features within the Denver Basin.

Movement on basement faults may generate folds by passive draping of sedimentary rocks over faults. Several fields such as the Borie, Horse Creek, and Fort Collins hydrocarbon fields along the east flank of the Front Range and Laramie Mountains, are drape folds with up to 125 m of structural relief (Bolyard and Katich, 1963). These folds formed by the passive drape of sedimentary rocks over

differentially uplifted and rotated basement blocks (Matthews and Work, 1978). Many of these folds have planar limbs with one steeply and one gently dipping limb. Along the Front Range, the upper surface of most basement blocks (and, therefore, the gently dipping limb of the drape folds) dips eastward. The process of draping is far more complex than simple bending or forced folding of sedimentary rock over some discrete vertical displacement in the basement surface. The process includes a number of mechanisms that, in various combinations with the dynamics of basement deformation, determine the resultant fold geometry. These deformation mechanisms include lateral sliding along bedding surfaces, general buckling, brittle cataclasis, and fracturing and faulting. The steep limb of a fold may undergo tectonic thinning by extensional fracturing parallel with the major basement fault to create a loss of continuity in the folded strata. Matthews and Work (1978), suggest that it is a possibility that the Carter Lake Anticline located along the eastern flank of the Front Range near Loveland developed in this manner. Cook (1978) reported that strike-slip faults in the sedimentary column may be important features in facilitating lateral movement and sliding of sedimentary rocks over the basement. These faults would trend parallel or subparallel with the direction of lateral transport and their presence would signal the existence of zones of intense fracturing in the sedimentary rock overlying the basement blocks.

On Landsat-4 imagery, drape folds are extremely well displayed and appear as closed circular anomalies transected by or immediately adjacent to prominent linear features. Drape folds associated with regional lineaments commonly occur adjacent to a principal lineament and are associated with subordinate features of similar orientation and relative displacement.

The sedimentary rock overlying a basement fault may be deformed into drag folds if movement along the fault has a significant horizontal component. Drag folds associated with regional wrenching will trend 20 degrees or less to the major wrench direction.

Many of the small hydrocarbon fields of the Denver Basin produce from small anticlines of low structural relief (e.g., Torrington, Pine Bluffs). These small folds, although not related to regional lineaments, may be associated with locally strong lineament trends and small circular anomalies that may be seen on Landsat-4 imagery. These folds take the form of anticlines, domes, or simple nosing of subsurface strata. These features may be broad, gentle features, but most likely they will be small isolated folds. Most folds of all origins are associated with a unique set of features that formed at the same time and in response to the same stress field that produced the fold. For example, the crest of anticlines and the troughs of synclines are marked by well-developed fractures parallel with the fold axes. On a plunging fold, these features commonly converge toward the nose of the fold. Many shear and buckle folds have conjugate shear fractures that

trend approximately 60 degrees to the fold axes. Fracture orientation frequently is sensitive to changes in trend of fold axes. Deflections in fold axes are accompanied by an increase in both fracture frequency and diversity of the fracture orientation. Therefore, areas seen on Landsat-4 imagery that contain multiple fracture directions, even if they are not associated with apparent surface closure, possibly overlie folds.

Within the Greeley study area, buried topographic highs may be found on the Precambrian, Pennsylvanian, pre-Triassic, and pre-Cretaceous surfaces. Differential compaction of folds may have formed over these erosional highs along the unconformity surfaces. Differential compaction folds affect both Paleozoic and Mesozoic rocks in the Denver Basin. Differential compaction and thinning of Cretaceous units along the Transcontinental Arch is responsible for trapping of hydrocarbon along the Wattenburg Trend of the Denver Basin.

4.2.4 Hydrocarbon Potential of the Denver Basin

The Denver Basin contains over 4,000 m of sediment. Two basin deeps exist within the Denver Basin, one near Cheyenne, Wyoming and the other near Denver. The area within and around the Denver deep has been proven to be very productive (Figure 17). The depths to the top of the oil-generating window within the Denver deep is about 1,675 m, assuming initial hydrocarbon generation at $65^{\circ}C$ and ambient surface temperatures of $10^{\circ}C$ as well as geothermal gradient of $1^{\circ}C$ per 30 m. This suggests
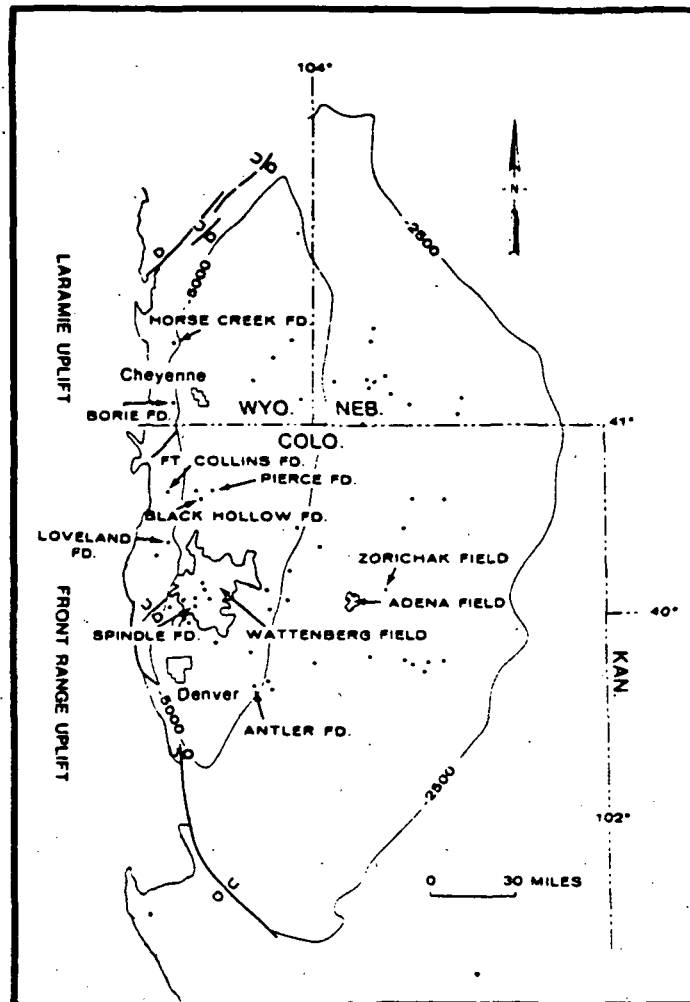
Figure 17   Precambrian basement structure contour map of
the Denver basin (contours in feet) showing
locations of major oil fields (from Clayton and
Swetland, 1977).

that Cretaceous rocks of the Denver deep are currently within the oil- or gas-generating window.

Mallory (1977) reported the presence of petroleum-filled fracture voids in the Pierre Shale and the Niobrara Formation, particularly in the Loveland, Berthoud and Boulder Fields, located north of Denver. He suggests that other areas with the potential for this type of reservoir are located elsewhere within the Denver Basin, possibly occurring associated with northeast-trending lineaments which may have been reactivated by Laramide deformation. According to Mallory, tensional cracks develop on the convex side of a flexure or along faults. These fractures develop in more brittle sedimentary facies such as silty or calcareous units of certain formations such as the Pierre or Niobrara Formations. The interbedded plastic shales provide a trapping seal for fractured, brittle shale reservoirs, thus creating a network of fracture voids in an essentially impermeable rock. Since the petroleum accumulation in these types of traps is not directly controlled by anticlinal closure, exploration should concentrate on fracture density rather than delineating subsurface flexures.

Thus, in otherwise unattractive reservoir rocks, fractures can provide porosity and permeability. Traps formed by induced porosity or permeability in otherwise tight reservoir rocks will be expressed on Landsat-4 imagery as areas having a high density of lineaments. In most areas, one fracture direction will be more prevalent than others. Therefore, areas that exhibit an unusually high number of different fracture orientations, as well as unusually high

density of fractures, are prime areas to be considered for fracture-induced hydrocarbon traps. An approximation of the geometry of such a trap can be derived because linear features seen at the surface are often a good approximation of subsurface trends.

Most of the fractures in rocks result from regional stresses. Folding and/or faulting initiated by regional stresses tend to fracture the rock locally in a very complex manner. In addition, fractures may be developed by upward propagation of basement features or by differential compaction of younger strata over structural highs in the subsurface.

In addition to fracture void reservoirs in the Denver Basin, a number of workers have reported that growth faults are responsible for fracture-induced porosity and permeability in tight reservoirs. Moredock and Williams (1976) reported that the high density of growth faults cutting the tight Upper Cretaceous strata facilitates production through fracture-induced porosity and permeability from the Single Tree, Spindle and Surrey Fields located just north of Denver. Fentress (1955) reported that most of the wells drilled in the Little Bear Field of Colorado are cut by faults confined to this stratigraphic interval. Fentress also implies that these faults significantly increase reservoir porosity and permeability.

The possibilities for basin centered gas in the Denver Basin are very good. Masters (1979) summarized the major characteristics of basin centered gas:

1. Water is produced updip in porous and permeable sands and gas is produced downdip in less porous and less permeable, shalier sands.

2. Meteoric water flows downdip in a water saturated section toward the basin center. The water saturated section grades imperceptably through a transition zone (consisting of saline water) several miles wide into a gas-saturated zone. Wells drilled in these three zones produce water, water and gas, and gas, respectively.

3. No evidence exists for stratigraphic or structural barriers between the water and gas saturated zones, except perhaps a small change in porosity (the gas zone being less porous). A typical example is 20% porosity, 15md permeability in the water zone and 10% porosity, 1-2md permeability in the gas zone.

4. The entire gas zone is gas-saturated, including every stratigraphic lens.

5. All rocks in the gas zone exceed 20 ohms resistivity.

According to Masters, the primary trapping mechanism of basin centered gas is a function of gas permeability in a water-saturated, low permeability rock. As water saturation increases, gas permeability in the water-saturated low permeability rock decreases. This permeability difference might be a result of the difference in surface tension of gas relative to that of water. Surface tension of water is significantly greater than that of gas. This enables water molecules to

become absorbed in pore walls which may lead to blocking of the pore throats (provided that the rock is water-saturated and low enough in permeability). Meteoric water flowing downdip from the edge of the basin will have a hydrostatic head behind it, contributing to the efficiency of such a water block.

Methane can be dissolved in water (Levorson, 1967). Since the water in basin-centered gas situations is continuously in motion (governed by a hydrodynamic gradient), any dissolved methane is effectively removed from the reservoir. Thus, for a sizable accumulation of gas to exist today, the rate of gas generation must be greater than the rate of gas lost through this solution in water.

Masters (1979) suggested that the primary trapping mechanism at the Wattenberg Field (lower-center area of the Greeley Landsat-4 scene) is an area of basin-centered gas. According to Matuszczak (1976), the primary trapping mechanism at Wattenberg is some type of unspecified permeability barrier, in that along the north and northeast portions of the Wattenberg Field, quartz cementation plays a contributary role. Gas in the Wattenberg Field is produced from fine sands and silts deposited in a subsidiary delta lobe rather than the main delta lobe (the Greeley lobe to the north). The main delta lobe consists of a thick sequence of delta front and delta plain deposits having relatively high permeability and porosity. Pruit's (1978) potentiometric surface map of the J sand shows a strong gradient downdip, indicating meteoric water moving downdip, along the flank of the Denver Basin. The Wattenberg Field is located over the deepest part of the Denver

Basin on a small high between the two basin deeps (one near

Denver and one near Cheyenne). The Wattenberg Field is

hydrodynamically and structurally analogous to other basin

centered gas fields such as the Milk River Field of Canada and

the San Juan Basin of New Mexico. Both these basin-centered

gas fields are located in low permeability rocks in the center

of the basin, downdip of a basin sloping potentiometric

gradient.

4.2.5 Qualitative Assessment of Thematic Mapper Imagery,

Greeley, Colorado

The TM image of the Greeley, Colorado area, image no.

40123-17052, was acquired on 16 November 1982 when large

portions of the imaged area were covered with snow. Clouds

also compounded the problem of selecting a clear subscene for

analysis. The southwest quadrant of the image provided the

best area for evaluation. The area is largely a high plains

environment, with the foothills of the folded Front Range along

the western margin. The plains at the edge of the foothills

are highly urbanized. Much of the remaining plains, which are

not too deeply buried by windblown sand, are cultivated. In

spite of the lateness in season of imagery acquisition, much of

the cultivated area exibits green vegetation.

After evaluation of various image processes on

EarthSat's GEOMAS system, the color images produced were band

combinations 1,2,3; 1,3,4 decor; 4,5,7; 7,5,4, and IHS. The

interpretability for geological information of the 4,5,7 and

7,5,4 images is substantially better than the other images, in

both mountain and plains areas. Good data quality of most of
the bands used allowed sharp, clear images to be produced.
Although cultivated areas show great variation in color, the
spectral and spatial resolution of the imagery is so good that
subtle tonal variations, indicating lineaments, are mappable.
The predominant northwest-trending pattern in the sand cover is
distinct and it is believed that these "windpatterns" have been
distinguished from the geological structure in most cases.
Structures significant to recent petroleum discoveries in this
area nearly parallel the linear sand dunes so evident in much
of the image.

An IHS image was produced for this area, but the quality
was poor and the image was not used in the analysis or produced
as a deliverable product.

The 1,2,3 image was considered to be inferior to the
4,5,7 or 7,5,4 images for structural interpretation. The
overall contrast of the natural color image is lower or more
neutral than the above mentioned images, disguising subtle
tonal differences. Also the data for both bands 1 and 2 are
noisy, thus degrading the image quality. Red beds are present
in the foothills and in localized areas. This color can be
distinguished on the natural color image.

The decor 2,3,4 image was seriously degraded by the poor
quality band 2 data that "destroyed" much of the subtle tonal
and textural detail essential for lineament analysis. However,
the red beds in the foothills are distinguishable on this image
to a greater degree than on any of the other color composites

produced, thus aiding the accurate mapping of stratigraphy and therefore, structure.

4.3. <u>Bluff, Utah</u>

4.3.1 <u>Regional Structure of the Bluff Area</u>

The Bluff, Utah area falls within the Four Corners area which includes the states of Utah, Colorado, Arizona, and New Mexico, and it is transected by the San Juan River (Figure 18).

The major exposed structural features in this area are the north-trending Comb Ridge monocline, the Raplee and Lime Ridge anticlines and the Mexican Hat syncline. All of these structural features are spectacularly exposed on the Landsat-4 Bluff scene. The Comb Ridge monocline forms the eastern structural boundary of the large north-trending Monument uplift (Figure 19; Kelley, 1979). The Monument uplift is a 75 km wide structural feature that stretches for over 150 km northward from Kayenta, Arizona to the confluence of the green and Colorado Rivers in southeastern Utah. The northeast-trending, southeast-facing Organ Rock monocline of northwestern Arizona forms the southern boundary of the Monument uplift. To the east of the Comb Ridge monocline is the Blanding Basin, a shallow structural basin about 75 km wide. The giant Aneth Field produces hydrocarbon from this basin.

Bedding exposed along the Comb Ridge monocline dips moderately to steeply eastward. The dips of bedding decrease along the length of the Comb Ridge monocline both north and south of where the San Juan River cuts through the Comb Ridge monocline. The north-trending Raplee and Lime Ridge anticlines
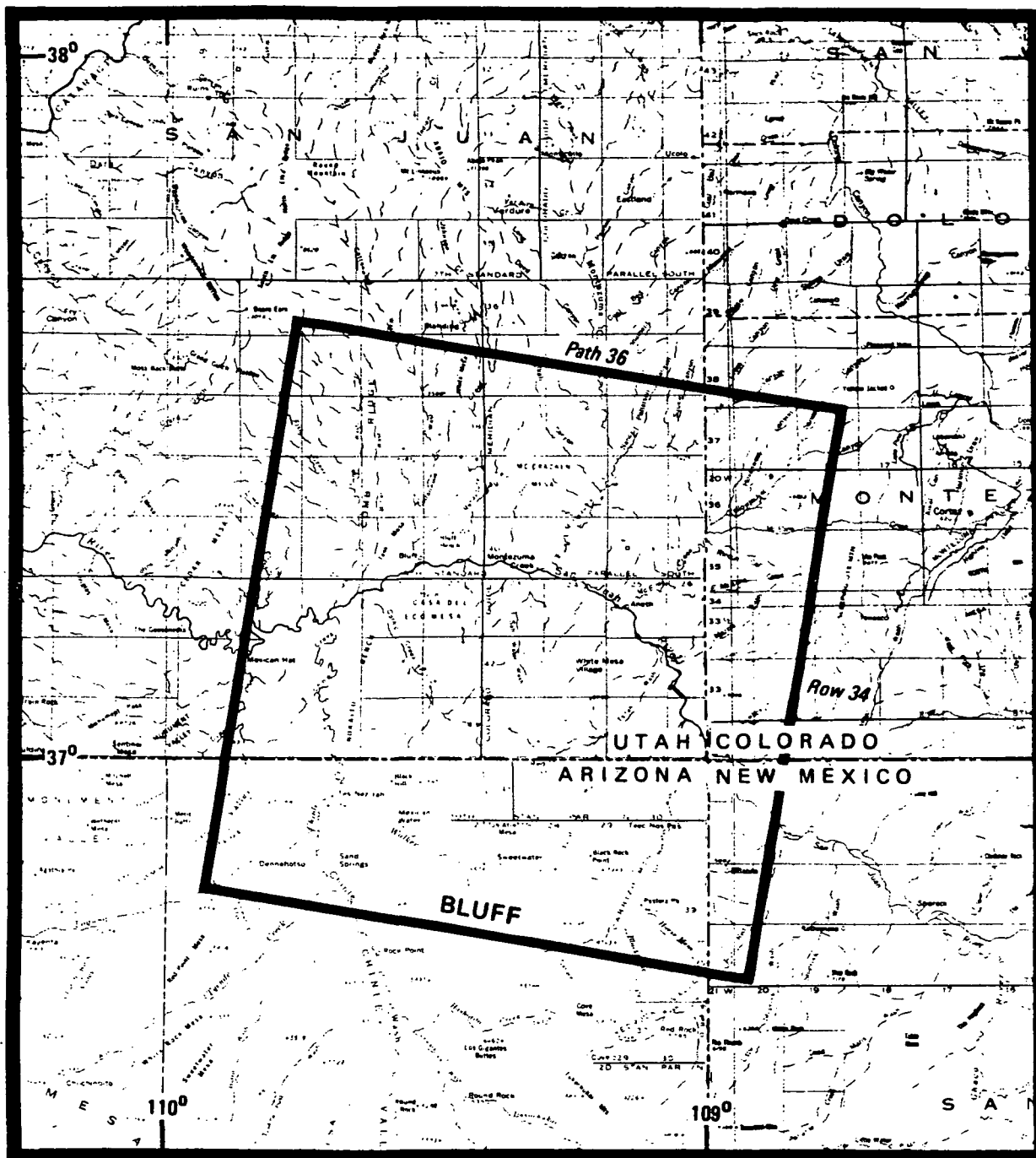
Figure 18   Bluff, Utah, location map

        Region delineated is the area covered by Landsat 4 frame 40176-17252,
8 January 1983, Path 36/Row 34. A Geologic Interpretation was
performed on this Landsat scene.

and the Mexican Hat syncline are found within the Monument
uplift or just west of the Comb Ridge monocline. The Lime
Ridge and Raplee anticlines are surface expressions of a pair
of branching anticlines. The Raplee anticline comprises the
west limb of this branching structural, whereas the Lime Ridge
anticline forms its eastern limb (O'Sullivan, 1965). The Lime
Ridge anticline is a relatively flat topped, kinked-style, fold
extending several kilometres northeast of the Raplee anticline.
The Raplee anticline is a more rounded and better exposed
structure with more closure than the Lime Ridge anticline.
Both anticlines are capped by indurated Pennsylvanian-Permian
strata of the Rico Formation. Structural contours on the top
of the Rico Formation indicate that both the Lime Ridge and
Raplee anticlines are asymmetrical structures with the steepest
limbs on the east side of the Lime Ridge anticline and the west
side of the Raplee anticline. The east limb of the Lime Ridge
anticline is continuous with steeply dipping beds of the Comb
Ridge monocline (O'Sullivan, 1965).

The Comb Ridge monocline is pervasively jointed both in
the direction of strike and perpendicular to the strike of this
ridge. Brittle subsidiary faulting is associated with both the
Raplee and Lime Ridge anticlines and the Comb Ridge monocline
(Sears, 1966). A system of steeply dipping normal faults with
minor amounts of dip-slip are found along the western side of
the Comb Ridge monocline. The Jurassic Navajo sandstone holds
up the most prominent ridge along the Comb Ridge monocline.
West of this monocline on the Monument uplift, mainly
Pennsylvanian and Permian units are exposed at the surface. In

the structurally lower area to the east, younger Cretaceous and Jurassic units are found at the surface.

There is very little surficial structure mapped within the area east of the Comb Ridge monocline where surficial units are nearly horizontal. However, a broadly plunging east-west-trending anticline has been identified along the Ismay Field by subsurface mapping supported by seismic data. Other anti-clines, too subtle to be perceived without detailed subsurface data, also exist in this region. One such fold, an east-west-trending anticline running through the northern part of the giant Aneth Field and initally identified by subsurface mapping, can be recognised on Landsat-4 imagery. Landsat-4 imagery also reveals the presence of a complex and pervasive series of both northeast and northwest-trending lineaments transecting the study area. These trends appear to have influenced production in many of the oil fields of this area. Specifically, the productive zones at the Ismay and Aneth Fields are sedimentary features which are elongate in a north-east direction. A northeast-trending basement fabric may have controlled the favorable development of reservoir facies in this area. Other folds east of the Comb Ridge monocline depicted on the interpretive overlay of the Bluff scene are derived from subsurface data of this region.

The Monument uplift is part of a family of north-trending uplifts found along the western side of the Colorado Plateau structural block (Figure 19; Kelley, 1955; Kelley and Clinton, 1960). Other important north-trending uplifts of the western Colorado Plateau include the Defiance, Circle and
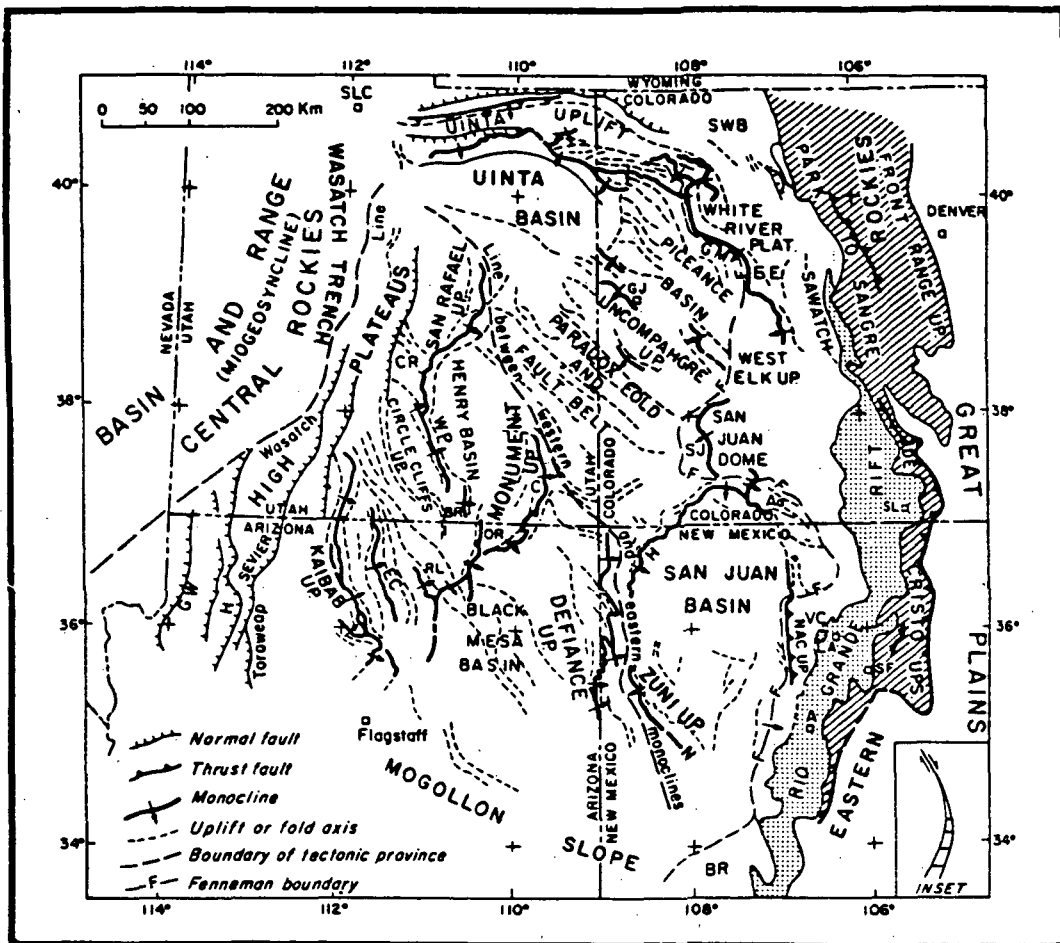
Figure 19 The Bluff Landsat 4 scene lies along the central part of the Comb Ridge monocline in Utah (diagram from Kelley, 1979).

Tectonic map of the Colorado Plateau in relationship to Central Rockies, Eastern Rockies, and Rio Grande rift. (Uplifts: NAC = Nacimiento; EE = East Elk. Monoclines: GM = Grand; SJ = San Juan; H = Hogback; N = Nutria; C = Comb Ridge; OR = Organ Rock; RL = Red Lake; EC = Echo Cliffs; and WP = Waterpocket. Fold Belts: CR = Capitol Reef; Aa = Archuleta. Faults: GW = Grand Wash; H = Hurricane. Other: VC = Valles caldera; BR = Basin and Range; SWB = San Wash basin; SLC = Salt Lake City; GJ = Grand Junction; SF = Santa Fe; SL = San Luis; A = Albuquerque.)

Kaibab uplifts (Kelley, 1979). These uplifts are commonly defined by east-facing monoclines that bound their eastern side. In contrast to this structural style are the monoclines and folds found along the eastern and northeastern portion of the Colorado Plateau where structures generally trend north to northwestward with southwest facing monoclines bounding the southwestern sides of the uplifts (Figure 19; Kelley, 1979). The northwest-trending salt-cored Paradox Fold Belt, found just to the north of the Comb Ridge study area, is part of the structural pattern of the eastern and northeastern Colorado Plateau area. Therefore, the dividing line between eastern and western structural styles of the Colorado Plateau is found between these areas (Kelley, 1979).

Monoclines and subsidiary folds are the major structural features of the Colorado Plateau. These structures are a result of horizontal compressive stress and formed above deep seated thrust faults (Kelley, 1955). A majority of the monoclines and various folds of the Colorado Plateau block are products of the Laramide orogeny. The Comb Ridge monocline and Raplee and Lime Ridge anticlines formed during the Laramide orogeny. As discussed in the Owl Creek section of this report the Laramide orogeny is a complex 2-stage orogenic event. The 2-stage nature of the Laramide orogeny has been recently recognized by Gries (1981), and Chapin and Cather (1981). This work is based on a regional synthesis of the Laramide foreland from southern New Mexico to northern Montana. However, a very similar 2-stage deformation model for formation of the Laramide monoclines and folds within the Colorado Plateau was proposed

25 years ago by Kelley and Clinton (1960). This does not

detract from the models of Gries or Chapin and Cather, but it

does show the insight in which Kelley and Clinton viewed the

structures of the Colorado Plateau areas. Kelley and Clinton

recognized that there are two dominant and very similar trends

of the major monoclinal feature of the Colorado Plateau. They

hypothesized that these two trends could be explained by

invoking two episodes of Laramide deformation, each with its

own principal horizontal compressive stress direction. An

early phase of Laramide deformation with an east-west-trending

horizontal compressive stress would have formed the north to

northeast-trending monoclines of the western half of the

Colorado Plateau. A later phase of Laramide deformation with a

northeast-trending principal horizontal compressive stress may

have formed the northwest-trending monoclines that characterize

the eastern and northeastern parts of the Colorado Plateau

(Kelley and Clinton, 1960). Northeast directed shortening of

the Colorado Plateau during the late Laramide phase of

deformation would also necessitate right-lateral, strike-slip

deformation between the eastern edge of the Colorado Plateau

and the southern Rockies of Colorado and New Mexico (Kelley,

1955, 1979; Chapin and Cather, 1981). This 2-stage

evolutionary model of Laramide structures would also explain

the more sinuous nature of the early formed north to

northeast-trending monoclines of the western Colorado Plateau

such as the southern Comb Ridge, Hogback, and Defiance

monoclines (Figure 19; Kelley and Clinton, 1960). The

sinuosity of the early formed north to northeast-trending

monoclines may have resulted from re-deformation of these structures during late Laramide compression. This would have occurred because late Laramide compression was directed towards the northeast or nearly parallel to the strike of many of the early formed monoclines. This would have refolded the northeast-trending monoclines along northwest-trending flexures resulting in sinuosity in the trends of the early formed monoclines (Kelley and Clinton, 1960).

4.3.2 Stratigraphy

The area covered by the Landsat-4 Bluff scene contains surficial exposures of rocks that range in age from the Pennsylvanian to Recent. The stratigraphy is complicated by complex lateral variations in several formations in both lithology and thickness (Sears, 1956). Separation of certain units (such as the Cutler Formation) into several intertonguing members further complicates the stratigraphy.

The Devonian rocks of this region consist of shelf carbonates deposited east of the Cordilleran Hingeline. These units include the McCracken Sandstone, the Elbert Formation and the Ouray Limestone. These rocks were deposited on a relatively shallow but extensive marine shelf with partly restricted bays.

Mississippian rocks of the Four Corners area are shelf carbonates of the Leadville Formations deposited in a shallow northwest-trending trough. Northwest tilting of the region in Late Mississippian time caused considerable erosion of Mississippian strata. Erosion resulted in the thinning of the

section to the southeast and the development of karst topo-
graphy throughout the upper member of the Mississippian Lead-
ville Formation.

The Pennsylvanian section consists of mainly evaporites
with interbedded carbonates and arkosic sandstones. Shelf
carbonates (Hermosa Group) contain several facies favorable to
hydrocarbon accumulation, specifically porous algal bioherms,
leached oolitic and bioclastic limestones, and fine-grained
dolomite beds with secondary porosity. The Cutler Group
consists of conglomerate, red arkose, and red and green shale
with minor amounts of carbonate and black shale. The evaporite
sequence of the Paradox Formation of the Hermosa Group is
composed of salt and andyrite with a depositional thickness of
1,524-1,829 m.

The Permian section contains complex interfingering
continental red beds, dune, beach and littoral sandstones and
marine shales, carbonates and anhydrite. The Permian section
in the Bluff area consists mainly of limestones deposited in an
extensive, shallow Permian Sea such as the Cutler Group, the
DeChelly Sandstone and the Kaibab Formation.

The Moenkopi Formation is the basal member of the
Triassic System and gradationally overlies the Permian
sediments. The Moenkopi Formation consists of dark brown
interbedded shales and sandstones. Overlying the Moenkopi
Formation is the Upper Triassic Chinle Formation. Although
some authors (O' Sullivan, 1965) have subdivided the Chinle
into as many as six members, Sears' (1956) maps of the Chinle
Formation display distinct lithologic variability.

Within the study area, the Chinle Formation commonly consists of red, brown, and gray sandstones interbedded with shales. The shales are variously colored and lenticular, appearing pale blue, light greenish gray, or pale red. The shales may include whitish accumulations of gypsum. Above the Chinle Formation is the Wingate Sandstone. The Wingate Formation is a massive cliff forming orange-red sandstone which is characterized by large-scale cross-bedding. The Wingate Sandstone is one of the most conspicuous cliff forming units in the entire study area. In the cliffs, the Wingate displays pervasive vertical joints allowing huge blocks to spaul from the cliff and litter the slopes of the Chinle Formation below.

The Kayenta Formation is the oldest member of the Lower Jurassic System. The Kayenta is well-exposed along Comb Ridge. The Kayenta is distinguished from the underlying, massive Wingate Sandstone and the overlying massive Navajo Sandstone as a thin, irregularly bedded, alternating sandstone, siltstone, limestone, and shale sequence. The Navajo Formation is the upper member of the Lower Jurassic System. The unit is composed of grayish-orange, fine grained quartz sandstones. The large-scale cross-bedding is very evident in outcrop. Navajo Formation comprises most of the east slope of Comb Ridge. The Carmel Formation overlies the Navajo and is placed in the Middle Jurassic System. The Carmel Formation consists of alternating clays, mudstones, and sandstones. Its overall aspect is that of soft, easily weathered red beds. Upper Jurassic Entrada Sandstone conformably overlies the Carmel Formation. The Entrada is divided into an upper and lower

member which are lithologically distinct (Sears, 1956). The
lower unit is a resistant ledge forming gray to buff sandstone.
The upper member of the Entrada is comprised of thin bedded red
shaly sandstones.

The Summerville Formation is another Jurassic unit that
overlies the Entrada Formation and is composed of an assemblage
of gray, brown, and tan thin-bedded sandstones, siltstones and
shaly beds. The Upper Jurassic Bluff Sandstone overlies the
Summerville Formation. The Bluff Formation is a thick, gray,
massive sandstone composed of fine, rounded grains of quartz
with minor amounts of feldspar, chert, and dark accessory
minerals (O'Sullivan, 1965). Large-scale, high-angle, sweeping
cross-beds dip east and northeast in the study area, and are
particularly prominent in the upper Bluff horizons (O'Sullivan,
1965). The Bluff Formation forms prominent cliffs in the
eastern part of the study area.

The Morrison Formation overlies the Bluff Sandstone.
The Upper Jurassic Morrison Formation is divided into two
members, the Salt Wash Member and the Brushy Basin Member.
Both units of the Morrison Formation are highly varied with
respect to lithology color, texture, and bedding relations.
The Salt Wash Member forms thick resistant ledges of yellow,
gray, buff, and rusty red sandstone. Salt Wash Sandstone beds
contain interbedded red shales and mudstones with thin local
lenses of dense gray limestone present. The Brushy Basin
Member of the Morrison Formation overlies the Salt Wash Member
and consists primarily of variously colored bentonitic shales
and mudstones with intercalated beds of conglomeratic sandstone

and limestone. The basal unit of the Cretaceous Series is the Burro Canyon Formation. The unit consists of alternating conglomeratic sandstones separated by variegated mudstones with sparse beds of chert and limestone.

4.3.3 Hydrocarbon Potential of the Bluff Region

Prolific amounts of hydrocarbon have been produced within this study area. Approximately 400 million barrels of oil reserves are found within the confines of the Bluff Landsat-4 scene. Over half of this oil is found in the giant Aneth Field, the largest oil field in the southern Rocky Mountain region.

Multiple reservoir and source rock horizons are present in the Blanding Basin area. Known producing reservoir rocks include: the porous sand bars of the Devonian McCracken Sand; the porous dolomitized crinoid biomicrite bank deposits of the Mississippian Leadville; the porous carbonate mound deposits of the Pennsylvanian Paradox Formation; the tight (fracture induced porosity and permeability) Cane Creek black shale member of the Paradox Formation; and porous clastics of the Honaker Trail (Upper Pennsylvanian) and Cutler (Permian) Formations. Potential reservoir rocks include porous Chaetetid coral beds of the Paradox Formation and black shale members of the Paradox Formation. These potential reservoir rocks will probably require natural fracture induced porosity and permeability to be significant reservoirs. Source rocks include regionally extensive black shale (8-15% organic carbon, Hite

and Buckner, 1981) members of the Paradox Formation and the black shale of the Devonian Aneth Formation.

The hydrocarbon potential of this area is governed by the tectonic activity coupled with the contemporaneous depositional history. The four major plays are: winnowed porous clastic sediments (McCracken Sand) or porous crinoid bank deposits (Mississippian Leadville) localized along paleotectonic highs present in the Devonian and/or Mississippian Sea; oolitic and/or algal carbonate buildups (Paradox Formation) localized on paleotectonic highs present in the Pennsylvanian Sea; wedgeouts of porous clastic Upper Pennsylvanian (Honaker Trail) and Permian (Cutler) sediments against deformed salt walls; and fracture induced porosity and permeability of the black shale member(s) of the Paradox Formation. Some of these plays are clearly interrelated to one another in both time and in space.

Numerous hydrocarbon seeps, or evidence of seeps, have been reported to occur within this area. Wengerd (1973) reported that numerous oil seeps occur near the town of Mexican Hat and facilitated the discovery of the Mexican Hat oil field. Baars (1973) reported that oil seeps from the White Rim Member of the Cutler Formation along the northwest edge of the Monument Uplift.

Production from the Hermosa Group occurs in the Aneth, Ismay, Desert Creek, and North Boundary Butte fields and accounts for the majority of the oil produced in this area. The interrelationship between the cyclically deposited marine carbonate reservoirs and organic rich hydrocarbon source beds

in the Paradox Formation makes this formation an excellent

hydrocarbon production horizon. Peterson and Hite (1969) point

out the excellent preservation of organic matter under saline

conditions, and measurements by Hite show that the black marine

shales of the Paradox Formation (the major source rocks)

average 8-9 percent by weight organic carbon. The ubiquity of

hydrocarbons in the Pennsylvanian section is demonstrated by

the fact that almost every well that has penetrated the section

reveals at least shows of oil and/or gas.

The bathymetry of the Pennsylvanian seafloor of the

Paradox region was governed by the geographic distribution and

relative displacement of paleotectonic features (Elias, 1963;

Peterson and Ohlen, 1963; Peterson and Hite, 1969). Because

the sea was relatively shallow, these features controlled the

distribution and thickness of facies. Carbonate mounds,

comprised of significant quantities of bioclastic debris,

accumulated on slightly elevated highs in the shallow regions

of the basin. Micrite, dolomite, anhydrite, and black shale

accumulated between these highs, and evaporate deposition was

largely confined to the deeper portions of the basin. The

carbonate mounds of the Paradox Basin contain excellent

reservoirs that produce hydrocarbons in numerous localities

(e.g., Aneth and Ismay Fields). These mounds are primarily

leached algal or oolitic micrite carbonate buildups that were

apparently localized along paleotectonic features.

Northwest-trending paleotectonic features (Szabo and

Wengerd, 1975) crosscut by northeast-trending paleotectonic

features (Hite, 1975) were apparently responsible for governing

the bathymetry of the Pennsylvanian seafloor and thus, the distribution of carbonate mounds. Carbonate mounds occur along broad northwest-trending zones that stretch across the basin.

The Pennsylvanian carbonate mounds of this region are confined to the Paradox Formation, which consists of a cyclicly deposited suite of carbonate, evaporate, and clastic sediments. These three laterally equivalent facies of the Paradox Formation differ in geographic extent within the Paradox Basin. The thickest and most areally extensive carbonate mounds (and mound related reservoir rocks) are present in the Desert Creek and Ismay Members of the Paradox Formation. The preferred location of the mounds appears to be along northwest-trending structural features.

The carbonate mounds of the Paradox Formation are lens shaped buildups, primarily composed of partially dolomitized carbonate mud with a locally abundant oolitic and bioclastic debris. The bioclastic debris predominately consists of phylloid algae (Ivanovia) plus lesser quantities of fusulinids, coral, crinoids, and brachiopods. The typical reservoir consists of porous, partially dolomitized, leached algal and oolitic micrite. These rocks may be interbedded with micrite or bioclastic micrite marked by desiccation cracks (Martin, 1981; Krivanek, 1981). The apparent thickening of the mounds is principally caused by the vertical stacking of algal or oolitic carbonates separated by intervals of micrite, pellet or biomicrite (Ball et al., 1977; Mazzullo, 1982). In several localities, the mounds are vertically stacked providing multiple producing horizons (e.g., Aneth Field, Peterson,

1966). The largest mound, Aneth, is about two hundred feet thick and comprised of about one hundred feet of leached oolite overlying about one hundred feet of algal carbonate of the Upper Desert Creek Member (Peterson, 1966). More typically, carbonate mounds may be several tens of feet thick and a few square miles in area, such as the Bug Field (Krivanek, 1981).

The distribution of mounds appears to have been governed by paleotectonic features that controlled bathymetry and, in addition, it appears that bathymetry had a significant influence on the diagenetic processes that lead to the development of reservoir porosity. The carbonate mounds were bathymetrically higher than the surrounding seafloor and were deposited in subtidal environments that underwent periodic episodes of intertidal to supratidal exposure (e.g., mounds contain limestones marked by desiccation cracks; Martin, 1981; Krivanek, 1981). This means that leaching of aragonite grains (i.e., oolite, Ivanovia debris) and lithification and local dolomitization of the largely micrite mounds occurred during these periods of exposure when meteoric water migrated through the mound. Because these aragonite grains were coated with calcite micrite envelopes, open molds of micrite envelopes of the former aragonite grains were produced during leaching by meteoric water. Additionally in places, dolomitization of carbonate mud and leaching of carbonate grains occurred to produce a very porous and partially dolomitized micrite. The result is a reservoir quality, partially dolomitized, porous and permeable algal or oolitic micrite in which the porosity is

principally comprised of molds of what were formerly aragonite grains swimming in a matrix of micrite.

The best method to explore for carbonate mounds is to map those paleotectonic features that governed the bathymetry of the Pennsylvanian seafloor. The regionally extensive northwest-trending paleotectonic features mapped by Baars (1966) and Wengerd (1973) appear to have governed the basinwide distribution of mounds, whereas the northeast-trends (Hite, 1975) appear to have governed the shape and local limits of individual mounds. Most of the individual mounds appear to be elongated in a northwest direction and are abruptly terminated by northeast-trends (Peterson and Hite, 1969; Elias, 1963). In places where drilling has been dense (e.g., the Ismay Field) isopach data of some mounds show that the individual thicks or "pods" within the field are aligned northeast whereas, the overall trend of the individual fields are northwest (Elias, 1963; Reid and Berghorn, 1981). This suggests that the northeast-trends play a significant role, locally, in defining the occurrence and shape of the mounds.

Szabo and Wengerd (1975) suggested that contemporaneous structural growth had a significant impact on the regional distribution of Paradox facies during the Pennsylvanian. According to their model, the subsidence of the Paradox basin during the deposition of the evaporite-carbonate facies took place along a series of northwest-trending faults that were initially sites of monoclinal folding. Movement along these faults was intermittent, with the oldest and largest faults occurring nearest the center of the basin. These northwest-

trending faults of Szabo and Wengerd (1975) are depicted on the overlay of the Bluff scene as the Aneth flex axis, Aneth line and the Boundary Battle line. These faults were active during deposition of the carbonate mounds and served to localize deposition of these mounds.

Landsat-4 imagery can be used to delineate and precisely locate these northwest-trending faults that define the basement blocks along which carbonate mounds developed. Examination of this imagery also shows numerous crosscutting northeast-trending fractures which appear to be important in defining the local limits of the mounds. Examination of the Landsat-4 interpretation of the Bluff scene illustrates the dominant pattern of crosscutting northeast and northwest-trending linear features identified in this area. In the eastern part of the Bluff image, the control of topography by northeast-trending fractures is quite prominent. Control of topography by the northwest-trending linears is most distinct along the northern half of the Bluff scene. Defining the location of these two sets of linear features is a critical factor in hydrocarbon exploration in this region. Not only do the linears define local limits of the hydrocarbon-bearing carbonate mounds but they delineate fracture systems that may have induced secondary porosity and permeability in the hydrocarbon-rich stratigraphic section.

Fractures can provide sufficient permeability to facilitate production of hydrocarbons from otherwise tight rocks. Several fracture porosity fields (e.g., Long Canyon, Verde) are present just outside the project area. Fractures

provide permeability which enhance production in numerous other fields within the Blanding Basin (Fassett et al., 1978). Traps formed by fracture induced porosity and permeability in otherwise tight reservoir rocks will be expressed on Landsat-4 imagery as areas of high lineament density. An approximation of the geometry of such a trap can be derived because the linear features seen at the surface are often a good approximation of subsurface trends.

4.3.4 Qualitative Assessment of Thematic Mapper Imagery, Bluff, Utah

After an evaluation of the various image processing techniques on the interactive system, the Bluff, Utah Landsat-4 TM scene 40176-17252 was processed in the following band combinations: 1,2,3; 1,4,5; 1,5,7; Principle Component 1,2,3; and IHS. For this IHS scene, we used Eigenband 1 for the Intensity, Eigenband 2 for the Hue, and Eigenband 3 for the Saturation.

The quality of the Landsat-4 Bluff scene is superior to the Greeley and Owl Creek Landsat-4 scenes in the sharpness of the hard copy picture and in the resolution of fine details. This is most likely due to better atmospheric conditions during data acquisition even though there is·a scattered, thin cirrus cloud cover. This area is sparsely populated and therefore uncluttered by agricultural or urban features and minimally affected by atmospheric pollution.

TM 1,2,3 and 1,4,5 scenes are both excellent images for mapping geologic features such as bedding, lineaments, and

tonal anomalies. The 1,4,5 scene is slightly better than the 1,2,3 scene because of its sharper picture quality. Also, the 1,4,5 image has slightly more contrast, giving the illusion of "deeper" topography which is a great aid in mapping linear features. There is also a wider variety of colors in the 1,4,5 scene, making bedding and tonal anomalies somewhat more prominent and visible. Topographic details of snow-covered areas such as the Carizzo Mountains are also better on the 1,4,5 scene than the 1,2,3 scene   The 1,5,7 scene presents more color combinations and therefore highlights in more detail the stratigraphy of the region. This is best seen in the east dipping shaley units between the Lime Ridge anticline and Comb Ridge monocline where more purple and green tints of the 1,5,7 image more clearly highlight the bedding. In summary, the 1,2,3; 1,4,5 and 1,5,7 scenes are all excellent in quality, but the 1,4,5 and 1,5,7 scenes are slightly better in overall spatial and spectral resolution.

The Eigen 1,2,3 and IHS images are markedly different in appearance from the above mentioned images and exhibit somewhat "wild-colored" depictions of the Landsat-4 data. However, from a geologic point of view, these images provide a better picture of the more regional (scene-wide) linear features. The 1,4,5 scene tends to obscure regional linear features by "breaking" them into a series of detached shorter linear segments. It is more difficult for the human eye to integrate these short linear segments into the regional pattern. This problem is best resolved with the Eigen 1,2,3 image. This is best illustrated by comparing the northeast portion of the 1,4,5 and

the Eigen 1,2,3 images. Northwest-trending regional lineaments are clearly visible on the Eigen 1,2,3 image. The sharp detail on the 1,4,5 image clearly shows the individual lineaments that compose the regional linear feature, but it is more difficult to readily see the regional trend. On the IHS image, northwest- and northeast-trending regional lineaments are best displayed in the southeastern section of the image. Again, the same regional lineaments are difficult to see on the 1,4,5 image.

The TM 6 thermal scene is a black-and-white image that lacks the spatial resolution of the other processed TM images. However, it delineates some regional linears that are difficult to observe even on the Eigen 1,2,3. The most notable regional lineament is a west-northwest-trending feature found in the lower half of the image. This lineament can be readily seen on the TM 6 image as extending across the northern part of Carizzo Mountain westward through the Comb Ridge monocline and along the southern terminus of the Raplee anticline. This lineament is only partly visible on the Eigen 1,2,3 and 1,4,5 scenes. A second northeast-trending linear feature cutting through the center of the Raplee anticline and across the Comb Ridge monocline is easily seen on TM 6 but difficult to distinguish on the other TM scenes.

4.4 Cement/Velma, Oklahoma

4.4.1 Introduction

Surface expressions of oil and gas seepage from sub-surface petroleum reservoirs have long been used in exploration for hydrocarbons. Prior to the twentieth century, most commercial oil accumulations were discovered from surface discharges of oils which indicated the presence of subsurface oil reservoirs. Recently, however, attention has turned to geochemical, geobotanical, and radiometric techniques designed to reveal alteration of surface rocks that can be attributed to trace amounts of hydrocarbon leakage from underlying reserves of oil and gas.

Techniques that sense diagenetic alteration phenomena are a type of direct detection, unlike indirect exploration methods that seek to relate favorable structure or stratigraphy to hypothesized zones of petroleum production. What the direct methods "see" are the physical, geochemical, and geobotanical effects of hydrocarbons on the surface environment. Methods of direct detection are increasingly providing low cost alternatives to conventional structural and stratigraphic exploration techniques. In particular, direct detection methods are valuable in development of exploration target areas, thus eliminating many non-prospective lands from consideration and narrowing the area where expensive and intensive indirect exploration efforts should be applied. In addition, direct detection methods may provide evidence of stratigraphic traps which indirect techniques commonly fail to discern (Duchscherer, 1980).

Evidence of hydrocarbon leakage may include a suite of closely interrelated geomorphic, chemical, and mineralogical, anomalies, and magnetic, radiation, and related physical anomalies. Additionally, since plant physiology is strongly affected by soil chemistry, alterations of the soil can have geobotanical consequences. Any one or combination of these anomalies may be detected by remotely sensed data in the appropriate exploration environment. Research into direct detection of reliable signatures caused by alteration phenomena is the forefront of remote sensing in oil and gas exploration.

The Cement Field of Caddo and Grady Counties and the Velma Field of Stephens County in southwestern Oklahoma are well documented examples of hydrocarbon induced diagenetic alteration. The locations of these field are shown in Figure 20. A suite of surface and shallow subsurface anomalies provides abundant evidence for hydrocarbon induced alteration at both fields; however, the Cement Field has received more attention than the Velma Field in the literature concerning late diagenetic alteration in the Anadarko Basin.

The various hydrocarbon induced mineralogical anomalies present in the study area are chemically and physically measurable and many authors have related these anomalies to stratigraphic and structural controls on the distribution of oil and gas reserves. Abundant subsurface data revealed during the sixty year history of oil field development have contributed to increasing understanding of the mechanisms and geological controls on the phenomenon of hydrocarbon induced alteration at Cement and Velma.
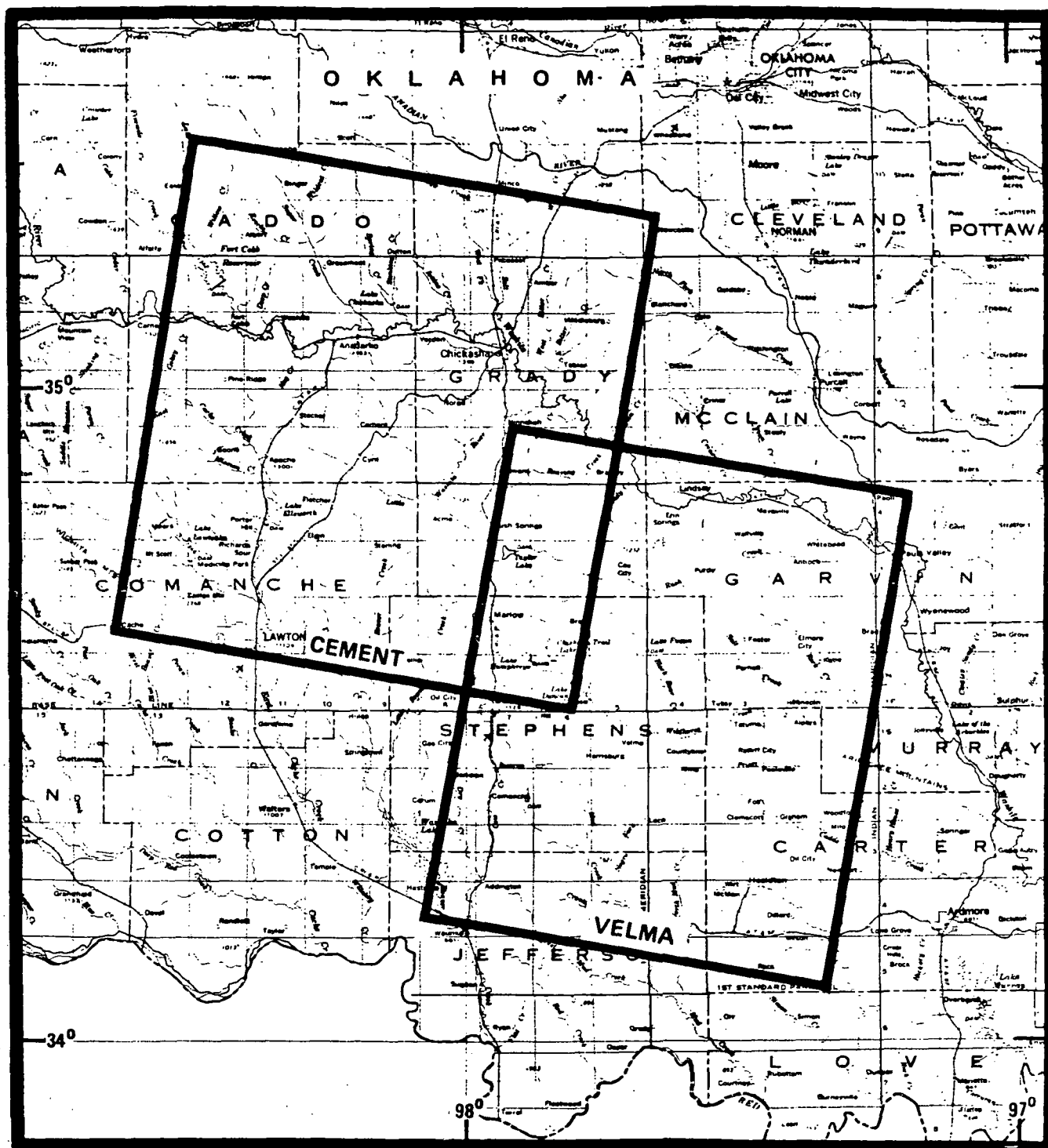
Figure 20   Cement, Oklahoma, and Velma, Oklahoma, location map

Regions delineated are portions of the area covered by Landsat 4
frame 40136-16362, 29 November 1982, Path 28/Row 36. Geologic
interpretations were performed on these scenes.

The alteration of surface materials is attributed to the effects of vertical leakage of hydrocarbons (Donovan, 1972, 1974; Donovan and Dalziel, 1977; Donovan et al., 1974, 1981, 1979a, 1979b, 1979c; Al-Shaieb et al., 1982; Lilburn and Al-Shaieb, 1983). A brief discussion of the phenomenon of vertical migration is discussed in Section 4.4.3. Following that will be discussions of the regional tectonic history of the Anadarko Basin, the structure and stratigraphy of the Cement and Velma anticlines, and descriptions of alteration anomalies and the causative mechanisms of the alterations documented at the Cement and Velma oil fields.

4.4.2 Hydrocarbon Potential of the Cement/Velma Area of the Anadarko Basin

The Cement and Velma Fields are located at the extreme southeast end of the Anadarko Basin, an area of prolific oil production. Both fields are structurally controlled but lie on different, though genetically related, fault systems. The Cement Field has produced nearly 150,000,000 barrels of oil since discovery. The Sho-Vel-Tum Field, to which the Velma Field is connected, was discovered in 1914 and has produced nearly a billion barrels of oil. Numerous significant fields lie within the area covered by the TM imagery. The Chickasha Field, to the immediate southeast of Cement, is a large producer, as is the Knox Field north of Velma and the Sho-Vel-Tum Field. The Golden Trend Field, on the east shelf of the Anadarko Basin, is an agglomeration of smaller fields that have probably produced a half billion barrels of oil.

Although most of the major fields had been discovered by 1950, numerous smaller fields have been, and are continuing to be, discovered. The Paleozoic structure is complex, making exploration difficult but, properly used, the insights concerning structure derived from the interpretation of the TM imagery should be of great value in directing further exploration in the area.

4.4.3 Hydrocarbon Leakage

A hydrocarbon trap is a dynamic membrane that processes fluids, permitting aqueous fluids to leak, while inhibiting the flow of hydrocarbons (Roberts, 1980). The current state of knowledge concerning petroleum entrapment suggests that most petroleum reservoirs leak, allowing upward seepage of hydrocarbon fluids.

There are three principal mechanisms of hydrocarbon seepage from oil and gas fields (Hunt, 1979; Donovan and Dalziel, 1977, and Donovan, 1981). The first of the mechanisms is effusion of hydrocarbons, usually occurring as macroseepage of large quantities of oil and gas through inadequately compacted roofrocks and along fractures and faults. Examples of effusive hydrocarbon leakage from a thrust fault and through permeable roofrocks are present at Cement (Donovan, 1974, Henry and Donovan, 1978). Joint controlled leakage is an effusion mechanism suggested by Al-Shaieb et al. (1982) to be contributing to anomalous uranium mineralization at Cement. Faulting along the edges of horst and graben blocks is an important contributor to vertical permeability at the Velma Field (Ferguson, 1979).

The second mechanism cited by Donovan and Dalziel (1977) is solution of hydrocarbons. Typically the low molecular weight fractions or "light ends" are dissolved in small amounts in meteoric water or in clay interlayer groundwater. Circulating groundwaters are subject to field potential gradients which may not necessarily apply to in situ hydrocarbons. Under the influence of a variety of field gradients, circulating groundwater may transport its load of dissolved hydrocarbons away from the petroleum reservoir. Common field potentials which can effect transport include hydrodynamic head pressure, pressures caused by differential compaction of deep sediments during basin maturation, or pressure gradients caused by differences in chemical activity (such as osmotic imbalance) on opposite sides of clay beds (Henry and Donovan, 1978).

In most groundwater leakage mechanisms, the direction and rate of flow are principally functions of hydrostatic pressure gradients. Typically, the vertical hydrodynamic pressure gradient is stronger than the horizontal gradient, thus imparting upward pressure on hydrocarbon migration (Davidson, 1982). It appears that situations where hydrocarbons migrate in solution in a direction significantly different from vertical are extremely unlikely in the absence of effusion through structurally controlled pathways.

Donovan and Dalziel (1977) cite evidence that osmotic drive is an important mechanism for hydrocarbon leakage at Cement. The osmotic drive is a result of a chemical imbalance which is itself strongly dependent on relative salinities of the interstitial formation waters. Increased salinity decreases hydrocarbon solubility as follows: In the range of lower salinities, a gradual reduction in solubility begins at around 25,000 ppm of NaCl.

-117-

Formation water salinities of around 150,000 ppm of NaCl effect a significant exsolution of previously dissolved hydrocarbons, and a salinity of 350,000 ppm of NaCl is sufficient to cause a 95% reduction in hydrocarbon solubility (Henry and Donovan, 1978). Although the quantitative relations between hydrocarbon solubility and salinity may vary with different types of hydrocarbon and different salts present in the formation waters, the concept of salinity driven transport is valid in many hydrocarbon solubility mechanisms.

If saline formation water either is diluted, passed through a filtering shale bed, or otherwise desalted, drastic dissolution of hydrocarbon may result (Henry and Donovan, 1978). At Cement, osmotic drive caused by the high salinity of formation waters at depth and the lower salinity of shallower waters is a potential gradient which forces water upward through the sedimentary column. As the saline waters pass through intervening shale layers, they are physically desalted by micropore filtration. The lower salinity migrating waters then dissolve hydrocarbons which are present in the shales or in superjacent formations and transport the hydrocarbons upward in response to potential gradients. A corollary to this phenonomenon is that an increase in salinity of any rock unit in the sedimentary column saturated with gaseous hydrocarbon, such as a hydrocarbon generating shale body, will decrease the solubility of gas in that body and force it into the newly desalted waters (MacElvain, 1963, 1969). Thus, shale micropore filtration may decrease the salinity of the circulating waters, while increasing the tendency of gaseous hydrocarbons to migrate. Isotopic evidence supports Donovan's (1981) contention that some of the mineralogical

anomalies observed at Cement are the result of osmotically driven
(salinity controlled) solubility leakage of hydrocarbons.

The third mechanism of hydrocarbon seepage is that of gaseous
diffusion of hydrocarbon in an acqueous water phase (Donovan and
Dalziel, 1977). MacElvain (1969) states that methane in water is an
inert gas which behaves as individual molecules of methane--not as
bubbles of methane. Thus methane will move in response to concen-
tration gradients in the direction of least concentration. In
hydrocarbon generating environments, concentration gradients
generally favor upward diffusion. Gaseous diffusion may occur at
geologically significant rates (MacElvain, 1969) and is probably
independent of the pore size of the containing rock. However, as
upward diffusion occurs, the gas expands 0.6 m laterally for every
foot of vertical ascent. The upward expanding gas acts as an
evaporating agent for formation waters. Thermodynamically, The
amount of water vapor in expanding gas increases rapidly at depths
of less than 1,000 feet. Thus, upward diffusion and dissolution of
formation waters can be expected to result in concentration of
residual minerals in shallow portions of the anticline or along
preferred migration pathways where subsurface to surface communi-
cation of expanding gas is least impeded (Donovan, 1974; Nisle,
1941). However, upward diffusion is physically a dispersing or
diluting phenomenon which cannot alone account for concentrated
effects of surface seepage such as those observed at Cement.

The mechanisms of hydrocarbon leakage are complex and inter-
related with a variety of subsurface chemical and physical factors.
Understanding which mechanisms are dominant in a specific
exploration setting is crucial to the successful characterization of

hydrocarbon leakage phenomena. Isotopic evidence, together with geochemistry and conventional geologic insights, provide the tools necessary to unravel the genetic controls on hydrocarbon induced alteration phenomena.

4.4.3.1 Hydrocarbon Induced Diagenetic Alteration

While there are a variety of diverse manifestations of hydrocarbon induced alteration, many anomalies are directly attributed to an essential pattern. Leaking hydrocarbons and associated reductants such as hydrogen sulfide produce a reducing environment, thereby initiating late diagenetic Eh/pH controlled reactions in the rocks and soil above hydrocarbon accumulations. These chemical reactions cause mobilization or precipitation of minerals present in the stratigraphic column above the leaking reservoir. Mineralogic changes may, in turn, promote geomorphic or physical alteration of the surface and near surface projections of the hydrocarbon reservoir.

The central zone of alteration attributed to hydrocarbon seepage is commonly known as the "alteration chimney". In many places, the alteration chimney is surrounded by a "halo" of geo-chemical influences that also are genetically related to the alteration and leakage phenomenon (Duchscherer, 1982). A distinction is made between the chimney and halo, since they may represent dual expressions of hydrocarbon induced alteration which are seemingly contradictory (such as a radiation low surrounded by a radiation high). The chimney and halo together comprise the alteration "aureole". A schematic diagram of a geochemical aureole is shown in Figure 21. The geometric configuration of the
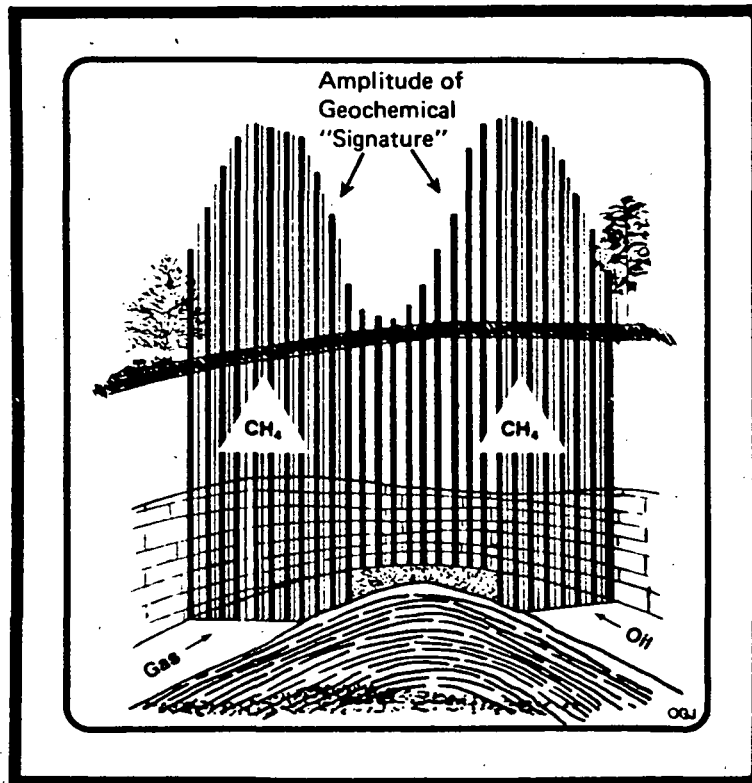
Figure 21   Schematic diagram of a Geochemical Aureole
             (from Duchscherer, 1982)

alteration aureole, however, may be complicated by faulting,
structural aspects of the trapping mechanism, and the chemical
nature of the rocks and minerals that comprise the overlying
strata.

Many of the alteration effects in the aureole are
discernible as remotely sensed spectral, textural, geobotanical, or
topographical anomalies. Moreover, integration of observed effects
with laboratory geochemical analysis and other techniques may allow
the determination of a specific mechanism of alteration which can
reveal aspects of subsurface geology.

4.4.4 <u>Regional Structure of Southern Oklahoma</u>

Present day structural configuration of Southern
Oklahoma is the result of several major documentable
deformation episodes that have sequentially left their imprint
on the area (Figure 22). The earliest of these was a
Precambrian-early Cambrian extensional event that seems to have
set the stage for subsequent deformation with regard to
important directions that were later reactivated and along
which major structures formed. The Precambrian-Cambrian
extensional event was a rifting episode related to the
formation of a triple junction immediately southeast of present
day southern Oklahoma. The area that we now know as the
Anadarko, Ardmore, and Marietta Basins occupy the site of the
northwest arm of the triple junction (Figure 23). This arm
failed to develop fully as a rift, although thinning of the
continental crust and intrusive and extrusive rocks are
evidence of the beginning stages of rift formation. The other
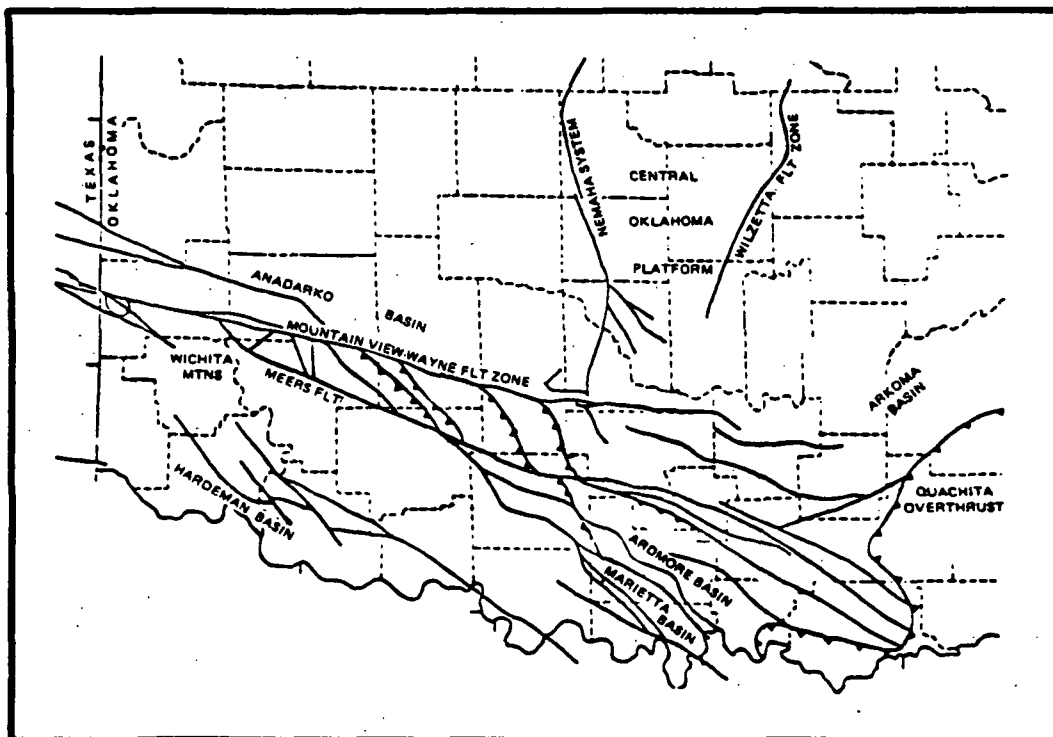
Figure 22   Regional structure of southern Oklahoma
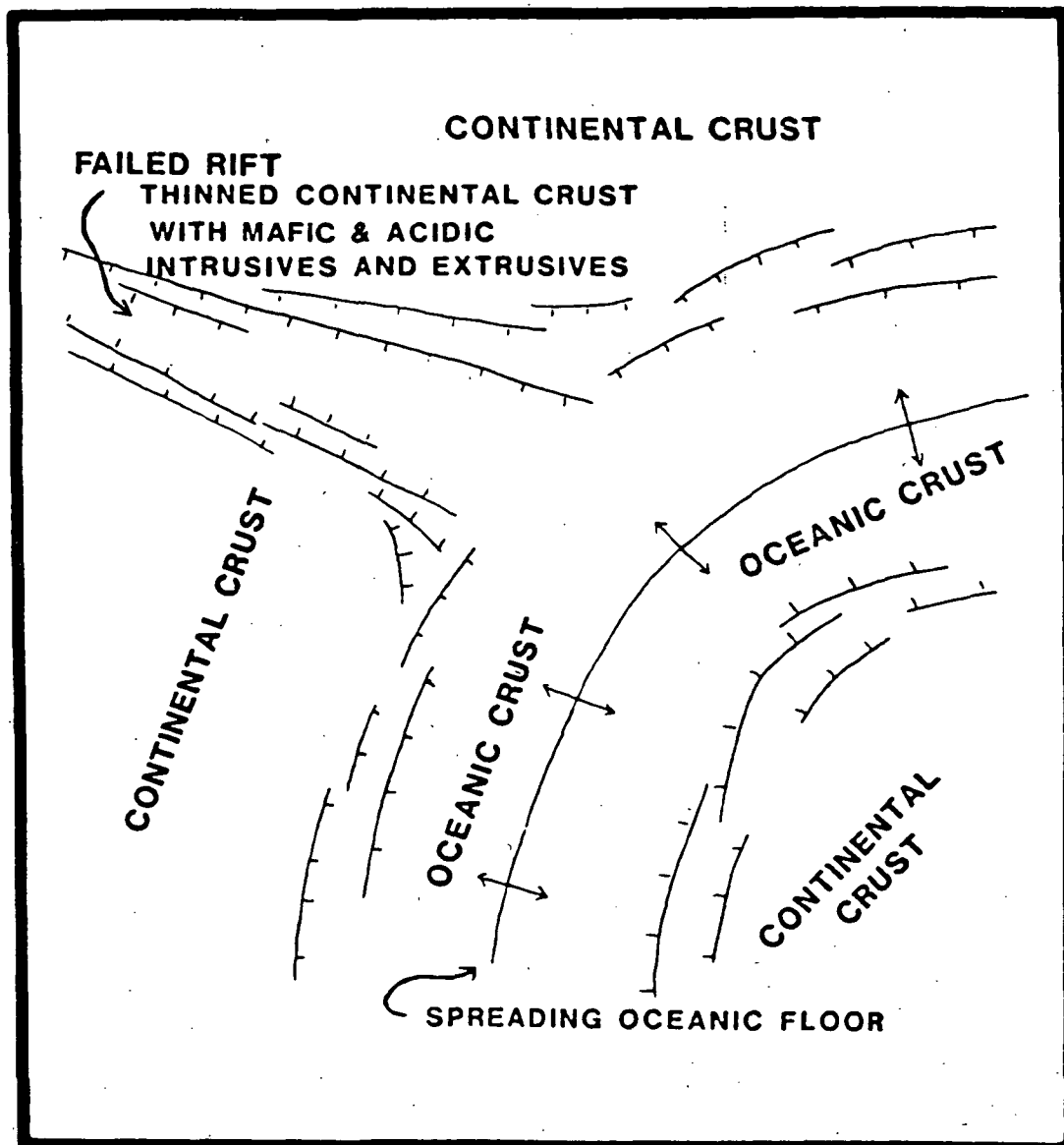(modified from Axtmann, 1983)

Figure 23   Diagrammatic sketch of the triple junction that formed
            the Anadarko Aulacogen (from Axtmann, 1983)

124

two arms continued as rifts and continental crust was separated

from present day southeastern Oklahoma by newly formed oceanic

crustal material. Subsidence continued in the failed arm of

the triple junction and a deep basin began to form with cooling

of mafic materials and continued extension. Deposition of the

Cambrian Reagan Sandstone ensued from erosion and redeposition

of the granites and rhyolites. Subsidence continued through

the Cambrian and Ordovician and shallow water deposition

typified the region during this time period.

The next period of major tectonism in the Anadarko Basin

occurred during the Silurian-Devonian interval. Axtmann (1983)

suggests that the present Ouachita Mountain area was in a

compressive regime as early as late Ordovician. This corre-

sponds to the rise of the Taconic Highlands (Axtmann 1983, and

Bird and Dewey, 1970) and marks the onset of pervasive

compressional deformation across much of the southern United

States that lasted through the Permian period. This

compressional deformation began in the northeastern United

States and progressed in a continuum fashion to the southwest.

Figure 24 shows the relative timing of the east coast orogenic

events that appear to have had an influence on the structural

development of the southern Oklahoma Region. As stated, this

continuum of compressive events began with the Ordovician

Taconic orogeny, proceeded through the Devonian Acadian

orogeny, and culminated in Southern Oklahoma with the

Pennsylvanian-Permian Ouachita orogeny. In short, the

structural history of Southern Oklahoma has been dominated by

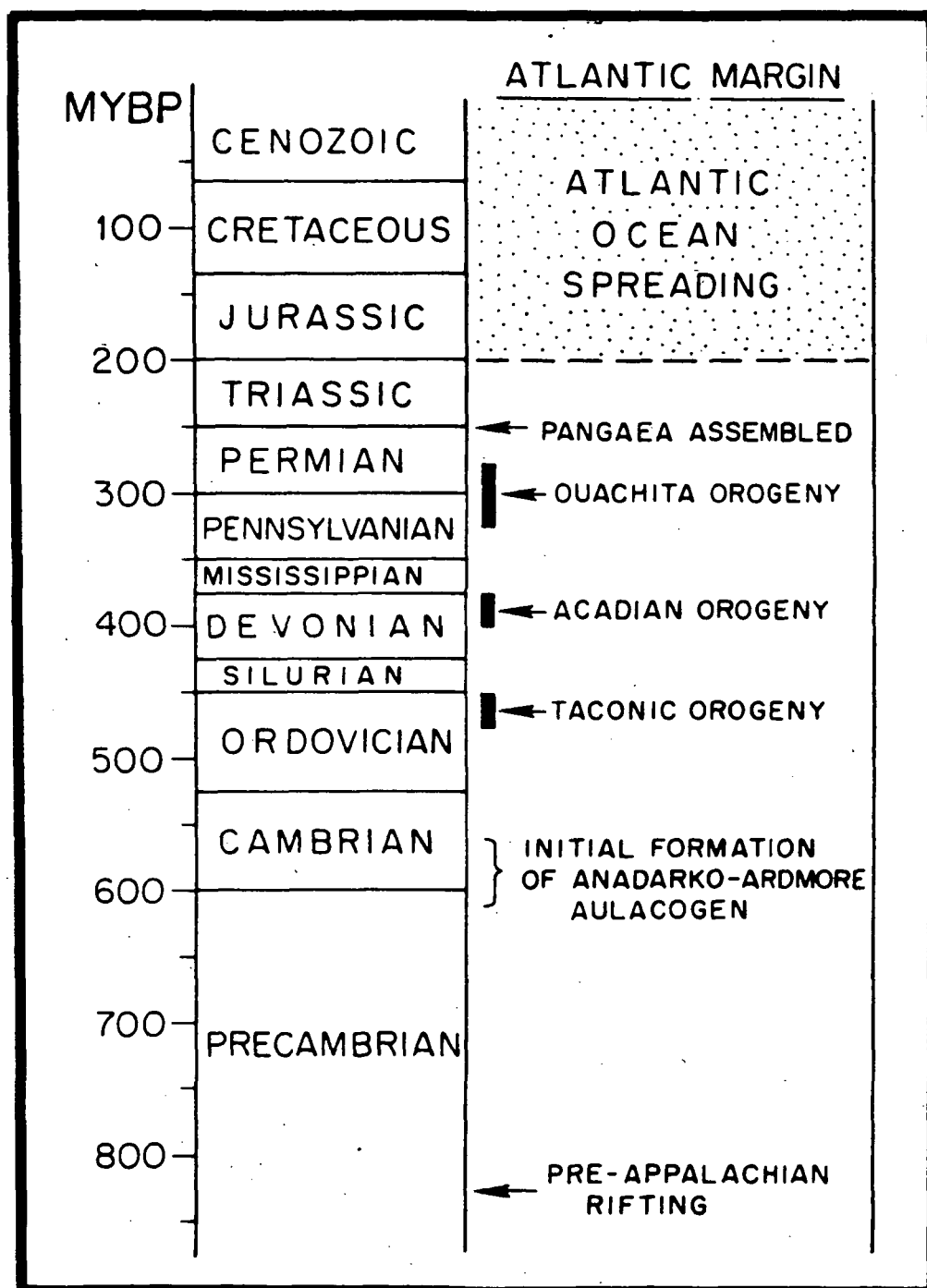compressional regimes on a plate tectonic scale.

Figure 24   Approximate timing of important events affecting Eastern
North American Margin (modified from Dickinson, 1977)

Within the Southern Oklahoma area, the manifestation of post aulocogen compressional tectonics is in large scale folding and faulting. Strike-slip movement dominates regionally with associated thrusting and normal faulting on a more local scale. Although senses of motion on most of the faults in the Anadarko/Ardmore Basin region have been documented for years, it has been difficult to place them in regional context prior to the advent of plate tectonics theory. Although details still need to be worked out for individual areas, it is now clear that the interaction between plates was the overall driving force behind the variety of Cambrian through Permian tectonic events that affected the area.

Specifically, Figures 22 and 25 illustrate details of the regional structure in Southern Oklahoma. Although it has always been difficult to integrate the various structural styles present (strike-slip, thrusts and normal faults), plate tectonics and application of theory developed from rock mechanics work, e.g., the strain-ellipse (Figure 26) has enabled a more or less unified story to be constructed that accounts for most of the larger-scale features that have been known for years. When adapted to the regional compression as provided by plate tectonic theory, the strain-ellipse (Figure 26) predicts not only what types of deformation will occur, but also the approximate orientation of any particular type of possible deformational event. If the strain ellipse of Figure 26 is compared to the structural representations in Figures 22 and 25, it becomes readily evident that the association of strike-slip, thrust, and normal faults agrees with predictions
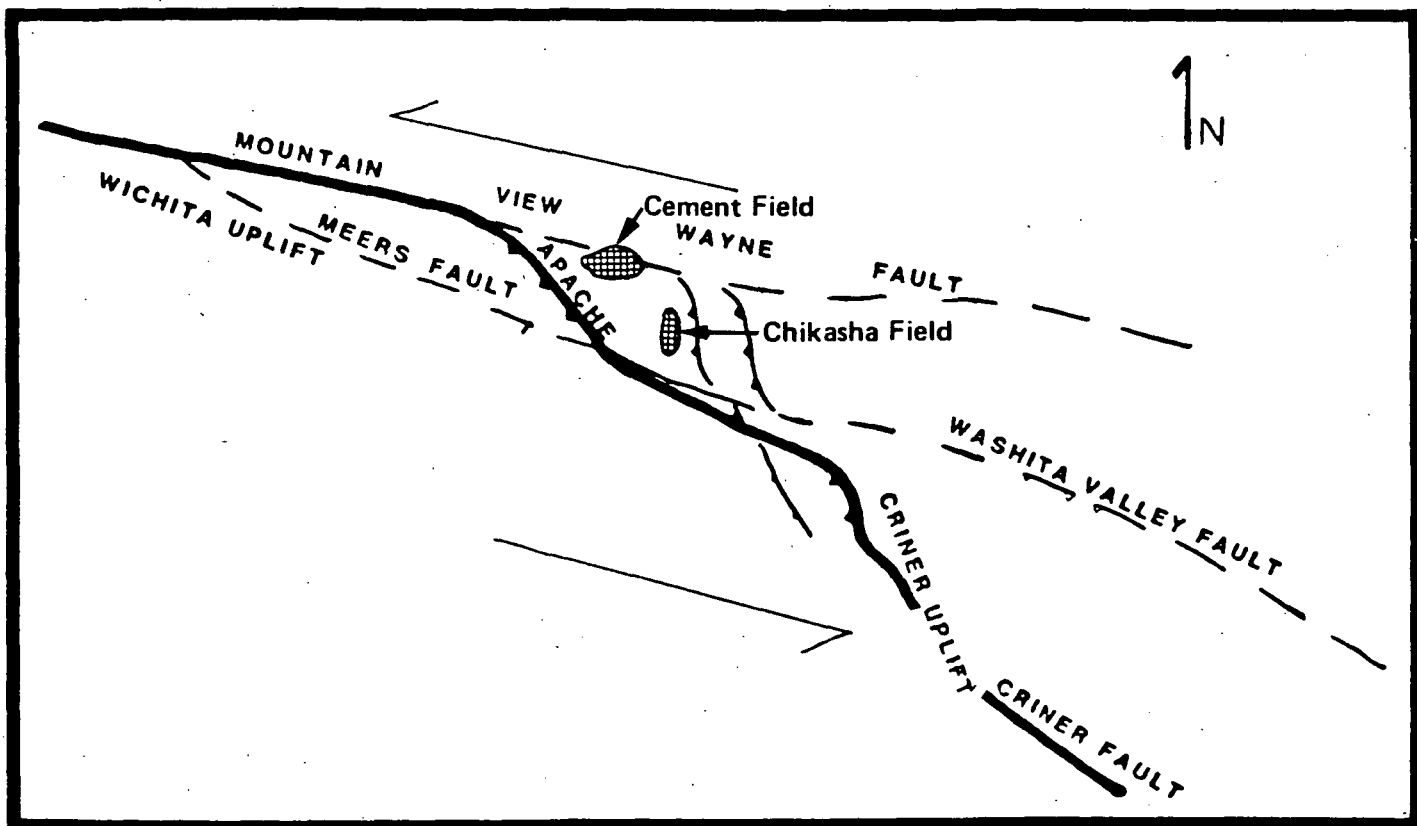
Figure 25   Diagrammatic detail of regional structural components of southern Oklahoma
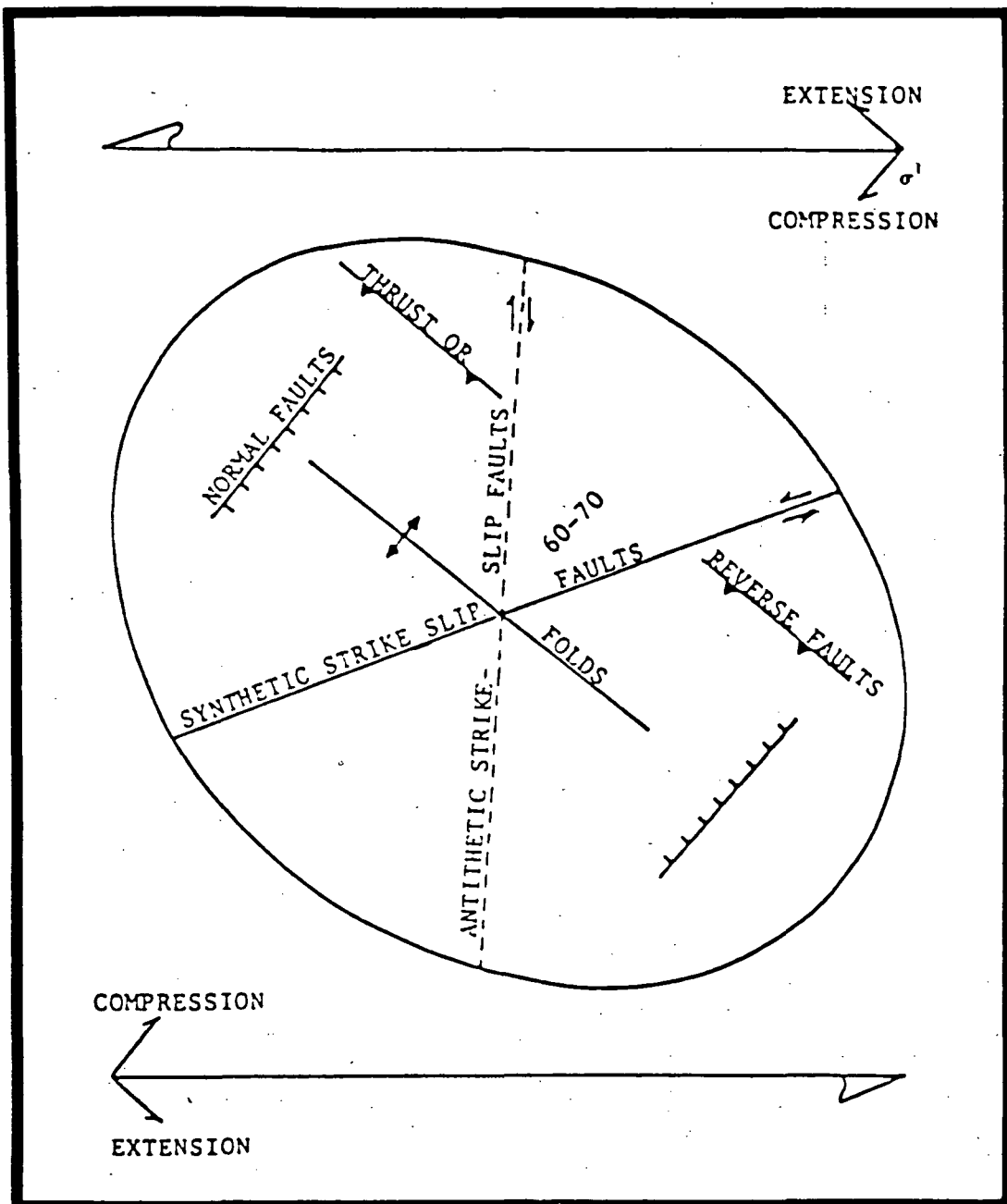(modified from Axtmann, 1983)

Figure 26   Left-slip wrench system: strain ellipse and composite of forces and structures that can result (after Harding, 1974)

based on utilization of the strain ellipse. Many complications

will become evident at a more local level, especially since the

orientation of the principal compressive stress (Sigma-1)

changed through time as deformational events progressed from

northeast to southwest along the line of continental collision.

Indeed, depending on reconstruction of events and shape of

continental edges, Sigma-1 may have rotated through almost 180

degrees from Ordovician to Permian. Additionally, the major

northwest trending strike-slip faults of the region have at

times been oblique slip features that have given rise to

features termed "flower structure" by Lowell (1972). Sections

4.4.5 and 4.4.7 describe the details of this overall system

with respect to Cement and Velma fields.

4.4.5 Structure of the Cement and Velma Oil Fields

The Cement Oil Field is situated in a doubly plunging

west-northwest striking anticline. The anticline is approximately

17 km long and 3.2 km wide (Reeves, 1921). Outcropping rocks at the

crest of the structure dip south at about 1 to 3 degrees. Dips on

the north flank are slightly steeper than dips on the south flank,

indicating a slightly asymmetrical structure at the surface

(Herrmann, 1961), though the asymmetry of the structure increases

dramatically with depth (Donovan, 1974). A structural cross-section

is shown in Figure 27.

The Cement structure consists of a severely deformed and

faulted Pennsylvanian sedimentary section which is unconformably

overlain by a thick series of unfaulted Permian red beds. The

Pennsylvanian section is tightly folded, and provides abundant

Figure 27   Structural Cross Section of Cement Field (from Herrmann, 1961)

131
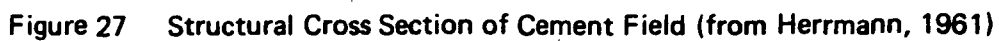
evidence of severe compressive diastrophism. The Permian red beds are about 770 m thick and are gently folded into a nearly symmetrical anticline with its axis almost exactly coinciding with the pre-Permian fold axis (Al-Shaieb et al., 1982). An angular unconformity exists between the Permian and Pennsylvanian sections in the upper portions of the structure where the topographically positive portions of the pre-Permian structure were beveled by erosion (Al-Shaieb et al., 1982).

There are two well-defined domes developed along the anticlinal axial highs. These domes are approximately 13.5 km apart. One dome crests immediately south of the town of Cement (Sec. 3, T5N, R9W) and the other in section 36 of T6N, R10W (Harlton, 1960). The two domes support oil fields named East Cement and West Cement, respectively. Structural closure of the East Cement dome is about 18 m, and the West Cement dome has structural closure of about 40 m (Donovan, 1974). Between the two domes is a crestal saddle. Most production is restricted to the structurally highest portions of the domes (Donovan, 1974).

The Cement anticline is bounded on the north by a major northwest striking, south dipping thrust fault. The trend of the fault is parallel to the axial strike of the anticline. The thrust fault is expressed at the Hoxbar level (Missourian Series) about 2.4 km north of the anticlinal axis. The steep north flank of the anticline reflects the influence of the high angle thrust fault as rollover and drag folding of the penecontemporaneous beds (Donovan, 1974). The south dipping flank of the anticline is more gently folded and shows no evidence of thrust faulting.

The thrust fault is upthrown on the south (Donovan, 1974). Although the thrust fault is situated near the the axis of the Pennsylvanian anticline, it does not appear to penetrate the Permian rocks which comprise the youngest strata of the structure (Donovan and Dalziel, 1977). Instead, the fault is truncated by the pre-Permian unconformity at the top of the Pennsylvanian section. At the Hoxbar horizon (Missourian Series), the throw on the thrust fault is about 300 m at West Cement and about 850 m at East Cement (Herrmann, 1961).

A north dipping normal fault with varied throw trends roughly parallel to the anticlinal axis and is located between the thrust fault and the axial plane. Like all the faults in the structure, this fault also has been truncated at the pre-Permian unconformity (Al-Shaieb et al., 1982). This fault has 850 m of throw at the Hoxbar level at West Cement and 30 m of throw at the Hoxbar level at East Cement. The normal fault merges with the thrust fault below the Deese horizon (Desmoinesian Series) at 2,300 m (Harlton, 1960).

Cross faults and subsidiary faults are present at both East and West Cement (Herrmann, 1961, Harlton, 1960). One cross fault striking north-northeast cuts the East Cement dome at the Hoxbar level immediately west of the domal culmination. Five northeast striking cross faults are mapped at the West Cement field. These faults break the West Cement dome into fault blocks and offset the anticlinal axis. There is one northwesterly cross fault in the West Cement dome mapped by Herrmann (1961). These and other as yet unmapped faults may act as pathways of hydrocarbon migration, possibly allowing effusion leakage from the reservoir to the surface.

The Velma anticline, like the Cement structure, is a severely deformed Pennsylvanian anticline unconformably overlain by a gently folded Permian red bed sequence. The Velma anticline is a northwest-southeast striking asymmetric structure formed by the diastrophic events which affected the entire Anadarko Basin and which deformed the Cement structure. The Velma structure, however, is significantly more structurally complex than the Cement structure, consisting of an apical horst bounded by flanking grabens. The horst and graben structures are entirely Pennsylvanian in age. Stratigraphic evidence suggests that deformation began during Morrowan time and continued through the Arbuckle orogeny (Ferguson, 1979). Unconformities are common throughout the Pennsylvanian section, and a final post Pennsylvanian unconformity has truncated and beveled all the horsts and grabens.

Permian clastic sediments unconformably overlie the beveled Pennsylvanian section, as shown in the structural cross section of the Velma Field in Figure 28. The thickness of the Permian rocks is about 350 m at the crest of the structure and thickens to about 800 m along the anticlinal flanks (Donovan et al., 1981). The Permian rocks are folded into a gentle anticline forming a north-northwest ridge at the surface. The axis of the Permian anticline is located directly above the central horst of the Pennsylvanian structure (Ferguson, 1979).

High-angle reverse faults bound the tipped graben and horst blocks and run parallel to the anticlinal axis for the entire length of the structure. The faults are prominently displaced in the Pennsylvanian section, but there is no known structural expression of these faults in the Permian rocks or at the surface (Ferguson,
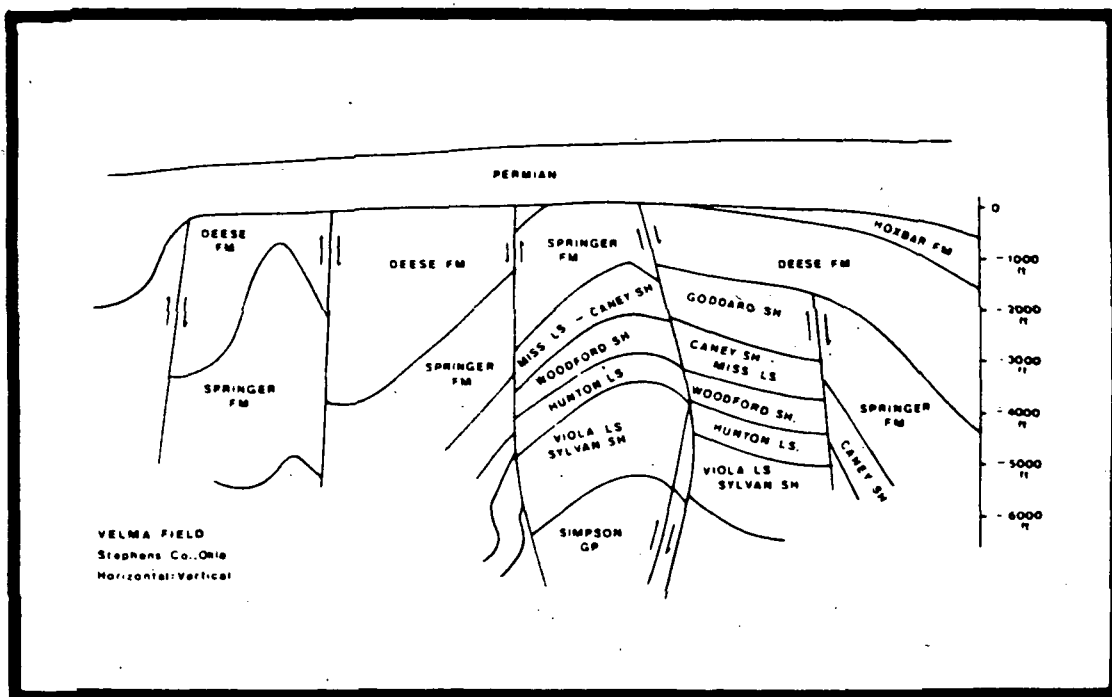
Figure 28 Structural Cross Section of the Velma Field (from Ferguson, 1979)

135

1979). Isotopic and mineralogical evidence suggests that many of the faults may provide pathways for the migration of petroleum from the subsurface reservoir to the surface, causing late diagenetic alterations to surface rocks.

4.4.6   Producing Horizons of the Cement and Velma Fields

Reeves (1921) mapped the Cement anticline based on outcrop and drilling records from approximately five years of oil field development. Subsequent work by Harlton (1960) and Herrmann (1961) applied modern methods and stratigraphic nomenclature to the study of the Cement Field. The formation names at Cement used in this report reflect the work of Donovan (1974) whose stratigraphic column as adapted from Harlton and Herrmann is shown in Figure 29.

Rocks from the Middle and Late Permian System (Guadalupian Series) to the late Early Mississippian System (Osagean Series) have been penetrated by drilling at Cement. Between the Mississippian and Permian rocks each stratigraphic system is represented, with only one major unconformity occurring between the Pennsylvanian and Permian Systems (Herrmann, 1961). Each system has been subdivided formally into formations and groups as shown in the stratigraphic column. Prior to the Mississippian, the presence of older systems through the Ordovician, while not revealed by drilling, is inferred from drilling records in the Carter-Knox, Bradley, and other nearby oil fields (Herrmann, 1961).

The multizone accumulation of the Cement Field has produced over 120 million barrels of oil as of 1968, with estimated remaining reserves of 14.5 million barrels (Donovan, 1974). Over 120 million standard cubic feet of gas and 30 million barrels of oil had been

SYSTEM	SERIES	GROUP	FORMATION	SUBDIVISIONS		
PERMIAN	Guadalupian		Cloud Chief	Cyril Gypsum Member		
		Whitehorse	Rush Springs			
			Marlow			
		El Reno	Chickasha			
			Duncan Sandstone			
		Clear Fork	Hennessey			
			Garber Sandstone			
	Leonardian ?	Wichita		Fortuna sandstone		
				Noble Olson sandstone		
	Wolfcampian	Pontotoc		Basal Permian limestone		
PENNSYLVANIAN	Virgilian	Cisco		Upper Gregory limestone		
				Garner sandstone		
				Griffin sandstone		
				Rowe limestone		
				Rowe sandstone		
	?	?		Niles sandstone and limestone		
	Missourian	Hoxbar		Upper oolitic limestone Yule Funk sandstone Ostracod sandstone Oolitic limestone Wade sandstone Hedlund sandstone Marchand-Medrano sandstone Culp-Melton zone		
	?					
	Desmoinesian	Deese		**West Cement field** Upper Kistler sandstone Lower Kistler sandstone Sams sandstone Pooler sandstone U. Deese sandstone	**East Cement field** Glover sandstone Charleston sandstone LAH Pooler sandstone Lower Pooler sandstone Mona sandstone	
	Atokan	Dornick Hills	Upper	Primrose Member of Golf Course Formation, near base		
	Morrowan		Lower			
	? ?		Springer	Sandstone		
				Shale		
				Goddard Shale Member		
MISSISSIPPIAN	Chesterian					
	Meramecian		Caney Shale			
	Osagean		Sycamore limestone			

Figure 29   Stratigraphic column, Cement field and vicinity (from Donovan, 1974)

produced as of 1966 from the Medrano Sand alone, most of this after unitization of the field in 1947 (Weaver and Anderson, 1966). Though the Pennsylvanian Medrano-Marchand Sandstone is the most productive single unit in the field, production occurs from over fourteen distinct zones of Permian and Pennsylvanian age.

Pennsylvanian rocks include the Cisco, Hoxbar, Deese, and Dornick Hills Groups. Each of these is further subdivided into stratigraphic members with names from local oil field usage. Of note, the Medrano - Marchand Sandstone of the Hoxbar Group is the most prolific producer in the Pennsylvanian section (Herrmann, 1961). The other producing members of the Pennsylvanian section are, in order of decreasing potential, the Rowe, Niles, Yule-Funk, Melton, Griffin, Garner, Deese, Edwards, Springer, and upper Cisco horizons (Herrmann, 1961).

In the Permian section at Cement, the Guadalupian Series is represented by the outcropping rocks of the Cloud Chief Formation (Cyril Gypsum Member), the Rush Springs Sandstone, and the associated red beds of the Marlow, Chickasha, and Duncan Sandstone Formations. The Clear Fork Group containing the Hennessey and Garber Sandstone Formations, and the Wichita Group comprised of the Fortuna Sandstone and Noble Olson Sandstone members, are the representatives of the Leonardian Series. The Pontotoc Formation of the Wolfcampian Series is the basal Permian limestone which unconformably overlies the Pennsylvanian section. The Fortuna Sandstones, Noble Olson Sandstones, and Pontotoc limestones are the major Permian producing members (Herrmann, 1961).

The Velma Field was discovered on the basis of plentiful oil seeps which initiated surface mapping in 1917 (Donovan et al.,

1981). At the Velma Field, oil and gas are produced from Ordovician through Permian rocks. The Sho-Vel-Tum Field, which includes the Velma Field, has produced nearly a billion barrels of oil and unrecorded amounts of gas.

The most important economic units in the Velma structure are the Springer Group horizons of Mississippian and Pennsylvanian age. These include three persistent and hydrocarbon productive sandstone units and a thick and diverse assemblage of shales, with a maximum thickness of about 150 m expressed in the vicinity of the Carter-Knox oil field (Peace, 1965). The Springer Group is truncated by an unconformity at the top of the Pennsylvanian structure and is over-lain by late Pennsylvanian and Permian rocks.

Other hydrocarbon productive zones include the Ordovician Simpson Group, the Devonian Hunton Group, the Mississippian Sycamore Limestone, and the Deese and Hoxbar Formations of Pennsylvanian age. A small amount of oil and gas has been produced from depths of 100 to 300 m in the Permian section (Ferguson, 1979; Rutledge, 1954). Permian units present in the Velma Field include the Wichita Formation, the Wellington Formation, and the Garber Sandstone, which outcrops over most of the structure.

4.4.7 Tectonic Development of the Cement and Velma Anticlines

Structural and stratigraphic development of the oil and gas regions of southwestern Oklahoma is believed to have begun with a Late Precambrian structural trough named the Southern Oklahoma Aulocogen (Pruatt, 1975). The aulocogen is interpreted to represent a failed arm of a three-armed radial rift system (refer to Section 4.4.4). Rifting of the aulocogen through Middle Cambrian time was

accompanied by extensional normal faulting, basaltic and rhyolytic extrusions, and emplacement of gabbros and granites. The structure in late Cambrian time was a graben with igneous and metasedimentary rocks comprising the bottom (Ferguson, 1979).

A Late Cambrian to Early Devonian subsidence stage allowed marine transgression and deposition of 3,100 m carbonates through Early Devonian time (Ferguson, 1979). Subsidence of the developing Anadarko and Ardmore Basins was contemporaneous with uplift of the Wichita-Criner and Arbuckle mountain systems, providing a sediment source during the extended deformational phase that occupied Devonian to Permian time. Compressional diastrophism uplifted the nearby igneous mountains allowing erosion of plentiful clastic detritus off the topographically positive areas. Rapid sedimentation occurred through Guadalupian or Ochoan time in tectonically loaded basins adjacent to the uplifts, including the Anadarko Basin (Ferguson, 1979).

The compressive deformation responsible for the development of the Cement structure was apparently intermittent and long lasting throughout the Pennsylvanian. Early Morrowan units thin at the crest of the structure, indicating early Pennsylvanian growth. Thinning of all post Morrowan Pennsylvanian units at the Cement Field suggests persistent recurrence of intense diastrophism until the Permian (Herrmann, 1961, and Donovan, 1974).

Asymmetrical folds, thrust faults parallel to the axial plane, and associated normal faults at oblique angles to the axial strike of the anticline are evidence of the intense Pennsylvanian compression. According to Herrmann (1961), the major normal and thrust faults began their growth in Atokan time and proceeded with

continuous deposition of sediments until Wolfcampian time. Evidence
of simultaneous deposition and faulting is provided by thickening of
the Atokan through the Cisco rocks on the downthrown sides of the
major faults in the Cement structure (Donovan, 1974). From the
record of stratigraphic relations, the most rapid period of
structural growth and thrust faulting in the East Cement Field was
during Atokan and Desmoinesian time.

At the end of Pennsylvanian time, the Cement anticline was
topographically positive along its crest. This is indicated by the
unconformity present at the base of the basal Permian Pontotoc Group
(Harlton, 1960). Post-Pennsylvanian beveling of the Cisco Group
rocks and subsequent deposition of the basal Permian sediments
resulted in an angular unconformity at the base of the Permian. The
structure is deeply etched by erosion on its crest, but not on the
lower flanks where the angular unconformity also loses its angular
relationship with the underlying Pennsylvanian units (Harlton,
1961). This evidence and the pinching out of many of the sandstone
units along the flank of the anticline suggest that only the crestal
portions of the anticline were topographically positive at the end
of the Pennsylvanian, and that sedimentation was relatively
uninterrupted at the lower portions of the structure where
strandline conditions persisted (Herrmann, 1961).

The Velma structure was uplifted, folded and faulted during
episodic diastrophism during the Morrowan Late Wichita deformation
event through the Missourian and Virgilian aged Arbuckle orogeny
(Ferguson, 1979). The flanks of the anticline were steepened and
the central horst emerged from the anticline as compression
increased and movement occurred along high-angle reverse faults.

Post-Morrowan deposition of marine beds occurred in response to thrust loading of the lithosphere to the south during the continuing Ouachita continental collision. The Velma structure was broken into a series of tilted horst and graben fault blocks by the end of the Arbuckle compression, with substantial vertical displacement occurring along the faults (Ferguson, 1979).

Early Permian sedimentation in southwestern Oklahoma began with Pontotoc (Wolfcampian Series) detrital clastics consisting mainly of conglomerates (Harlton, 1961). Upward through the section, detrital marine sediments grade into restricted marine and marine mudflat sediments. The evaporites of the Cloud Chief Group are remnants of the dessicated shallow transgressive seas of later Permian time (Ferguson, 1979). Current directions in the Early Permian rocks imply sediment source areas to the southeast, suggesting Ouachita and Arbuckle Uplifts as the likely sources for Pontotoc sediments. Only the Ouachita Uplift was persistently positive throughout Permian time (ibid). A series of boulder conglomerates in alluvial fans and deltas in the Anadarko Basin attest to locally involved sediment sources such as the Wichita Mountains.

In Late Permian time, a shallow transgressive sea produced a depositional environment gradational between deltaic and brackish marine or marine mudflat conditions (Ferguson, 1979). The Rush Springs Sandstone (of the Whitehorse Group in the Guadalupian Series) is attributed to Ouachita uplifting leading to a significant influx of fine, sub-angular to sub-rounded clastics (Ferguson, 1979). The Rush Springs Sandstone has been variously interpreted as a coastal dune deposit (MacLachlan, 1967), as a marine strandline

deposit with associations with contemporaneous aeolian dunes (Al-Shaieb et al., 1982), and as a shallow marine embayment deposit (Tanaka and Davis, 1963). The Rush Springs unit is a deep red, cross-bedded sandstone 30 to 100 m thick in the Cement anticline. This unit, which is not present at Velma, bears the principal expression of much of the diagenetic alteration at Cement as bleaching and related discolorations on the top and flanks of the structure. At Velma, the Garber Sandstone is the outcropping Permian unit which is bleached and bears the expression of late diagenetic hydrocarbon induced alteration.

The Garber Sandstone is the youngest unit exposed at Velma (Ferguson, 1979). The youngest rock unit exposed at Cement is the Cyril Gypsum, the basal member of the Cloud Chief Group. This unit is a pink and white gypsum bed reflecting the evaporitic conclusion to the Permian sedimentation. Cyril Gypsum outliers locally overlie the Rush Springs Sandstone and vary in thickness from 3 to 12 m (Herrmann, 1961). The Cloud Chief Gypsum is altered to calcite over the top of the structure. This is one of the expressions of hydrocarbon induced diagenetic alteration at the Cement Field.

Late Permian diastrophism of a mild character created a gentle folding of the Cement and Velma structures. Outcrops of the subtle Permian age anticline allowed Reeves (1921) to map the Cement structure. Pennsylvanian units in both the Cement and Velma structures are significantly more dramatically folded than the unconformably overlying Permian rocks due to the intense Atokan and Desmoinesian compression discussed above (Ferguson, 1979; Herrmann, 1961).

4.4.8 <u>Alteration Anomalies Expressed at Cement and Velma</u>

Alteration of surface and subsurface rocks at the Cement and

Velma Fields has been documented by many authors including Reeves

(1921), Harlton (1960), Ferguson (1979), Lilburn and Al-Shaieb

(1983), Al-Shaieb et al. (1982), Donovan (1972, 1974, 1981), Donovan

and Dalziel, 1977, and Donovan et al. (1974, 1975, 1977, 1979a,

1979b, 1979c, 1981). Late diagenetic alterations have been more

thoroughly studied at the Cement Field, due to the extensive

exposure of altered rocks and the dramatic topographic anomaly

present. At Velma, the exposures are limited, thus most of the

study here of alteration has concentrated on subsurface expression

of mineralogy. From a remote sensing perspective, the surface

expressions are more important, thus the discussion herein will

concentrate on the Cement Field. The term "alteration" is used in

the literature to refer to anomalous features of the surface and

near surface portions of the Velma and Cement Fields which are

attributed to the effects of hydrocarbon leakage from oil and gas

accumulations below. Anomalies that have been studied include the

following general categories:

o   color anomalies of the surface rocks

o   topographic anomalies

o   magnetic anomalies

o   gamma radiation anomalies

o   cementation and calicification anomalies

o   isotopic anomalies

These anomalies have been interpreted as evidence for

hydrocarbon induced diagenetic alteration. Each of the above

anomaly classes will be discussed below, although they are in large

part interrelated and share many common physical and genetic characteristics.

4.4.8.1 Coloration Anomalies

The surface rocks overlying the anticlinal crest of the Cement structure display a variety of bleaching effects and related discolorations. The anomalous colorations at Cement were first noted by Reeves (1921) and have been further described by many other authors. The Rush Springs Sandstone, the Permian unit which outcrops over most of the field, is a typically reddish brown red bed formation. The Rush Springs is altered to lighter brown on the southwest flank of the structure and to pink on the northwest flank. On the south and east flanks, and toward the crest of the anticline, the colors grade to yellow variants. Near the anticlinal crest the rocks are almost white, and, at the very crest are altered to light gray (Donovan, 1974).

At the Velma Field, the bleaching of Permian red beds has been documented by several authors (Donvan, 1972; Harlton, 1960; Ferguson, 1979) and is similarly attributed to hydrocarbon leakage. The normally reddish brown red beds are bleached to yellow and white owing to iron loss (Donovan et al., 1981). Associated with the bleaching on the flanks of the Velma Anticline, Donovan et al. (1981) report abundant solid bitumen in some units on the flank.

The mechanism for the anomalous coloration at Cement and Velma is related to the Eh/pH stability field of iron within the alteration aureole. Under normal surface conditions in the absence of alteration, iron in Permian red beds is within the stability field of the ferric (Fe^{3+}) ion. Deposition of arkosic sandstones

(like the Rush Springs Formation) in oxygenated waters produces the red coloration typical of oxidized iron compounds. Reducing conditions or a strong acid can change the Eh/pH environment to the stability field of the ferrous (Fe^{2+}) ion. The stability field relations of iron are depicted in Figure 30.

Ferric iron is insoluble in waters that fall within the ferric stability field and the iron is easily adsorbed onto sand grains or incorporated into clays. Upon reduction or acidification, however, the ferric iron is changed to the soluble ferrous state, being easily dissociated by water from its adsorbed complexes. The presence of abundant calcite in the Permian section fixes the pH of the depositional environment at a minimum of 8.3, well within the acid/base stability environment of ferric iron. Therefore, to dissolve the iron, a strong reductant is necessary to place the iron in the ferrous stability field.

Hydrocarbons and associated compounds such as hydrogen sulfide leak vertically through the sedimentary column above a petroleum accumulation and create reducing conditions in the chimney of alteration. Iron in the alteration chimney can be reduced by the hydrocarbons and made soluble. Circulating groundwaters, if they are hypoxic, or ascending hydrocarbon brines can then flush the soluble iron out of the reduced zone. The resulting depletion of oxidized iron from the red bed leaves the formation with a bleached coloration. Bleaching may alter red beds to pink, indicating only slight alteration as at the flanks of the Cement anticline. Alternatively, bleaching may thoroughly alter the coloration to white as at the crest of the Cement anticline. The more severe bleaching at the crest of the structure suggests that geochemical
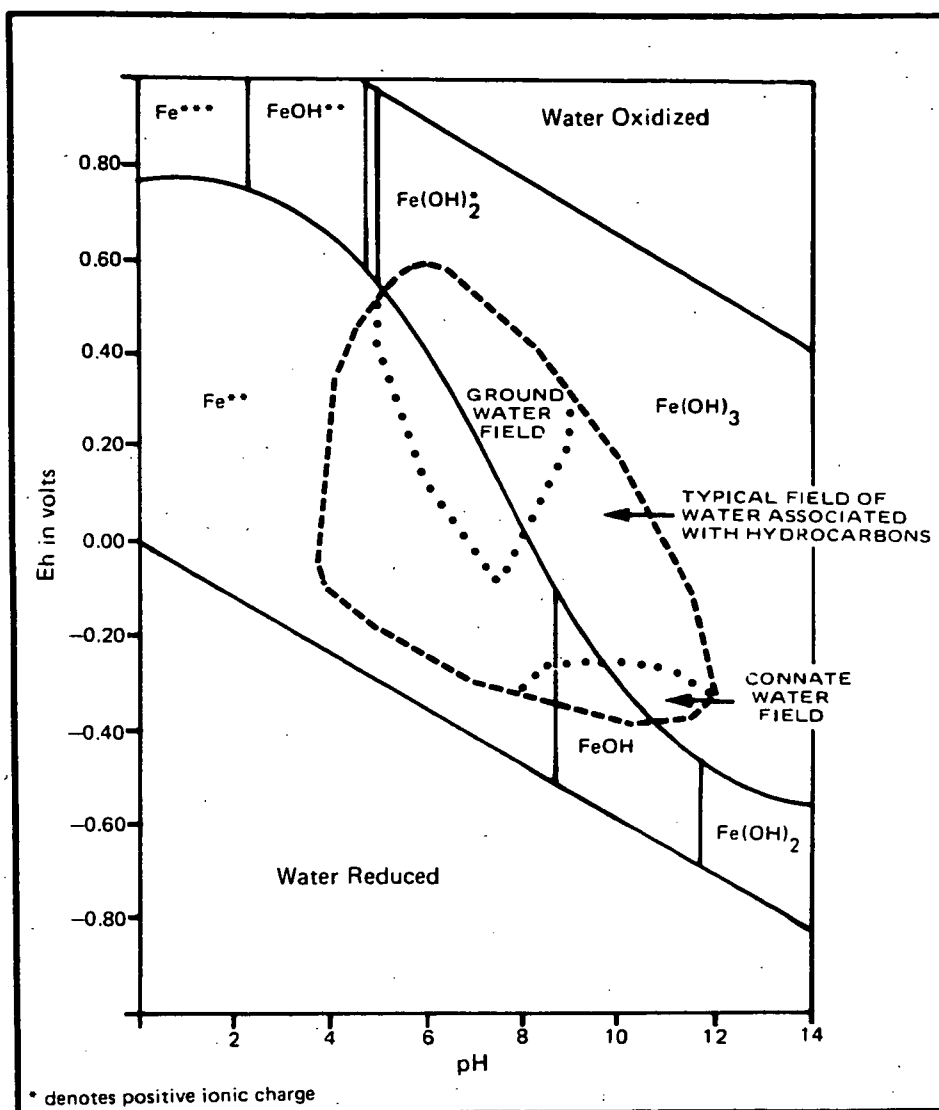
Figure 30 Stability Field Diagram for the Ferric-Ferrous System
(from Ferguson, 1979)

147

reduction has been more persistent or intense at that location. The intensity of reduction at the anticlinal crest or along faulted zones is attributed to the higher concentration of leaking hydrocarbons and to the more persistent leakage occuring in these zones through geologic time.

The yellow discoloration of the Rush Springs Sandstone observed by Donovan (1974) on the south and east flanks of the Cement structure is attributed to hydrocarbon reduction followed by incomplete oxidation of the dissolved ferrous iron as it is flushed away from the site of reduction. A variety of limonitic compounds, such as jarosite and lepidocrosite, are yellow in color and may represent semistable intermediate stages of ferrous oxidation responsible for the colors in the bleached portions of the anticline.

The gray coloration observed by Reeves (1921) at the very crest of the Cement anticline is the result of large concentrations of carbonate cement impregnating and indurating the sandstones overlying the crest. This carbonate cementation anomaly is discussed in detail below.

4.4.8.2 Topographic Anomalies

A prominent topographic high is coincident with the structural high of the Cement anticline and is locally referred to as the Keechi Hills (Harlton, 1960, Reeves, 1921). These hills consist of a series of barren rock ridges and isolated buttes which rise from 30 to 60 m above the drainage divide which marks the anticlinal axis of the structure below. Reeves (1921) calls the Keechi Hills the most prominent landscape feature of the Cement

region, and states that there is "no comparable topographic feature in the region," with the exception of the Wichita Uplift which the Keechi Hills resemble on a small-scale.

Although the entire axial plane of the anticline is topographically high, there are two areas of anomalously increased topography. Two concentrations of hills occur at East and West Cement, about four miles apart, which are coincident with the structurally high domal areas of the subsurface Hoxbar horizon (Donovan, 1974). Closure of the surface beds over the domal areas is as large as 60 m while closure at the Hoxar level is from 18 m at East Cement to 42 m at West Cement (Donovan, 1974).

The Keechi Hills are sandstone buttes which have been cemented by anomalously high concentrations of calcite cement or "calcrete" (Al Shaieb et al., 1982). The topographic anomaly is an expression of the resistance of the calcrete cemented sandstones to weathering. The anomalous calcrete concentration is attributed to vertical migration of hydrocarbons by effusion and solution through the crest of the anticline. The cementation mechanism leading to the topographic anomaly is discussed below.

4.4.8.3 Magnetic Anomalies

A low-altitude airborne aeromagnetic survey of the Cement Field was conducted. Flying at an elevation of 120 m the magnetometer made seven transects roughly perpendicular to the strike of the axial plane of the Cement Anticline. In addition, a systematic study of five borehole cuttings collected during development of the oil field was conducted by the investigators (Donovan et al, 1979a, 1979b, and Donovan, 1981).

The aeromagnetic survey revealed anomalous high wave number peaks against a background of rising magnetic field toward the northwest. The high wave number anomalies are evidence of shallow sources of magnetic field present in the sedimentary column (Donovan et al, 1979a, 1979b). Since magnetic susceptibility of sedimentary rocks is largely a measure of the amount of magnetite in the section, magnetite is the most likely source of the anomaly. The apparent rise of the magnetic field toward the northwest is, in contrast to the shallow anomalies, a regional phenomenon attributed to the regional trend in magnetic crystalline basement rock elevations rising in this portion of the Anadarko Basin (ibid).

Evidence of shallow sources of magnetism was corroborated by examinations of drill cuttings from five boreholes. The cuttings, which were available for depths of 300 to 80 m underwent magnetic separation and sampling for every 30 m of depth. The conclusion reached by the investigators was that the amount of ferrimagnetic material in the section increased toward the surface. X-ray diffraction of the ferrimagnetic material confirmed the material to be magnetite (Donovan et al, 1979a, 1979b).

Donovan (1981) suggests that vertical seepage of hydrocarbons and hydrogen sulfide has produced a reducing environment near the surface. The result is that ferric oxides present in the Rush Springs Formation and elsewhere in the Permian red beds have been reduced to hematite (Fe_2O_3) and subsequently to magnetite (Fe_3O_4, or, as Donovan expresses the formula of hematite, $Fe^{2+} Fe^{3+}_2 O_4$ reflecting the presence of a single reduced iron ion). Reduction of the iron, in this model, is insufficient to reduce all of the iron to soluble ferrous compounds that could be flushed out

of the sequence by ascending brines or circulating groundwaters.
Yet, the reduction is sufficient to maintain the presence of reduced
magnetite and allow a magnetically detectable anomaly to persist.
According to Donovan (1981) the presence of the ferrimagnetic
material near the surface is an indication of fossil petroleum
microseepage.

4.4.8.4 Radiation Anomalies

Deposits of uranium tend to associate with deposits of
petroleum in sedimentary terranes, leading to anomalous gamma
radiation concentrations that may have prospecting applications in
the appropriate geological and geochemical setting. Radiation
anomalies are hydrocarbon induced alteration phenomena which are
generally referred to as "radiation halos" (Armstrong and Heemstra,
1973). In general, radiation anomalies occur in conjunction with
more conventional geochemical halos, or in association with helium
concentration anomalies which also are attributed to the effects of
radioactive decay (Armstrong and Heemstra, 1973, Roberts et al.,
1978).

There are several types of radiation halos, and many
different mechanisms have been proposed to explain them. One type
of radiation halo consists of an anomalously low gamma radiation
count in the vicinity of the center of the associated petroleum
bearing structure, surrounded by an anomalously high radiation count
around the edges of the surface expression of the petroleum trap.
However, geometric complexities of the oil and gas trapping
mechanism, or lithological, structural, or other constraints on the
geology, may cause the halo to take alternative shapes. These may

include semicircular shapes, fan shapes, or even randomly contoured gamma anomalies that are difficult to interpret (Armstrong and Heemstra, 1973). In particular, fracture patterns, coning effects from diffusion, or hydrodynamic conditions can distort or shift the characteristic halo pattern (Weart and Heimberg, 1980)

The type of radiation anomaly present at the Cement anticline is caused by uranium mineralization of the Rush Springs Formation as a result of the vertical ascent of hydrocarbon associated fluids through the crest of the Cement structure. Instead of a halo of high gamma radiation values around the edge of the structure, the high radiation values are concentrated in and near the center of the structure, along the surface projection of the axial plane. The highest values of the radiation anomaly are truncated to the north at the location of the Permian thrust fault which bounds the north flank of the Cement Anticline (Donovan, 1981). The vertical leakage of hydrocarbon fluids along the axis and north flank of the structure is attributed by Donovan (1981) to the presence of preferred pathways for the vertical effusion mechanism of leakage. These preferred pathways consist of pre-Permian fractures and faults caused by the intense diastrophism of the Middle Pennsylvanian Period (Al-Shaieb et al., 1982).

The presence of uranium in the near surface portions of the sedimentary column at Cement is attributed to the vertical migration of hydrocarbons from the subsurface oil and gas accumulation. At Cement, the uranium emplaced by the vertical leakage has resulted in deposits of carnotite and tyuyamunite which, at East Cement, have been mined in small amounts (Donovan, 1981; Al-Shaieb et al., 1982). A combination of physical, geochemical, and geological mechanisms

are invoked to explain the mobilization and remineralization of uranium in the near surface. However, all mechanisms assume that ample uranium source rocks are contained within the sedimentary structure in contact with either circulating groundwaters or hydrocarbon brines. At the Cement Field, granite wash facies of Wolfcampian age are believed to be the uranium rich horizon that contributes to mineralization in the shallow portions of the structure. This arkosic uraniferous sandstone is believed to be derived from the uranium enriched Cambrian Quanah Granite of the Wichita Uplift (Al-Shaieb et al., 1982).

As in the mobilization of iron, the uranium mineralization phenomenon is essentially controlled by redox conditions in the subsurface. The Eh/pH stability fields of uranium are essentially opposite those of iron since uranium is insoluble in its reduced state and soluble when oxidized. Reducing conditions, such as those caused by the local presence of hydrocarbons, hydrogen sulfide, or compounds associated with petroleum reserves, tend to stablilize the reactive uranium ions, while oxidizing conditions, such as those encountered in circulating meteoric waters, tend to mobilize the uranium (Armstrong and Heemstra, 1973). Geologically, the problem in determination of a chemical mechanism for hydrocarbon induced uranium mineralization has been the complexity surrounding geological controls on oxidation and reduction conditions. In particular, the theories that are used to explain variations in redox conditions at different positions in the stratigraphic column and variations with respect to time have been a subject of controversy.

The mechanism for mineralization has been described in two dramatically diferent ways. One mechanism is similar to the formation of conventional geochemical halos, in which the uranium is adsorbed onto hydrocarbons leaking from the edges of the petroleum trap and transported vertically upwards. This mechanism forms the classic fan shaped or semicircular shaped gamma anomaly (Weart and Heimberg, 1980) and it explains the characteristic low radiation anomaly present above the center of the structure as the result of the shielding effect that petroleum trapping agents have on vertical migration immediately over the center of the trap. The anomalously high radiation values outside of the central structural high can thus be explained as leakage around the edges of the trap, like the conventional geochemical halo and aureole shown in Figure 21. Acceptance of this mechanism assumes that the reduction of uranium from a soluble form to an insoluble form occurs on the surface of an organic molecule such as a peat, wood, cellulose, kerogen, or other compound likely to be found in association with hydrocarbons (Armstrong and Heemstra, 1973). Evidence for this adsorption phenomenon is provided by the findings that uranium associations with ethylene, propylene, butylene, and other organic molecules are more stable than many other uranium organic complexes. Such evidence suggests that rising light fraction hydrocarbons could act as transporting agents for uranium mobilized from deep source rocks (ibid).

The alternative mechanism for uranium mineralization suggests that the uranium was brought into the vicinity of Cement in its oxidized (soluble) state by circulating groundwaters. In the upper portions of the structure, the uranium rich groundwater would

have contacted the vertically migrating hydrocarbons and other reductants leaking from the reservoir below (Donovan, 1981). Contact with rising reductants would be sufficient to reduce the uranium from the oxidized soluble state to an insoluble reduced state, thus causing precipitation of the uranium. However, the uranium is deposited in the structural crest of the Cement Anticline, and represents a secondary deposition event that almost certainly post dated the structural deformation that formed the anticline. Thus, the mechanism requires that uranium bearing groundwater move up the flanks of the anticline in order for it to contact reducing fluids and mineralize at the crest of the structure. This, in turn, requires that a significant hydrostatic head be invoked to drive the circulating groundwater up the flanks of the structure to the crest where it was precipitated. Since there is no evidence for such a hydrostatic head in the Cement vicinity, this mechanism seems unlikely (Donovan, 1981).

A third mechanism proposed by Donovan (1981) requires the introduction of uranium bearing groundwaters at depth within the Cement structure. In this mechanism, soluble uranium introduced in circulating groundwaters could have been precipitated from the groundwater and adsorbed onto vertically moving hydrocarbons and hydrocarbon associated compounds in connate brines squeezed by compaction pressure from the hydrocarbon source formations below. The problem with this mechanism is the tendency of the uranium to be precipitated at the site of contact where precipitation, leading to mineralization, would be expected to terminate the transport of the uranium. To resolve this problem, Donovan (1981) has suggested that

the uranium and hydrocarbons are cotransported in connate brines leaking upward from the hydrocarbon reservoir.

4.4.8.5 Cementation Anomalies

Anomalous concentrations of a variety of mineral phases are present in the near surface portions of the Cement structure over the zones of production. Principal among these is the saturation of pore spaces in the altered Permian Rush Springs Formation by calcium carbonate. Spatially, the impregnation occurs in the same general areas where the Rush Springs is bleached, though where the impregnation of the sandstones is especially strong, the color of the altered unit is gray. The anomalous induration of the sandstone by calcic cement is also the cause of the topographic anomaly discussed above.

Unaltered sandstones of the Rush Springs Formation are typically cemented by a hematitic grain coating and pore filling cement, imparting the red color to the unit. The unaltered Rush Springs Sandstones are also friable and easily eroded to gentle slopes or virtually flat topography.

At the Cement Field, the hematite cement has been removed by reduction and mobilization of the ferrous iron ions, contributing to the bleaching discussed above. In addition, the normally eroded Rush Springs forms a steep topographic anomaly where it is also bleached. Both of these phenomena are the result of calcite pore fillings, and replacement of the hematite cement by calcite cementing agents, which have imparted a gray color to the structural axis of the anticline and increased the resistance of the cemented zone to weathering.

Reeves (1921) relates the claim of drilling hands during
the early development of the oil field that sandstone beds over the
top of the structure are harder and more dificult to drill through
than stratigraphically equivalent beds along the flanks. This
effect was noted to a depth of several tens of metres the total
depth of the structure which had been tested at the time of Reeves'
work. Other authors (Donovan, 1972; Dalziel and Donovan, 1980) have
noted that cementation has apparently reduced the porosity of the
rock directly over the axis of the structure. The vertical extent
of the cementation is 760 m though at depth the effect is confined
to sandstone intervals.

Mechanisms for the carbonate mineralization are a result of
oxidation of hydrocarbons ascending vertically through the
sedimentary column. Light hydrocarbon gases in solution arrive in
the near surface portions of the structure and contact oxygen
bearing groundwaters. The hydrocarbons become oxidized, with the
liberation of carbon dioxide and a number of asphaltic byproducts of
incomplete oxidation. Carbon dioxide reacts with the siliceous
materials in the red beds to produce carbonates by decomposing the
silicates to calcium carbonate, silicates, and aluminosilicates. As
a result, the carbonates are embedded in pore fillings created by
the dissolution of the silicate material and occupy positions in the
crystal lattice structures of the grains of the red beds
(Duchscherer, 1982).

Another type of carbonate mineralization anomaly expressed
at Cement is the replacement of gypsum by calcite. Unaltered gypsum
beds of the Cloud Chief Formation are present on the flanks of the
anticline, but are altered abruptly to carbonate at the higher

locations on the structure (Donovan, 1972). The following reaction
mechanism is suggested for gypsum replacement (Kirkland and Evans,
1976):

$$CaSO_4 + CH_4 \text{ --- } H_2S + H_2O + CaCO_3 + energy.$$
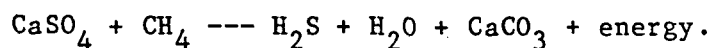
Evolved hydrogen sulfide from this reaction, by providing a source
of acid, may be associated with other mineralization phenomena at
Cement.

In Culberson County, Texas, a similar leakage case study
concerns leakage of hydrocarbons causing replacement of gypsum by
calcite. In this location, petrological analysis of the calcite
reveals sedimentary structures such as microstratification,
microfolding, lamaellar consistency, and overall texture of the
calcite which are characteristic of the unaltered banded gypsum
sediments replaced by the calcite (Kirkland and Evans, 1976).
At the Cement Field, the result of the calcrete substitution is a
resistive limestones with perfectly preserved gypsum crystal
morphology (Lilburn and Al-Shaieb, 1983). Other evidence supporting
a replacement mechanism for calcite mineralization at Cement
includes isotopic anomalies discussed below.

4.4.8.6 Isotopic Anomalies

Isotopic anomalies present at the Cement field support
the hypothesis of hydrocarbon leakage. Carbon, oxygen, and
sulfur isotopic ratios are anomalous in several areas which
spatially correspond to the areas of hydrocarbon production and
associated geochemical aureoles.

Carbonates formed during oxidation of leaking hydrocarbons (see Cementation Anomaly, above) are typically isotopically heavy, being enriched in carbon-13 relative to carbon-12 (Donovan et al., 1974). At the Cement field, the isotopic ratios, expressed in permil units against the PDB standard in Chicago, vary from -5.5 permil to -39 permil in 24 samples of the carbonate cements in the Rush Springs Sandstone (Donovan, 1974). Values of less than -25 permil are typical of petroleum derived carbonate isotope ratios, and the exceptionally light ratio value of -39 permil is believed to represent exceptionally rapid leakage (ibid). Values of -4 to +4 permil are typical of marine limestone carbon isotope ratios, and values of -5 to -18 permil are typical of freshwater limestones. The large variance of freshwater limestone ratios is a result of the inconsistency of the bicarbonate buffering capacity in the freshwater carbonate diagenetic environment (Donovan, 1974).

Oxygen isotopic ratios are also affected by leakage and display significant variance at the Cement field. In the Rush Springs Sandstone samples, oxygen isotopic ratios vary from +22.5 permil to +36.5 permil, as measured against the standard mean ocean water (SMOW) standard (Donovan, 1974). The anomalously heavy oxygen ratios reflect the increased representation of the oxygen-18 isotope relative to the oxygen-16 isotope. This phenomenon is attributed to selective evaporation of light water (bound with oxygen-16) relative to heavy water (bound with oxygen-18) in the groundwater table near the surface of the Cement structure. Heavy oxygen bearing groundwater, by

association with the precipitating carbonates, is fixed in late diagenetic pore filling cements of the Rush Springs Sandstone in the high portions of the structure.

Donovan (1974) recognizes four fundamentally different compositional types of carbonate cements in the Rush Springs Sandstone on the basis of their distinctive isotopic ratios. Types A and B are unaltered diagenetic limestones formed by solute precipitation as a result of micropore filtration of brines by shales. Type A consists of normal carbon and normal oxygen, and Type B consists of light carbon (ratio values of -27 to -36 permil) and normal oxygen. Donovan (1974) suggests that the A and B cements are both formed by normal diagenesis, except that the type B cement has oxidized petroleum as its source of carbon. Type C cement is enriched in carbon-12 and in heavy oxygen, with carbon values of -28 to -39 permil, and oxygen values of +28 to + 38 permil. Donovan (1974) interprets this cement to be the result of evaporation of formation waters in the presence of abundant oxidized hydrocarbon. The fourth cement, Type D, is composed of intermediate weight carbon (-16 to -26 permil) and heavy oxygen (+25 to +35 permil), representing a cement composition between that of freshwater bicarbonate and petroleum bicarbonate. Donovan suggests that this cement results from the mixing of carbonate from the normal diagenetic sources and the petroleum sources.

The significance of these types of cement is seen in Figure 31, in which the concentric arrangement of the cement types points clearly to a leaking reservoir. The type A cements form an outer zone around the West Cement dome, with Type D
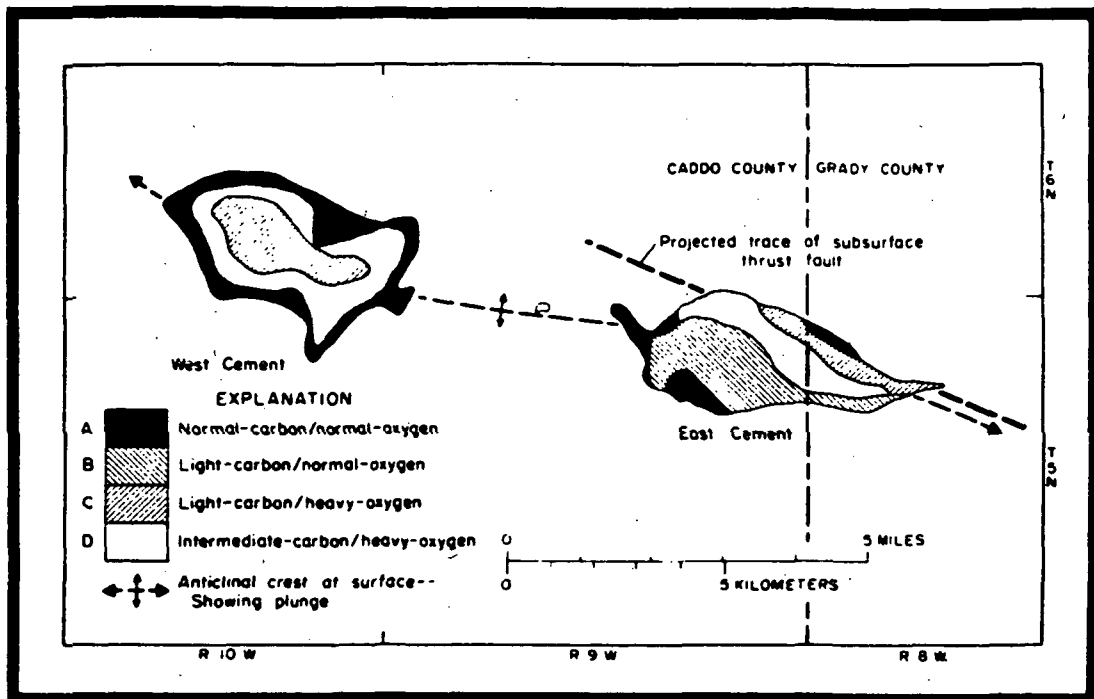
Figure 31   Areal distribution of carbonate cements according to isotopic composition in the Rush Springs Sandstone, Cement, Oklahoma (from Donovan, 1974)

forming an inner zone, and, at the top of the structure, Type C cement revealing a strongly petroleum based carbonate. The concurrence of the cement types with subsurface structure is clearest at West Cement, but also influences the surface isotopic ratios at East Cement. Here, the Type C cements are restricted to a narrow zone along the northeastern side of the productive area, directly overlying the surface trace of the major thrust fault bordering the structure. Donovan (1974) suggests that the fault has acted as a pathway for the leakage of hydrocarbons, and the gradient from Type C cement to Type B, D, and A away from the fault reflects the diminishing influence of leaking hydrocarbons away from the thrust fault.

At the Velma Field, the carbon isotopic ratios are exceptionally low over the crest of the anticline, ranging from -7.8 permil to -36.7 permil. These valuse are well within the range of values reported for a typical petroleum (Donovan et al., 1981). Oxygen isotopic ratios are also light along the crest of the structure relative to the flanks. Donovan et al. (1981) suggest that two mechanisms of fractionation have lead to the light oxygen isotope ratios in the near surface cements.

The first mechanism has caused enrichment of oxygen-18 isotopes in the reservoir fluids by virtue of gas expansion mechanisms like those operative at Cement. The selective evaporation of oxygen-16 waters from the reservoir fluids causes the enrichment of oxygen-18 in the reservoir fluids, leading to heavier isotopic ratios in the accumulation but allowing light oxygen to migrate to the surface where it intercuts with precipitating carbonates. The second mechanism involves

micropore filtration of the evaporating hydrocarbon saturated

formation waters as the fluids are transported vertically

through shale bodies between the reservoir and the surface.

Micropore fractionation results in selective removal of the

oxygen-16 isotopes leaving behind oxygen-18 in the intervening

shale bodies. Only the oxygen-16 is transported toward the

surface and subsequently incorporated into late diagenetic

carbonates. The findings that the oxygen isotope ratios are

light in the surface and near surface cements suggests that the

latter mechanism is dominating in the Velma diagenetic

environment (Donovan et al., 1981).

4.4.9 Field Work, Cement and Velma Areas

A two-day field study in the Cement and Velma oil fields

area on August 16 and 17, 1983 had the objectives of providing

ground truth concerning the character of various signatures

observed on the TM imagery and the appearance of anomalous rock

types and soil cover. An overflight in a small aircraft

provided an intermediate perspective closer to that provided by

the TM imagery.

An attempt was made during the overflight to correlate

the unbleached (red) and bleached (gray) areas with the spectral

characteristics displayed on the TM imagery. The results of

this effort were discouraging. Some subtle differences in soil

color associated with bleaching of the Permian red beds were

visible locally from the aircraft, but could not be identified

on the imagery. This can be explained, in part, as being due to

the extensive vegetation cover and deep soil profile. The

Cement field is associated with an elongated, northwest-trending hill and associated buttes called the Keechie Hills. These hills, which rise abruptly to over 45 m above the surrounding terrain are composed of erosional remnants of an area of well cemented and bleached Rush Springs Sandstone. Hydrocarbon leakage produced the bleaching and cementation. The topography of the Velma field is also expressed as an elongated, northwest-trending hill. It is less spectacular than the Keechie Hills, but is of similar relief.

Much of the area north of the Cement field is pasture-land (Figure 32) with a dense grass or tree cover. The exposures of ground are so limited in size that they are largely lost at the resolution of TM imagery. South of the Cement field the area is more extensively cultivated, but in most cases the soils are developed to such a depth that differences in coloration in the parent materials are disguised. Only on the Keechie Hills, is the lighter color of the bleached sandstone obvious. Even here, most of the hills have grass cover which obscures the unique coloration from detection by the TM sensors. Only where quarry operations have modified the surface (Figure 33) does the area appear anomolous on the Landsat imagery.

The Velma field in Stevens County lies on a structural trend parallel and related to the Cement field, and here also, Donovan (1974) reports evidence of surficial alteration due to microseepage of the hydrocarbons. The field, in part, lies along a low, elongated hill that apparently is the product of differential erosion of the more intensely cemented sandstone

Figure 32   A view to the southwest at the Keechie Hills showing mixed grassland and woodland cover north of the Cement Oil Field. The Keechie Hills, on the horizon, are the product of localized cementation of the Rush Springs sandstone resulting from vertical migration of hydrocarbons.

Figure 33   This aerial view to the northeast shows the extensive cementation and bleaching of the normally red colored Rush Springs sandstone. The numerous well locations on and to the south of the hills are evident as cleared areas of the end of or along the meandering roads.

165

associated with hydrocarbon leakage. Figure 34 shows the wooded ridge across the mid-portion of the photograph.

A unique suite of mineralization is associated with surface and near surface alteration (see Section 4.4.8) and this is partly revealed in the limited outcrops over the Velma field. There is an exposure of ironstone present (Figure 35) in a road cut about 0.5 km south of the northwest corner of Section 8, T2S, R4W, on the crest of the hill and near the crest of the structure. The ironstone is a cemented sandstone several metres thick, and is limonitic yellow to dark brown in color. This "caprock" is believed to represent iron in the red beds that was reduced to the ferrous state by ascending fluids and hydrocarbons, mobilized from the underlined sandstone strata and redeposited at an oxidizing horizon.

In a road cut on a steep hill in the southeast corner of Section 36, T1S, R5W, are exposures of bleached sandstone. This sand is light bluff in color, is in places friable, but near the top of the hill as shown in Figure 36, it is cemented by calcite into nodular (not concretionary) masses. The nodules range is size from about 4 cm to nearly 7 cm in diameter. This horizon is approximately a metre thick and appears to directly underlie the ironstone caprock, although only fragments of ironstone were found at this location.

At a cleared well site, in Section 35, T1S, R5W, an eroded slope shows the complex distribution of the bleached-unbleached facies that is believed to represent a condition that developed at or near the contact of the oxidizing and reducing horizons (see Figure 37). Present in both the bleached and

-166-

Figure 34   This northeasterly view of the Velma Oil Field shows the low, elongate hill associated with the area of extensive surface alteration resulting from microseepage of hydrocarbon.

Figure 35   Iron cemented sandstone is interpreted to be the result of re-deposition of ferrous iron mobilized by ascending hydrocarbons. Upon reaching an oxidizing zone, presumably near the surface, the iron is oxidized and deposited as ferric iron.

167

Figure 36   Nodular cementation by calcite in a sandstone bed near the crest of the structure of the Velma Oil Field. This horizon lies below the ironstone caprock. This unique cementation may be characteristic of the zonation of near-surface alterations produced by hydrocarbon microseepage.

Figure 37   An exposure in the Velma Oil Field that is believed to represent the redox contact of ascending fluids with a near-surface, oxidizing horizon. The highly irregular zone of bleached-unbleached sandstone contains abundant hematite nodules.

168

unbleached sandstone are aggregates of hematite that form

irregular "nodules" of cemented sandstone. The slope in the

lower-left corner of the picture is covered with these nodules.

Similar nodules extensively pave the grass covered slope for at

least 15 metres above this explosure.

Ground traverses provided valuable information concerning

details of the zonation associated with surface alteration

resulting from microseepage of hydrocarbons. However, accurate

delineation of the bleached-unbleached areas was not deemed

practical by this method in the environment around Cement and

Velma fields. Although not tested, as it is beyond the scope of

this study, the use of color aerial photography, supplemented

with low-altitude, reconnaissance overflights appear to provide

the best potential for mapping the boundaries of surface

alterations.

4.4.10   Qualitative Assessment of Thematic Mapper Imagery

Cement/Velma, Oaklahoma

The Cement and Velma areas are subscenes of the Lawton,

Oklahoma TM scene 40136-16362. As shown in Figure 20, the

Cement and Velma subscenes are located adjacent to each other

with only a small amount of overlap. Black-and-white prints of

each spectral band were produced as well as several color

combinations for each subscene area. Identical color composites

were not produced for each subscene. For Cement, a 2,3,4 band

color composite was produced, whereas for the Velma area a 1,3,4

color composite was made for comparative purposes. In addition

a 4,5,7 band combination was produced for the Cement area and a

7,5,4 was printed for the Velma area. Other color composites produced for both areas were 1,2,3 (natural color) and 1,4,5 (false-color).

Each color composite and individual black-and-white band print contributed some unique information to the study. Certain image products were, however, decidedly better than others. Little difference was found in the standard falsecolor 1,3,4 and 2,3,4 images for geological interpretation. For this scene, Band 1 data was more noisy than Band 2, so the technical quality of the 2,3,4 image is somewhat superior to the 1,3,4. The so called natural color version (1,2,3) is superior to standard false-color versions for soil tone distinctions, but even this version was inadequate to discriminate the areas of surface alteration associated with the Cement Oil Field. For structural interpretations in this area the 1,4,5 color composite was judged superior to the above mentioned images in that the contrasts between the different stages of cultivated lands and between cultivated land and rangeland is minimized. The exception is that green vegetation is rendered as bright green. Even so, the saturation of color in the 1,4,5 is less than in either the natural color or standard false-color versions. Consequently, subtle details of lineament traces can be mapped through these areas of growing vegetation with more confidence than on the other color versions.

Two final color versions were selected from the many examined on the CRT display of the interactive systems for bands 4,5 and 7. The 4,5,7 version was judged to be an excellent image for interpretation in the Greeley, Colorado area, but it

was considered somewhat inferior to the other color versions used in Oklahoma. The 7,5,4 version of the Velma area, on the other hand, was deemed to be equal to or superior to the other color images for structural interpretation. This version displays the green vegetation as red as does the standard false-color image, but overall the image appears "less busy" which facilitates the detection and mapping of the sometimes very subtle traces of lineaments.

The individual black-and-white bands were useful in interpretation and certain bands were more useful than others. The data for bands 1, 2, and to a degree for band 3 were degraded by excessive noise and were of little use for structural intepretation although the road network is prominent. For this particular TM scene, bands 4 and 5 are the most useful for geological analysis, and band 7 is nearly as good.

Band 6, the thermal band, is rather unique. The data shows excessive, but uniform banding between the detectors. The range of gray levels in the image is limited. As a result, the image appears to have been density sliced, and in general is a poor quality product. In spite of these apparent flaws, the image contains a large amount of valid data concerning major linear features of structural significance. As might be expected, those linear features having topographic expression, trending normal to the sun angle, appear to be emphasized. Moreover, several prominent lineaments parallel to the sun illumination are also mappable. As a result, the thermal band is considered to have produced the most useful information of the black-and-white images analyzed.

A Landsat-4 MSS image, obtained from an overpass of 15 December 1982, 17 days after the TM data was recorded, was processed to a standard false-color image. The spectral quality of the image is excellent, but image quality is seriously degraded by the pervasive "wood-grain" noise[2/] that is characteristic of the MSS system on Landsat-4. The data has some utility for structural mapping at 1:250,000 scale, but is nearly useless at 1:100,000 scale. NASA is not certain of the origin of the noise, but believe they have corrected the problem on Landsat-D'. Efforts are being made by some investigators to develop a processing procedure to eliminate or minimize the problem in existing data.

4.4.11   Thematic Mapper – Multispectral Scanner Comparison (Cement, Oklahoma)

A comparison of TM data with MSS data acquired for the Cement, Oklahoma area was performed. Lineaments were interpreted by two geologists from five image products as shown in (Table 7). The imagery included false-color infrared composite images from the Landsat-2 MSS and the Landsat-4 MSS and Thematic Mapper remote sensing systems. Each geologist interpreted the imagery without reference to the work of the other interpreter to insure complete independence of interpretations.

[2/]

A persistent characteristic of Landsat 4 MSS video data has been the presence of a distinctive noise pattern throughout. This pattern is most readily visible in the low-radiance flat fields and appears in geometrically uncorrected data as light, short diagonal stripes (sometimes referred to as a "woodgrain" pattern). The source of the noise is attributed to the spacecraft's multiplexer electronics.

Independent investigators have characterized the noise as occurring at spatial wavelengths of 2-15 pixels along a scan and ranging in level from 0.25 to 4 digital counts. Engineering analysis indicates that some components of the noise might possibly be accounted for as harmonics of a fundamental of 114.504 kHz. (There is a drifting voltage supply oscillator which operates at about 115 kHz.) All MSS data are affected by this. (NOAA Landsat Data Users Notes, no. 29, Dec., 1983).

TABLE 7:   SOURCES AND SCALES OF IMAGERY

Sensor		Scale
Landsat-2	MSS	1:250,000
Landsat-4	MSS	1:100,000
Landsat-4	MSS	1:250,000
Landsat-4	TM	1:100,000
Landsat-4	TM	1:250,000

The ten resulting interpretations were digitized with EarthSat's interactive graphics hardware. The interpretations were stored as ten filing areas according to the interpreter and image product interpreted. Statistical summaries of all the lineaments were created using the rose diagram format shown in Figures 38 through 42. These statistical summaries show the following three types of lineament distribution data: cumulative length of all lineaments in each compass direction; the cumulative frequency of all lineaments in each compass direction; and the average length of lineaments in each direction.

For ease of comparison, the rose diagrams are projected onto common axes and displayed together in the figures. In this way, smaller diagrams, representing small data sets of fewer or shorter lineaments, can be compared to the larger diagrams which contain either more or longer lineaments. The units of the axes are shown in Table 8.
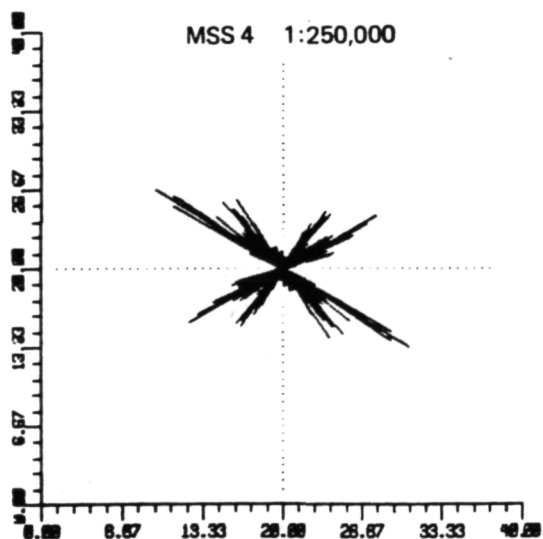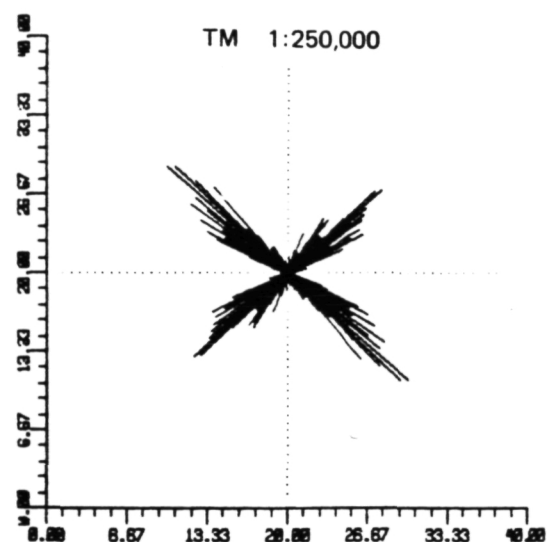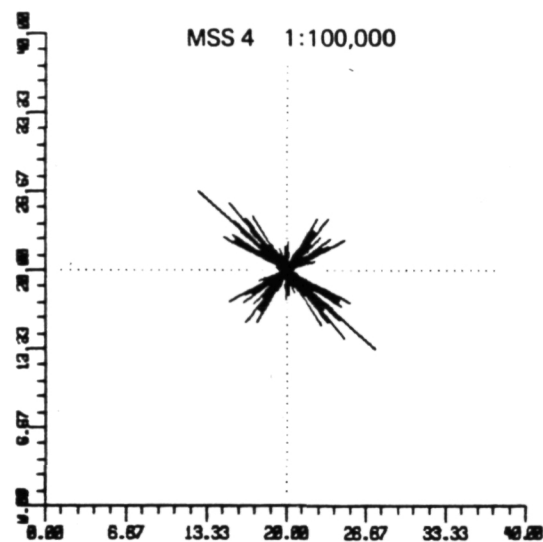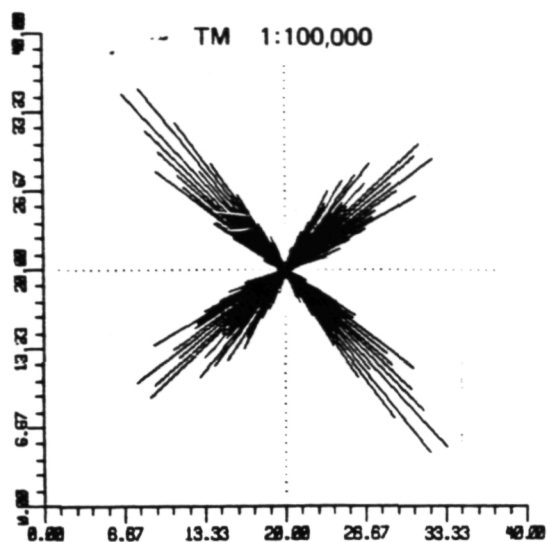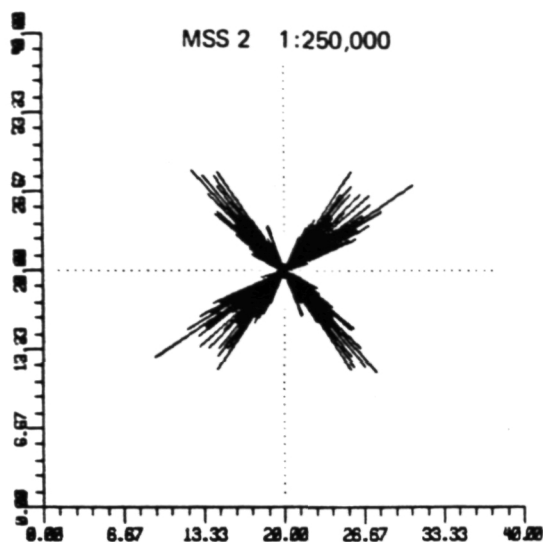
Figure 38   Rose diagrams showing cumulative length distributions for data from combined interpretations of interpreters R and S.

174
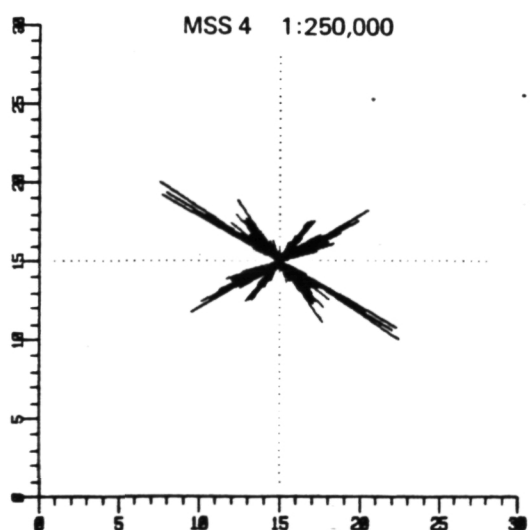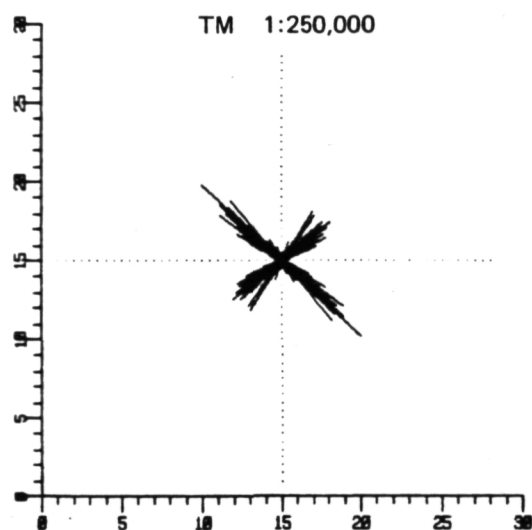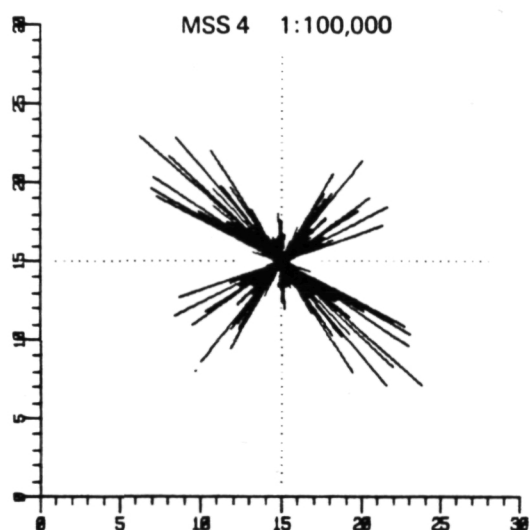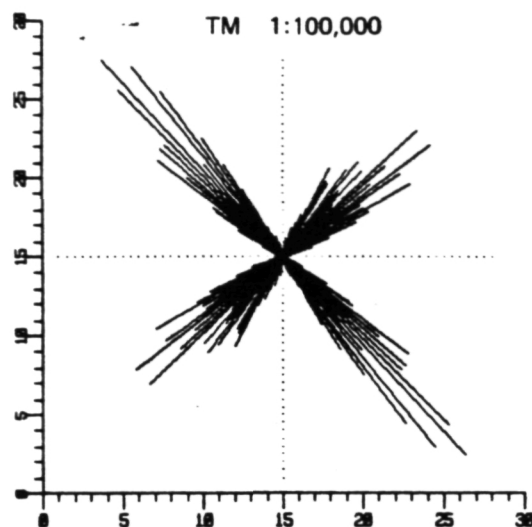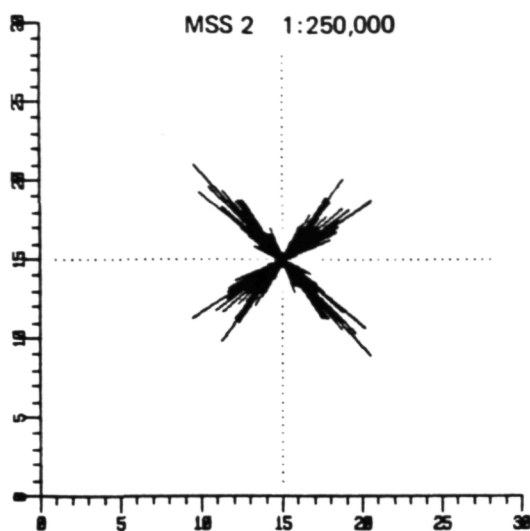
Figure 39   Rose diagrams showing frequency distributions for data from combined interpretations of interpreters R and S.
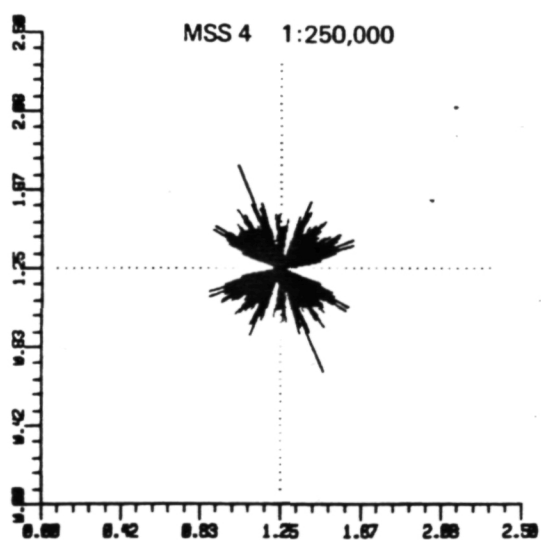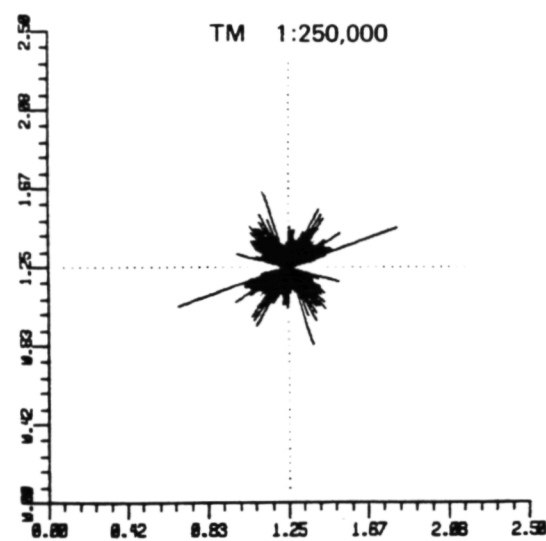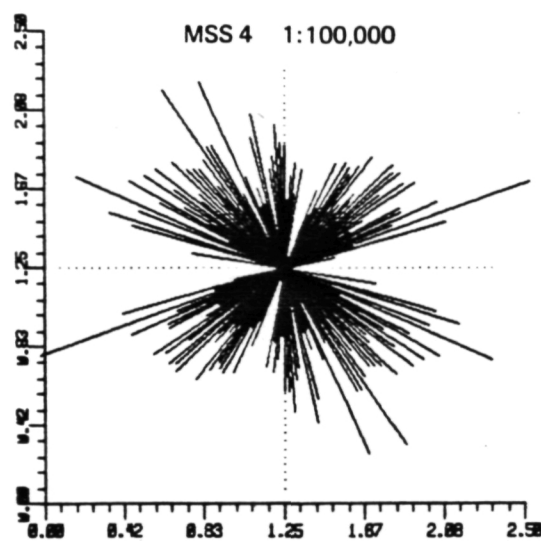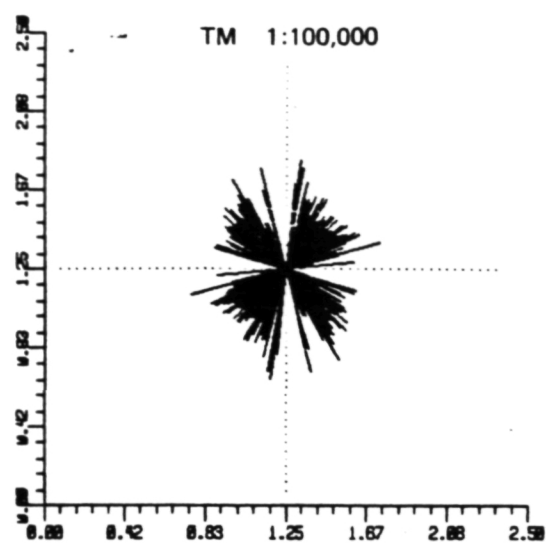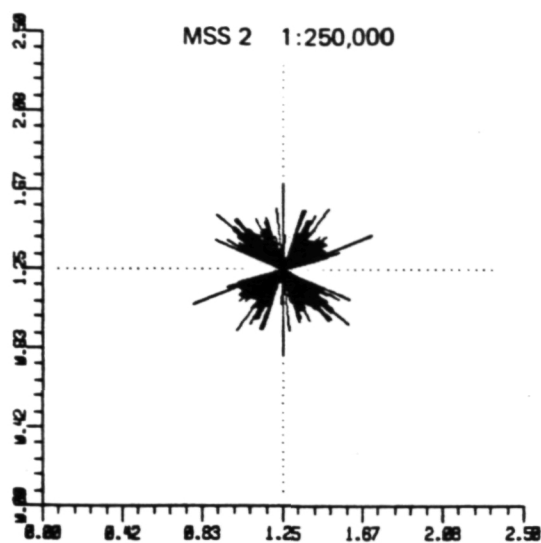
Figure 40   Rose diagrams showing average length distributions from combined interpretations of interpreters R and S.
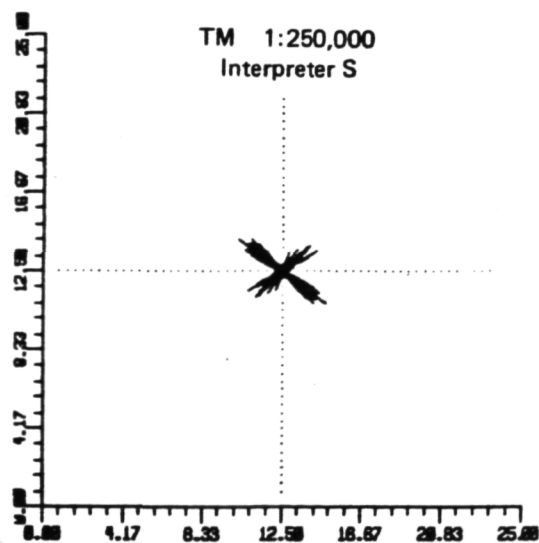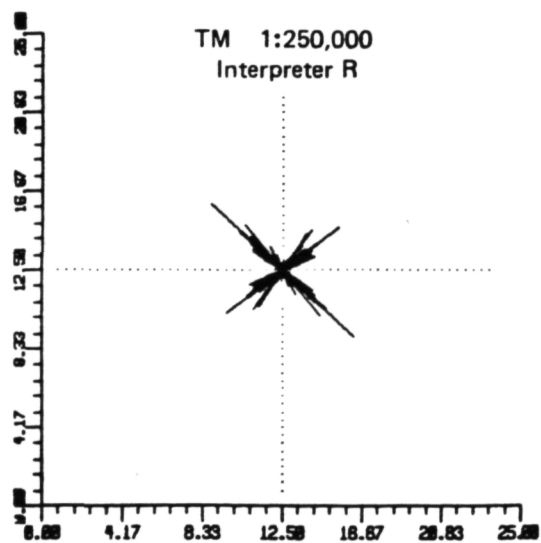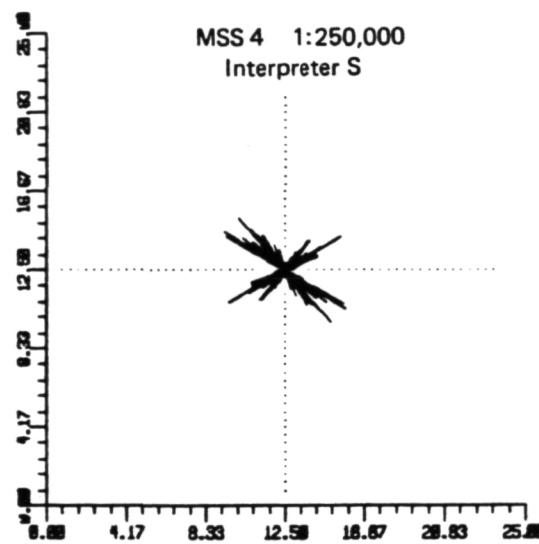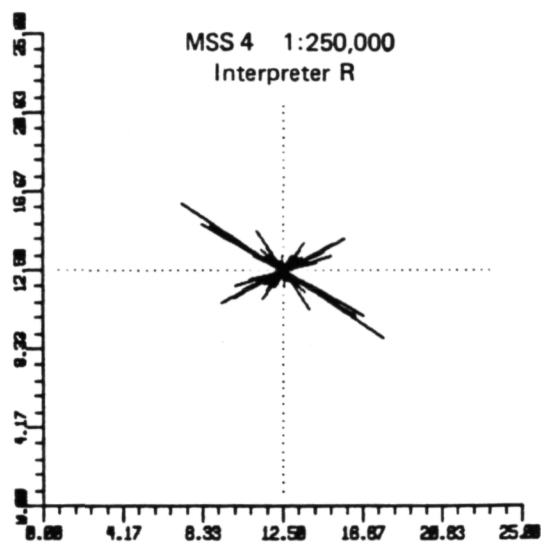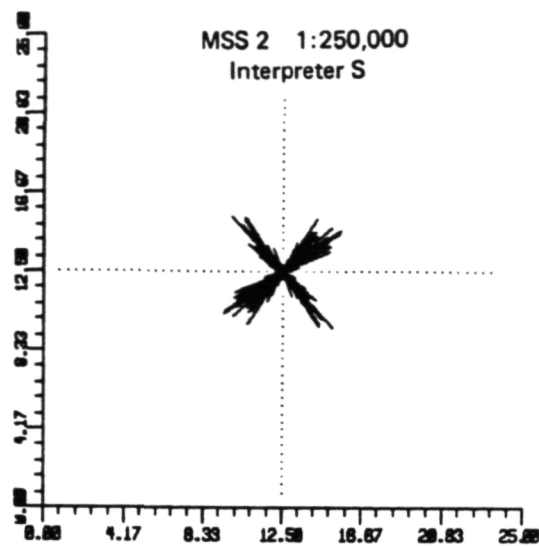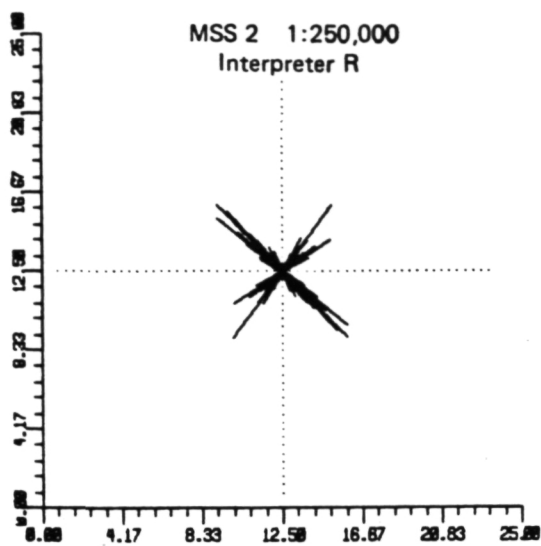
Figure 41   Rose diagrams showing cumulative length distribution for
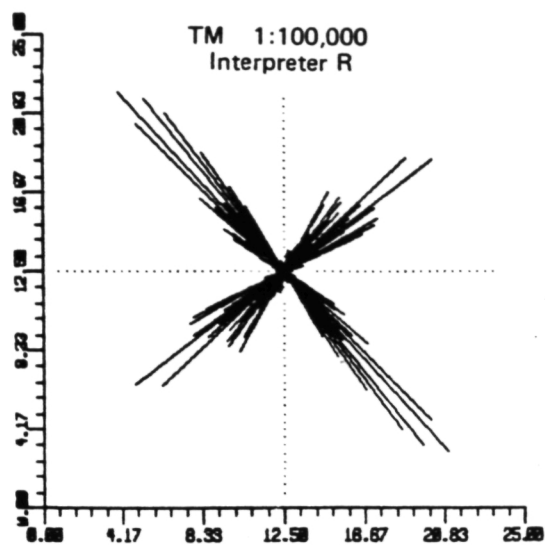independent interpretations of interpreters R and S.
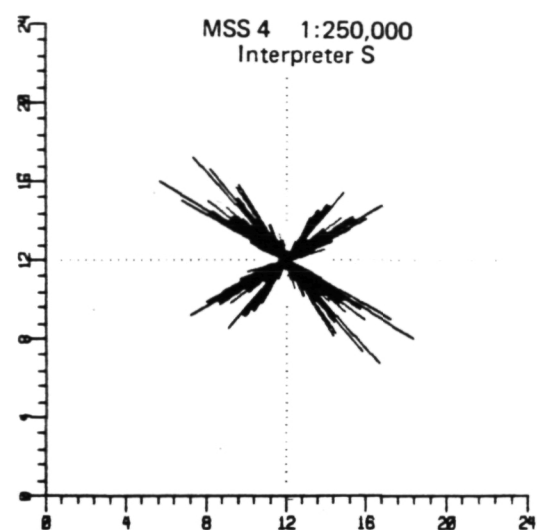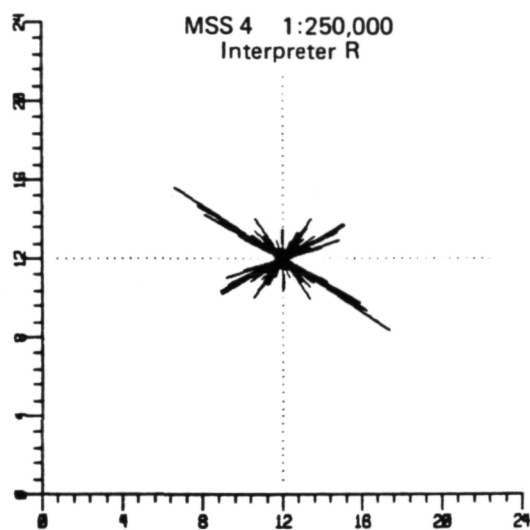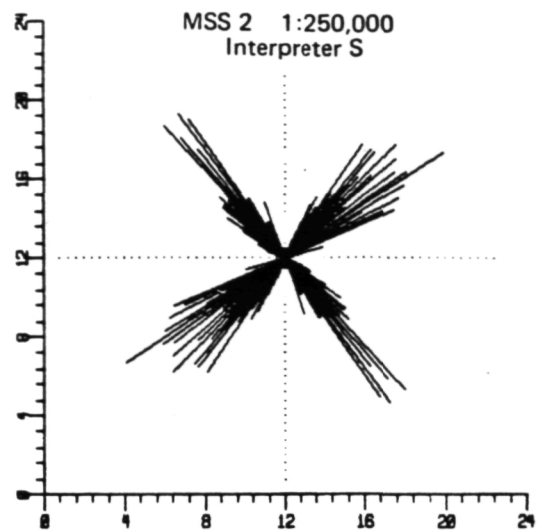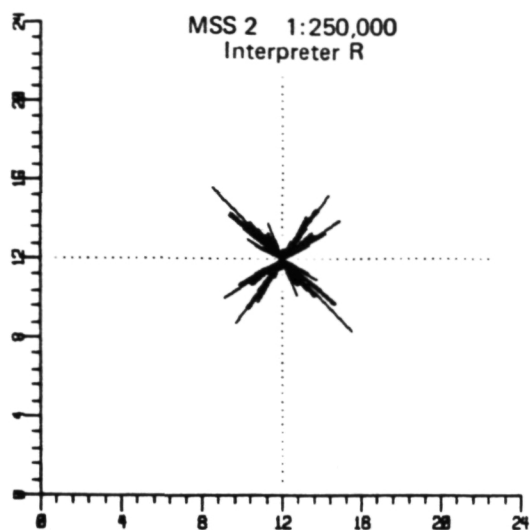
177
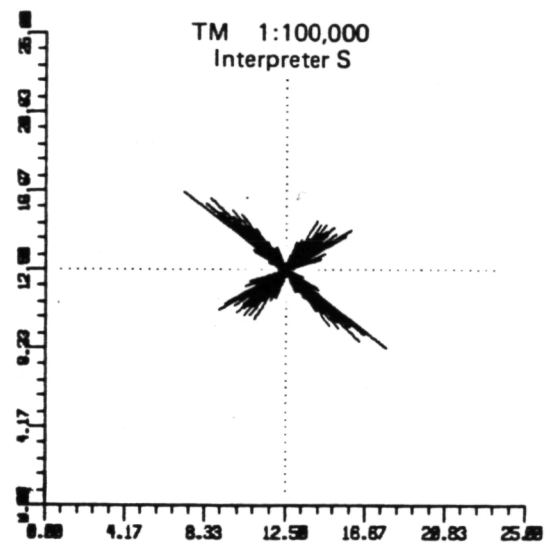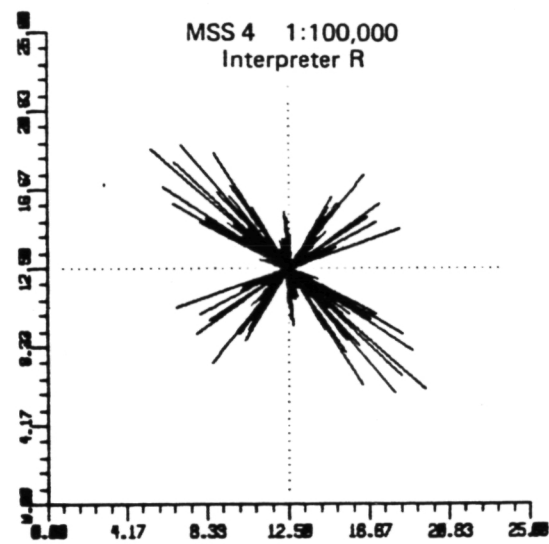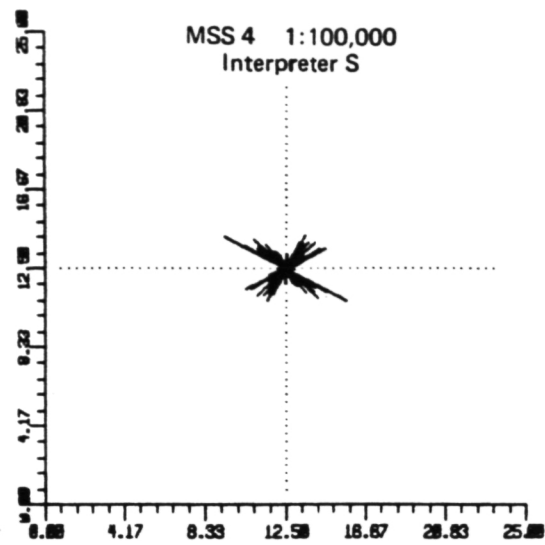
Figure 41 (continued)
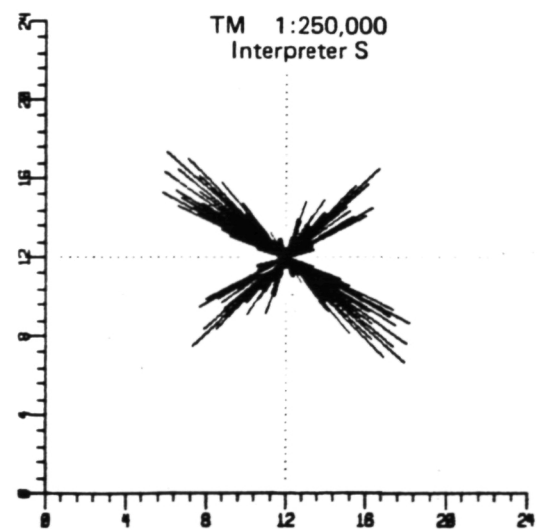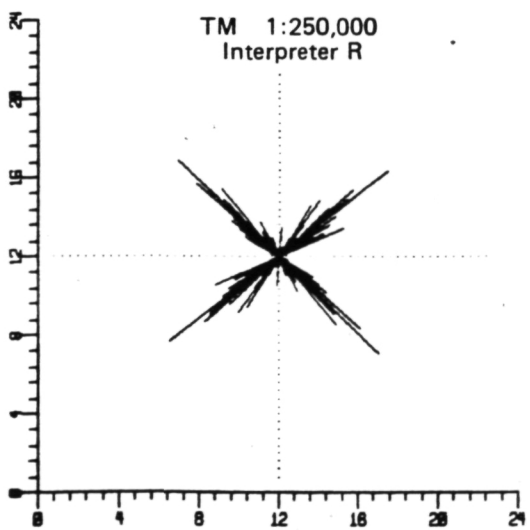
Figure 42   Rose diagrams showing frequency distributions for
independent interpretations of interpreters R and S.

Figure 42   (continued)

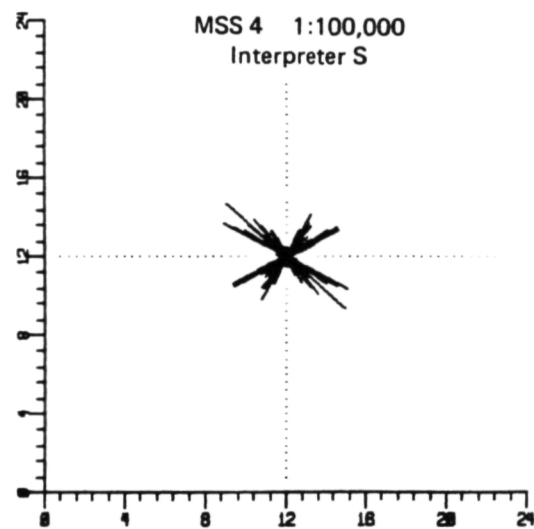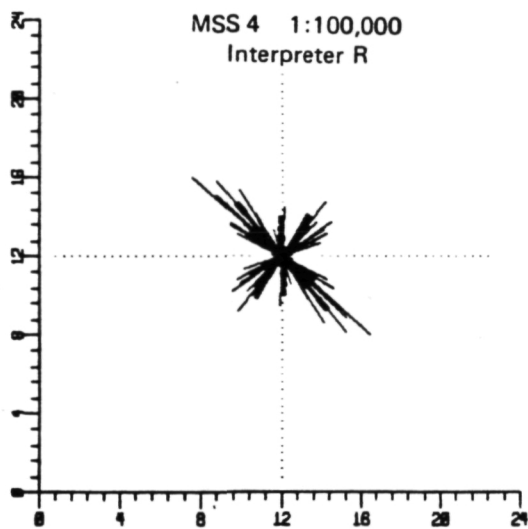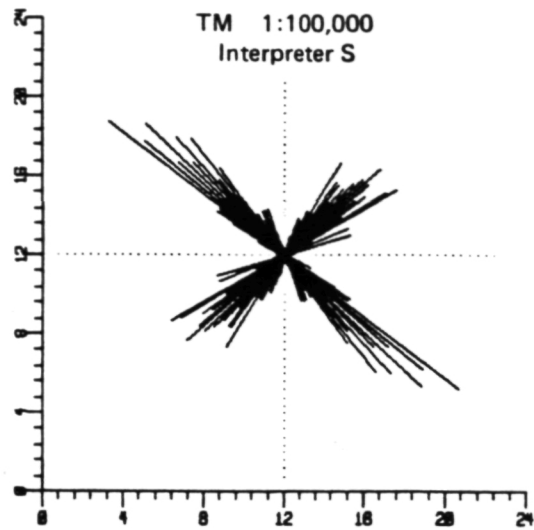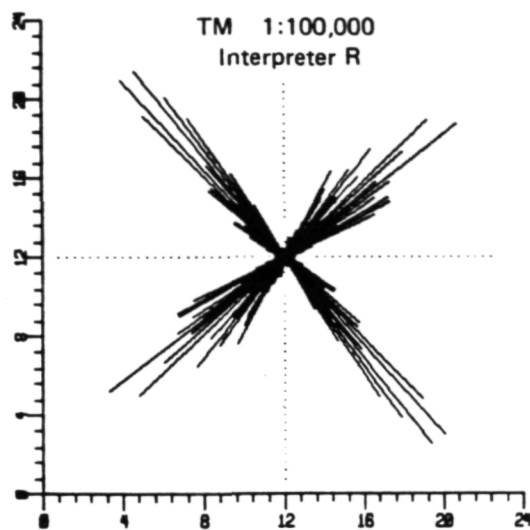| Plot Type	Axis Units
Rose diagram (cum. length)	map length (inches)
Rose diagram (frequency)	total number of lineaments (dimensionless)

In analyzing the distribution summaries, it should be noted that map inch measurements reflect the two different scales used in the study. Thus, one inch at a scale of 1:250,000 equals 2.5 inches at 1:100,000 scale.

Other products derived from the digital exercise include maps of the digitized lineaments representing both geologists interpretations compiled using a different line type for each interpretation. These maps were generated using scaling factors to a common 1:250,000 scale. Registration features were included in bold lines to facilitate comparison between the maps of each image product.

Table 9 is a summary of the cumulative length values, frequency values and their sums for each interpreter and each image product. The combined sum is the number and length of lineaments represented on the digitally derived maps and on the series of rose diagrams summarizing the data combined from both independant interpretations of each image product.

TABLE 9: SUMMARY OF CUMULATIVE LENGTH VALUES, FREQUENCY
VALUES, AND THEIR SUMS FOR EACH INTERPRETER AND IMAGE PRODUCT

Sensor	Interpreter	Frequency	Cumulative Length (Map Inches)
MSS 2 1:250,000	R	158	134.03
	S	445	187.49
	COMBINED	603	321.52
MSS 4 1:100,000	R	222	372.17
	S	143	113.22
	COMBINED	365	485.39
MSS 4 1:250,000	R	164	127.84
	S	311	160.46
	COMBINED	475	288.30
TM 1:100,000	R	429	386.80
	S	408	235.54
	COMBINED	837	622.34
TM 1:250,000	R	211	128.41
	S	369	120.41
	COMBINED	580	248.82

From the above table it is possible to determine a trend
concerning the length and frequency of lineaments generated by
the two interpreters. While interpreter R may map fewer
lineaments than interpreter S, the disparity is frequently
compensated for by the difference in lineament length mapped by
the two interpreters. For example, notice that in the TM
1:250,000 scale data set, the R and S interpretations resulted
in a virtually identical cumulative length of lineament (Figure
41), even though interpreter R only mapped about 60% of the
number of lineaments mapped by interpreter S (Figure 42). The
average length rose diagrams (Figure 40) for this data set are

a graphic illustration of this point, since the overall size of
the average length rosette for interpretation R is larger than
for interpreter S.

Table 9 also shows that between the MSS 4 1:250,000 scale
and TM 1:250,000 scale data sets, cumulative length is
approximately equal but frequency or number of lineaments is
much higher for the TM intepretation. This is an indication
that an interpreter would tend to map shorter linear feature
segments on the higher resolution TM data. This relationship
holds true for the 1:100,000 scale interpretation as well, and
points to the superiority of MSS data for regional mapping and
TM for more detailed work. Combining the results from the two
interpreters for each sensor and image product also gives the
same result.

In all of the data sets, the distribution of lineaments is
nearly identical between the two interpreters, although
differences in distribution are apparent in certain data sets.
For example, the TM 1:250,000 scale data set shows greater
spread of lineament distribution around two principal compass
directions: N50E, and N50W. Thus, although the two
interpreters mapped the same overall cumulative length, the
axial length (length of a single axis) of the S set is half of
the axial length of the R set (Figure 41) because more of the
cumulative length is dispersed around the principal directions
rather than being concentrated in a narrow range of compass
direction. Examination of the map representations of the data
reveals that many lineament trends are identified by both
interpreters, although they do not always lie spatially in

exactly the same location. On the whole, though, the

distributions of lineaments in both interpreters' data sets is

remarkably consistent.

Evaluation of the common axis projected rose diagrams for

the combined data sets (Figures 38 and 39) removes the

interpreter bias in the interpretation by combining both

interpretations into a single file. The combined distribution

summaries reveal distinct consistency between all of the data

sets. Perhaps the most noteworthy similarity between the data

sets is the virtual absence of lineaments interpreted in the

compass orientations of plus or minus 15 degrees around due

east-west. Secondly, the combined data sets show a distinct

bimodal distribution centered around the compass orientation of

N50W and N45E in each of the five sensors utilized.

It is suggested that these two distinctive components of

the lineament distributions are the result of several factors

related to the geology of the study area as well as to general

interpretive issues. First, the geological structure of the

region is dominated by major continental scale lineaments

trending generally westnorthwest and northeast. These include

the Texas and Wichita Lineament directions which trend about

N70W, the Nemaha Trend (N15E) and the Colorado Lineament

direction (N50E). These features control structure on a

continental scale, but may also have complex implications at

the smaller scale of the study area. There are two northeast

trends represented in the regional geology, and on many of the

rose diagrams, a distinct bimodal distribution of the northeast

quadrant lineaments is apparent. This is particulary well

expressed in the MSS 4 1:250,000 scale data set (Figure 38), where the two modes of northeasterly distribution are centered around N35E and N60E. It is noteworthy that the smaller scale 1:250,000 imagery expresses this continental scale distribution of northeasterly bimodality better than the 1:100,000 scale imagery interpretations. The apparent discrepancy between the rose diagram directions and the continental lineament directions may be a result of local smallscale rotation or similar smaller scale variation from the continental features.

The other factors affecting the absence of lineament distribution in the east-west orientation and, to a less obvious extent, in the north-south direction are probably artifacts of the sensor and of the land grid prevalent in the study area. Both MSS and TM imagery display scan lines that are oriented about N80W, which tend to give a false lineation in that orientation unless an interpreter carefully screens out this artifact from his interpretation. The scan line suppression routinely applied to the processing of the imagery helps to minimize the effect of scan lines, but does not entirely remove the problem. Consequently, the process of interpreting scanner imagery often results in overcompensatory avoidance of lineaments along the scan line direction, and could account for the absence of lineaments mapped in the N80W orientation. For similar reasons, interpreters tend to avoid lineaments oriented due north-south and due east-west because they are masked by the artificial lineation imposed by land line surveys as the Township and Range system used in the study area.

As noted in Table 9, three different MSS products were interpreted over the Cement, Oklahoma Study area. They were Landsat-4 1:100,000 and 1:250,000 scale and Landsat-2 1:250,000 scale images. The Landsat-2 data were included in this comparison to provide a corroborative data set for the Landsat-4 MSS data thus increasing the validity of comparisons drawn between the two remote sensing systems. Moreover, the Landsat-4 MSS data set is apparently more noisy than Landsat-2 data. The results of the interpretation of the data for the MSS 1:250,000 scale imagery perhaps reflect the difference in quality of the two data sets. For a given interpreter, the rose diagram plots show that different directions were predominant for both the length and frequency plots. In addition, the overall distribution between the two data sets is noticeably different. However, given any individual data set, there is substantial correlation between the interpretations of the two interpreters with respect to compass direction. The individual differences remain, however, where intepreter R tended to see fewer but longer lineaments than interpreter S.

The overall reaction of the two interpreters to the different image products was similar, differing only slightly in emphasis. Both interpreters thought that the detail in the TM data was far superior to that of the MSS. This increased detail allows better interpretation or definition of geomorphology as well as small-scale structural features. In an area such as Cement and Velma, a detailed understanding of the geomorphology can substantially enhance understanding of structural relationships.

Additionally, both interpreters felt that the TM data do not and should not replace the MSS data in a regional exploration program. The MSS can be used to faciliate regional geology and structure more easily and cheaply than TM data. Because TM data has better resolution, interpretation of the data tends to produce substantially shorter line lengths. Although these shorter lines or linear features are what actually comprise that which we know as regional lineaments and structural features, it can be difficult to connect them to get the overall regional picture provided by the more easily mapped throughgoing features that are readily seen on the lower resolution MSS data. In essence, this problem is similar to the "not being able to see the forest through the trees" adage.

TM data, on the other hand, are far superior to the MSS data for detailed work in local areas. In a large multi-frame program, the best way to proceed would be to use MSS for the regional view and to locally augment with TM data in areas of high interest. Besides providing a more readily available regional story, this approach can provide significant dollar savings in large areas when the price differential between TM and MSS data is considered.

4.5 Lithological Discrimination - Death Valley, California

Landsat-4 TM CCT's for the Death Valley, California scene were not included by NASA as part of this study. The data were purchased separately by EarthSat in the early months of the project. There is precious little potential for oil and gas

-187-

accumulation within this area. However, we felt that the near total lack of vegetation and the wide variety of exposed rock types offered an excellent data set with which to assess the utility of TM spectral data to discriminate between exposed surface lithologies. The results of this assessment demonstrated clearly that, in areas of good exposure, the TM data were able to provide clear and useful discriminations between juxtaposed rock types. Discriminations were based mainly on the iron content, clay content, total albedo, topography, and weathering textures.

The following discussion of the regional geology is drawn largely from the works of Hunt and Mabey (1966), Hill and Trexel (1966), and Burchfiel and Stewart (1966).

4.5.1 Regional Geology

Death Valley is located in southeastern California at the south edge of the Great Basin (Figures 43 and 44). The valley and the surrounding mountains have been the site of three major depositional episodes -- one during late Precambrian time, another during the Paleozoic, and a third during the early part of the Mesozoic Era.

During the Late Cretaceous the southern Great Basin was part of the Sevier orogenic belt. Rock units in this area were folded, thrust faulted, and invaded by granitic intrusions, shedding sediments to surrounding regions. Later, in the middle and late Cenozoic, the southern Great Basin became fragmented by both high- and low-angle block faulting into basins and ranges.
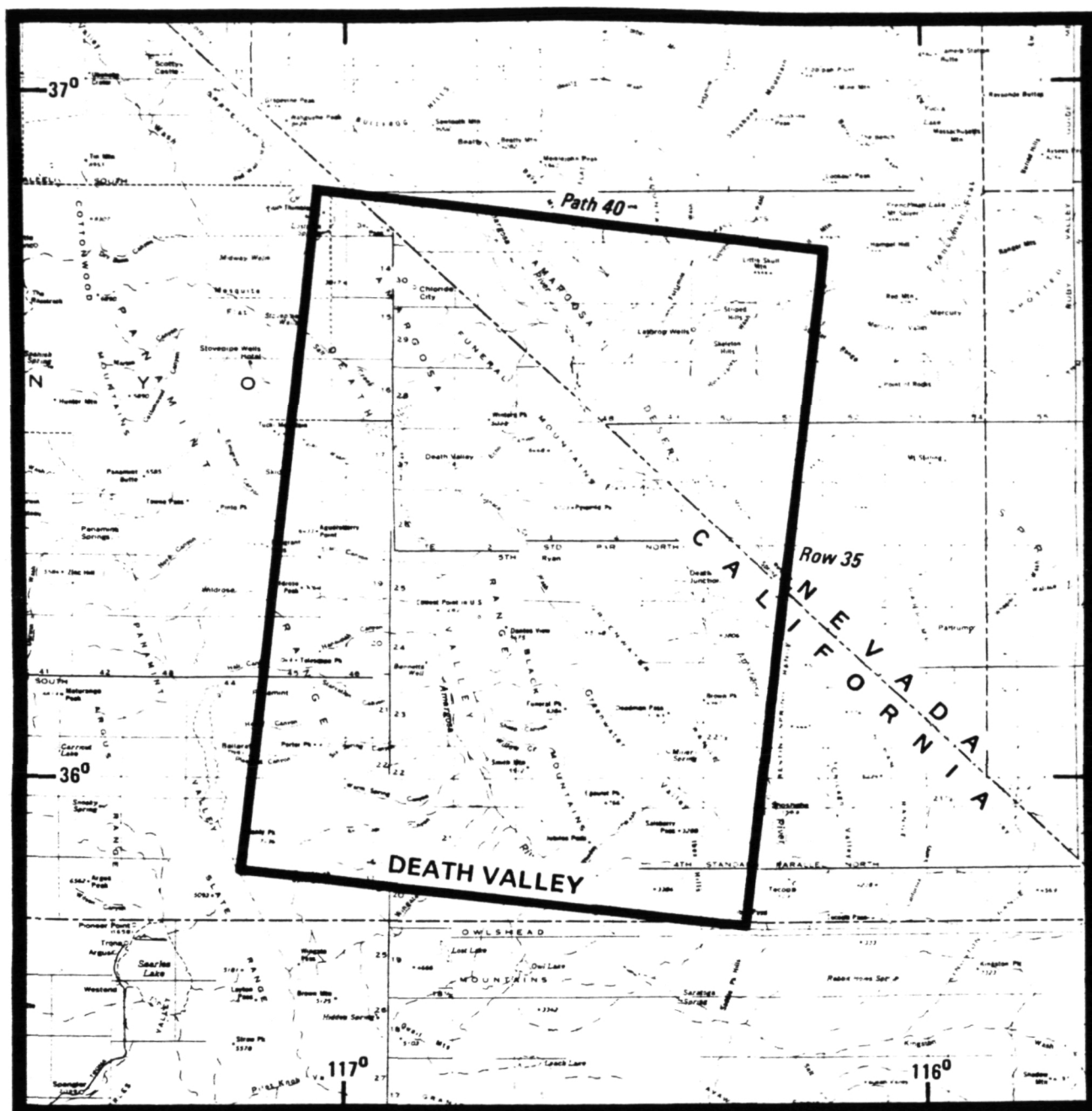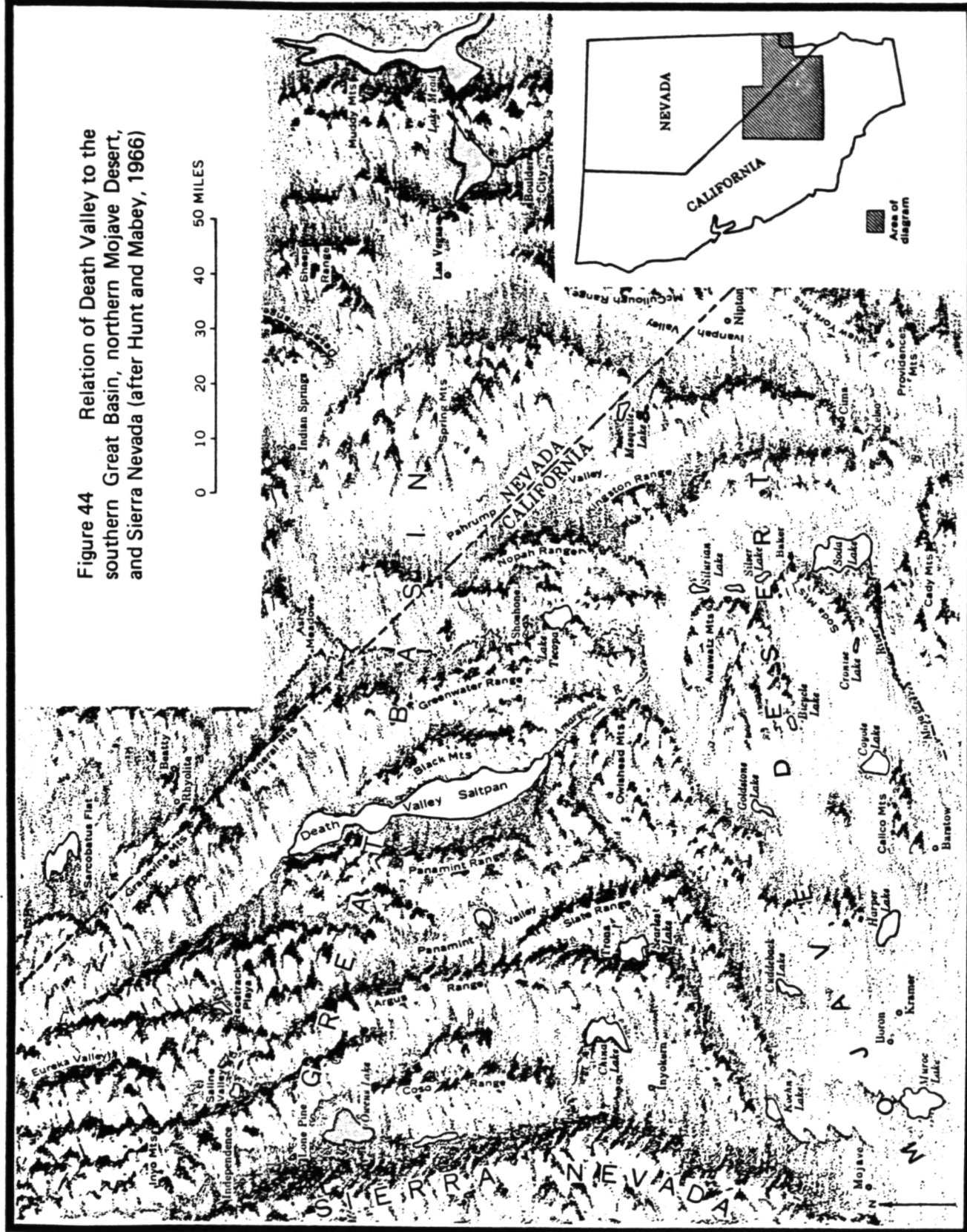
Figure 43   Death Valley, California and Nevada, location map

Region delineated is the area covered by Landsat 4 frame 40124-17495,
17 November 1982, Path 40/Row 35.

189

Figure 44   Relation of Death Valley to the southern Great Basin, northern Mojave Desert, and Sierra Nevada (after Hunt and Mabey, 1966)

190

Precambrian rocks are in three major groups. The oldest are crystalline metamorphic basement rocks representing the complex that have a structural and topographic relief of more than 900 m.

Overlying the basement complex is the Pahrump Series, which comprises much younger and only slightly metamorphosed clastic sedimentary rocks, with rare interbedded limestone and dolomite. This series is at least 3,000 m in thickness. They are not exposed one above the other in this area, rather their stratigraphic position is inferred from known relations elsewhere. Westward across the Panamint Range, each of the three formations of this series overlies metamorphic basement, probably as a result of thrust faulting rather than stratigraphic changes.

The third and youngest group of Precambrian rocks are clastic sedimentary units interbedded with dolomite and some limestone. These rocks are slightly less metamorphosed than those of the Pahrump Series. These units lie below the Olenellus fauna, which is taken to mark the base of the Cambrian. They have a total thickness of 2,000 m.

An unusually complete stratigraphic section of Paleozoic units are exposed in Tucki Mountain where 6,000 m of rocks ranging in age from Early Cambrian to Permian are found. The Lower Cambrian formations are mostly clastic sedimentary rocks. The rest of the Paleozoic units are chiefly limestone and dolomite. Permian rocks include much conglomerate and breccia derived from eroded Devonian and Carboniferous units. This is

a direct result of tectonic deformation during the latest
Pennsylvanian and Permian time.

At the south end of the Panamint Range, Triassic units
total 2,400 m in thickness. These units are composed of
volcanic and clastic sedimentary rocks, and represent a return
to conditions like those of the Precambrian. Moreover, the
thick remnants of the Triassic, like the thick remnants of the
Precambrian Pahrump Series, are restricted to a northwest-
trending belt approximately coinciding with the edge of the
Sierra Nevada batholith.

Two granitic intrusions lie within the mapped area.
They are referred to as the Hanaupah Canyon and Skidoo
granites. They probably are floored intrusions that spread
laterally along thrust faults and domed up the rocks of the
thrust plate. Batholithic intrusions along the Sierra Nevadas
are Latest Jurassic through Cretaceous in age. The granitic
intrusions in the Death Valley area are closely related to
middle Tertiary silicic volcanism.

Evidence for a close relationship between the granitic
intrusions and volcanism in the Death Valley area is found
along the hypothetical westward extension of the Amargosa low-
angle normal fault at the eastern edge of the Panamint Range
(this structure has classically been known as the Amargosa
Thrust, however, recent work by Stewart has demonstrated that
this structure is more correctly interpreted as a low-angle
normal fault). Precambrian augen gneiss cut by a granitic
intrusion and a swarm of still younger dikes underlies this
normal fault. A similar augen gneiss and similar granitic

intrusions underlie the Amargosa low-angle normal fault at the Virgin Springs district 32 km to the southeast across Death Valley. Zircons in the Precambrian rocks differ from those found in the dikes, and the granite contains both kinds of zircons.

Overlap of lavas and associated eruptives onto Paleozoic rocks of the Panamint Range shows that the eastward tilting of the range occurred half before, and half after, the eruptives were deposited.

The volcanic rocks along the belt of the Amargosa normal fault complex are Tertiary, as is indicated by the stratigraphy of the very similar volcanic rocks in the Tertiary formations along the east and north sides of Death Valley. Tertiary formations in the Black Mountains east of Death Valley are at least 3,700 m thick. The older deposits, volcanics 1,500 m thick in the Artists Drive area, are quite like those above the Amargosa normal fault. They are faulted onto the Precambrian core of the mountains. Northward these volcanics grade laterally into playa and other sedimentary deposits. They dip northward and thin under a syncline separating the Black and Funeral Mountains, and are tentatively correlated with it. In the trough of the syncline is the Furnace Creek Formation of Pliocene age, which is capped by, and intertongues with, the late Pliocene and early Pleistocene (?) Funeral Formation. Between the outcrops of the Furnace Creek and Titus Canyon (?) Formations is a faulted belt of different-looking sedimentary deposits which, on the basis of structural position, are assumed to be of an intermediate age and accordingly designated

Miocene.

The oldest deposits in Death Valley, classed as
Quaternary, are cemented fan gravels included with the Funeral
Formation. In places the Funeral Formation is conformable on,
and intertongues with, the playa deposits of the Furnace Creek
Formation of Pliocene age, but more commonly the Funeral
Formation rests with an angular unconformity on the older
rocks. The Funeral Formation has been displaced thousands of
feet by faulting and tilting during the late stages in the
structural development of Death Valley and the bordering
mountains.

Subsequent to most of that deformation, huge gravel fans
were built from the mountains to the floor of the valley. Some
of these are 10 km long and more than 300 m high. The oldest
of these fan gravel deposits, referred to as the No. 2 Gravel,
still has a distinct fan form which the older Funeral Formation
has lost because of deformation and erosion. Both the No. 2
Gravel and Funeral Formation have smooth surfaces of desert
pavement. Boulders and cobbles on these surfaces are deeply
weathered and have disintegrated to produce a new mantle of
angular rock fragments. The No. 2 Gravel is surely late
Pleistocene in age, but it may be pre-Wisconsin.

Other deposits of late Pleistocene age include a debris
avalanche at the front of the Black Mountains and some
isolated, poorly developed beach deposits of a late Pleistocene
lake, which had a maximum depth of about 180 m. The lake,
though, was of brief duration and evidently its level fluc-
tuated rapidly, so that beach deposits and other shore features

are poorly developed as compared with those around other Pleistocene lake basins in the Great Basin.

Younger gravels on the fans, referred to as No. 3, may include some late Pleistocene deposits and certainly include some Recent deposits.

Other deposits that may be of approximately this age are mounds of travertine at springs on the gravel fans. Some travertine, of course, is being deposited at present but the occurrence on these mounds of stone artifacts representing the earliest human occupation of the area indicates that the main parts of the mounds have considerable antiquity.

The youngest gravel on the fans, the No. 4 Gravel, is along the washes. These deposits are loose gravel composed of firm rocks without desert varnish.

On the 5/2 IHS imagery generated from the TM data (refer to Section 4.5.2.4) of the Death Valley scene, the spectral character of the gravels closely mirrors the spectral character of the rocks from which they were eroded. This, along with the geomorphologic information interpretable from the 10 m data, permits surprisingly accurate discrimination of the above gravel types.

During the Recent, but probably during the three millenia preceding the Christian Era, lakes flooded the floor of Death Valley to a maximum depth of 30 feet. The salt deposits comprising the saltpan were formed as a result of this lake.

The principal structural features of Quaternary age are (1) the north-south trough that is Death Valley and the border-

ing upfaulted mountain blocks; (2) the northwest-trending Furnace Creek fault zone and the downwarp that extends along Furnace Creek and northwestward across the northern part of Death Valley; (3) the northwest-trending Confidence Hills fault zone that extends into the south end of Death Valley; and (4) some features of Copper Canyon and Butte Valley. Deformation is going on at present, as indicated by measurable tilt at seven tiltmeter stations that have been established in the valley.

The composition and extent of the Furnace Creek Formation of Pliocene age indicate that it was deposited in a narrow trough that extended southeastward from Mesquite Flat across the Salt Creek Hills and Cottonball Basin and along the Texas Spring syncline and north end of the Black Mountains. The playas in which the formation was deposited existed long enough to accumulate 1,500 m of beds.

Much or most of the uplift of the Black Mountains occurred after the Furnace Creek Formation was deposited because the formation dips 45° or more off the north end of the mountains. Gravity data, however, indicate that the formation probably thins northward under the Texas Spring syncline, and presumably the thinning is by offlap from the mountains. If so, part of the uplift of the Black Mountains occurred while the Furnace Creek Formation was being deposited. It is inferred that roughly 1,200 m of uplift at the Black Mountains occurred while the Furnace Creek Formation was being deposited, and that another 1,000 m of uplift occurred in late Pleistocene and Recent time.

The Miocene (?) and older Tertiary formations exposed in fault blocks between the Funeral Mountains and the trough in which the Furnace Creek Formation was deposited are mostly coarse clastics that were derived from the Funeral Mountains. The mountains and the adjoining basin, therefore, were in existence in mid-Tertiary time.

The basins and ranges in this part of the Great Basin are at least as old as the Titus Canyon and Artist Drive Formations, although the structural limits of those basins and ranges probably were different from the present ones.

The structural history of the region during the Late Precambrian-Paleozoic depositional episode is obscure. The principal Cenozoic structural features are the westward-directed Amargosa low-angle normal fault and the chaos (breccia zone) that accompanies it, and smoothly exhumed surfaces of the low-angle normal fault locally known as turtlebacks, and the granitic intrusions that seem to have spread along the normal fault.

A short segment of the Amargosa normal fault is exposed along the east foot of the Panamint Range. The lower plate there, composed of Precambrian metamorphic rocks, is cut by a granitic intrusion. The metamorphic rocks include an augen gneiss; locally the augen are collected into small pegmatitic masses that grade into the dikes of Tertiary age that cut all the rocks in the lower plate. Part of the metamorphism of the lower plate of Precambrian rocks may have occurred at the time the granitic intrusion was emplaced.

The Paleozoic and Late Precambrian sedimentary rocks in the mountains bordering Death Valley occur in a series of fault-bounded slivers associated with the Amargosa normal fault system. Low-angle normal faulting moved younger rocks westward onto older ones. Within individual fault-bound slivers, rocks have uniform homoclinal dips, almost invariably to the east. The major structural units are grouped into four extensional allochthons and three window zones.

The most completely exposed area is at Tucki Mountain where Paleozoic formations ranging in age from Early Cambrian to Permian have been down-faulted toward the west onto the Klingston Peak Formation of Late Precambrian age. The extensional allochthon is further sliced-up by other low-angle normal faults that, toward the east, branch upward from the main one at the base. Along these branch faults the displacement is 6.5 km westward; along the main fault the displacement must be very much more than that.

The Panamint Range south of Tucki Mountain also is an extensional allochthon of east-dipping Paleozoic rocks down-faulted westward onto the Precambrian along the low-angle Amargosa normal fault which is exposed at the east foot of the range. Three Paleozoic formations in the upper plate dip east and rest on Precambrian metamorphic rocks in the lower plate. Other low-angle faults within the Paleozoic formations also seem to be branches extending upward from the Amargosa normal fault. Some of these branch faults are intruded by sills from the granite at Hanaupah Canyon.

The south end of the Funeral Mountains and the southern part of the Grapevine Mountains consist of extensional alloch-thons of Paleozoic formations thrust westward onto the Precam-brian. Between these two thrust plates is a structural window of Precambrian units forming the northern part of the Funeral Mountains. The two extensional allochthons may join under the Amargosa desert east of the Funeral Mountains.

A structural window in the northern part of the Funeral Mountains is formed by anticlinally domed Precambrian forma-tions. So also is the west side of Tucki Mountain, another window, and the Black Mountains. The uplift at the Black Mountains is divided into three structural windows, each a smooth-surfaced dome or turtleback. It is suggested that movement along extensional allochthons of the Amargosa normal fault tectonically denuded the turtlebacks.

Over the main part of the Panamint Range, Bouguer gravity-anomaly values are lower than over the mountains east of Death Valley and lower than those over the Slate Range to the southwest, suggesting that the Panamint Range is underlain by a granitic mass. In terms of deep crustal structure the geologic and gravity data suggest two possibilities. One is that deep under the Panamint Range is a large granitic intru-sion that connects westward with the Sierra Nevada batholith and forms a bulbous thickened edge of the batholith. A second possibility is that the edge of the batholith is in the area that is seismically active west of the Panamint Range and that the deeply buried granite is mostly Precambrian. By the latter interpretation the granites at Skidoo and Hanaupah Canyon, and

other granitic intrusions, could be attributed to palingenesis
of the Precambrian granitic rocks.

4.5.2 Geologic Observations Drawn From Specially Processed TM Imagery

The following sections will discuss each of the Thematic
Mapper image types generated for the Death Valley scene. For a
complete discussion of the image processing techniques, the
reader is directed to Section 3.3 of this report. To assist
the following discussion, a black-and-white (Plate 1) and a
color (Plate 2) collage of subsampled subscenes have been
generated from the Death Valley TM data. The Cotton and
Greenwater subscenes are sampled every other pixel on every
other line, creating a presented scale of 1:250,000. The
overview images (OV) on these two plates were sampled at
spacing of every 8th pixel on every 8th line, producing an
output scale of 1:1,000,000.

4.5.2.1 Natural and False-Color Composites

The natural (1,2,3) and false-color (2,3,4) composites
provide a clear, straightforward presentation of the visible
and near infrared spectral bands. When using the first four TM
bands, their extremely high degree of correlation in the Death
Valley scene (Table 5; in Section 3.3.1.1) creates very similar
looking natural and false-color imagery. The major differences
between the two are in their presentation of vegetation. In
the 1,3,4 false-color image, the presence of TM4 (IR band)
composited in red light causes the vegetation to appear as

various shades of red (compare the vegetation at the Furnace Creek Ranch on the northwest edge of the large alluvial fan on the Cotton subscene of Plate 2a).

Probably the most useful attribute of the natural color image is the ease in correlation of observed ground features with direct field observations. Both the natural and false-color image provide an excellent data base for photo-interpretation of lineaments, geomorphology, and other textural and spatial indicators of geologic structure and lithology. With the seven spectral bands of the TM system, six at 30-metre and one at 120-metre resolution, we are no longer constrained to the single available false-color composite of the MSS data. Rather there are a total of 35 possible three-band combinations of seven TM spectral bands, each with six color compositing permutations resulting in a grand total of 210 possible color images. This number is reduced somewhat by the observation that color permutations during compositing are usually most interpretable when the shorter to longer wavelength bands are composited with shorter to longer wavelength light (e.g., TM 1,4,5 composited as blue, green, red). This is not necessarily true when dealing with three IR bands; here we suggest that interactive analysis be used to select the most useful color permutations.

Using a determinant ranking method (see Section 3.3.1.1), we have selected the six TM band combinations determined to have the highest information content. The six color images of Plate 2b show the Cotton subscene of the Death Valley image color composited as each of these six combina-

tions. For comparison, we have also included the natural color (1,2,3) and the MSS-like false-color composite (1,3,4) on Plate 2a.

The Cotton subscene covers the northern half of the Death Valley Basin, bounded on the west by the Panamint Range and the northeast and east by the Furnace Creek and Black Mountains, respectively. To aid the location of significant features within the Death Valley Basin, the reader is referred to the 1:250,000 scale Death Valley sheet of the Geologic Map of California (Streitz and Stinson, 1974). The large conical fan in the upper center of the subscene drains the Furnace Creek Wash. On the northern edge of this fan is the Furnace Creek Ranch, the only major concentration of vegetation within the basin. The Panamint Range consists of Precambrian to Cambrian metasediments along the westernmost edge of the subscene. Two major outcropppings of eastward dipping Lower Paleozoic marine sediments overlie the metasediments. One lies just north of Tucki Wash in the northeast corner of the subscene, the other just to the south between Black Water Wash and Hanaupah Canyon (the Cotton subscene cuts this second, spectrally distinct outcrop off at the southern edge of the subscene along Death Valley Canyon). For convenience, we will refer to the northern and southern outcrops as the Tucki Mountain and Trail Wash sections, respectively. The Trail Wash section is further overlain along its eastern edge by three outcrops of Tertiary volcanics, hereon referred to as the Trail Volcanics.

In Plate 2a, the tight correlations (see Table 5) between the first four TM bands in the Death Valley scene create little spectral contrast when composited as the natural (1,2,3) or false-color (1,3,4) composites. Only the vegetation of the Furnace Creek Ranch shows as a marked spectral contrast on the 1,3,4 false-color composite. As noted in Section 3.3.1.1, these two band combinations placed 31st and 23rd, respectively, on the determinant rank information content list, leaving little question as to why they appear so spectrally flat. However, when the longer wavelength bands of the TM sensor are used, the spectral contrast between the lithologies becomes clearly apparent.

Referring to the 1,4,5 composite, note how clearly the Trail Mountain section is differentiated from the meta-sediments and the Trail Volcanics. When viewed on the single band prints of Plate 1a, the reason for the spectral contrast can be attributed to this unit's relatively high absorption of bands 5 and 7. Note that the detritus weathering from the Trail Wash section shows an extremely similar spectral character to the parent rock of the Trail Wash section. The increased absorption of the infrared bands 5 and 7 is most likely associated with an increased clay content within these units. The slightly younger section comprising the Tucki Mountain area shows a spectral character more similar to the Precambrian metasediments and is therefore believed to have a lower clay content than the older Trail Wash section. The Trail Volcanics are interpreted to have a higher surface iron content, which causes them to appear darker than the Tucki

Mountain section on all composites using bands 1 and/or 2

(bands characteristically suppressed by the presence of iron).

The best distinction of the Trail Volcanics from the Tucki

section is made on the 1,5,6 composite. The inherent lower

albedo of the volcanic rock has caused a higher thermal

emission, raising the gray level values of the TM 6 thermal

band and thus causing a distinct reddening on the color

composite.

Cross-referencing the different false-color composites

is a useful technique for lithologic mapping. However, without

question the most useful single image product for this purpose

in the Death Valley area was the 5/2 IHS image. The 5/2 IHS

image of the Cotton subscene is presented in Plate 2c. A

discussion of the geologic features identified on the 5/2 IHS

composite will be discussed at length in Section 4.5.2.4.

4.5.2.2 Principal Component Imagery

None of the subscene images presented on Plates 1 and

2 were processed as principal component imagery. For examples

of the imagery referred to in the following text, please refer

to the previously delivered principal component imagery of the

Death Valley scene. The color principal component imagery is a

popular approach to extracting geologic information from the

multispectral data. However, because of the nature of the

eigenstructure calculations, the directions of the individual

eigenvectors are data dependent. Therefore, the spectral res-

ponse of a given surface material cannot be reliably predicted

through interpretation of the principal component imagery.

The rationale for generating principal component imagery is that the decorrelated nature of the new eigenbands may provide color distinctions between areas that are strongly correlated in the normal TM color space. The advantages of this are immediately evident when comparing the principal component 1,2,3 composite with the tightly correlated natural 1,2,3 color composite.

A strong dependence on pixel albedo (total brightness) is a consistent characteristic of principal component imagery. Note, for example, that in the principal component 1,2,3 image, the shadowed areas consistently appear in various shades of green and the very bright areas appear in shades of blue.

The principal component 1,2,3 image contains a collective total of over 98% of the total scene variance (See Table 6; Section 3.3.1.1); whereas the principal component 4,2,3 image contains less than 17%. The similarity of the two images suggests that: 1) much of the unique spectral information is contained in eigenbands 2 and 3 (note that eigenband 3 is heavily weighted by the thermal band), and 2) the relative insensitivity of the human eye to blue light suppresses detection of contrast or information content between eigenbands 1 and 4 in their respective color composites.

It is our conclusion that the most useful geologic application of the principal component imagery is in mapping subtle differences between lithologies, vegetation cover, and other surface types in areas where the grosser, more generalized distinctions have already been drawn.

4.5.2.3 Thermal Band (TM6)

The thermal band (TM 6) of the TM system has a 120-metre pixel size, as opposed to the 30-metre resolution of the non-thermal bands. The TM 6 band is sensitive to radiation between 10.4 and 12.5 microns. Unlike the shorter wavelength bands, energy at these wavelengths is a measure of radiation that is emitted, rather than reflected, from the surface materials.

A subsampled version of TM 6 is presented, along with the first eigenband for comparison, at a scale of 1:1,000,000 on Plate 1d.

Although more experience is needed to fully understand the information content of the thermal data, it appears that the majority of the information in the Death Valley thermal imagery is in response to topography and reflective albedo. The topographic effects are obvious; the sunlight slopes are warmer (brighter), and the shaded sides are cooler (dark). The albedo effect is best seen in the highly reflective areas of the salt flats in Death Valley and in the dark low albedo alluvial fans and rock outcrops along the central portion of the lower edge of the image. Where the albedo is high, there has been near total reflection of the incoming sulight, and therefore, little absorption of the radiant energy. In the low albedo areas, a large percentage of the incoming sunlight has been absorbed and is being radiated back as longer wavelength thermal energy. The result is that low albedo surface

materials appear much brighter than high albedo surface
materials.

The use of TM 6 in color compositing has the serious
disadvantage of smoothing 30-metre spatial information due to
the larger pixel size (120-metre) of the thermal band.
However, referring to Plate 2b, the TM 1,5,6 false-color
composite shows a unique and useful representation of the
metasediment rocks of the Panamint Mountains. The pistachio
green rendition of these rocks is in response to their char-
acteristic low TM 6 and high TM 5 expression. It appears that,
in this example, the TM 6 is measuring a spectral characteris-
tic of the rock beyond a simple topographic or total albedo
effect.

4.5.2.4   IHS Imagery

The IHS method of image production is extremely useful
for merging data sets which possess different spatial and/or
spectral characteristics (see Section 3.3.1.3). For the Death
Valley scene, we have used the IHS approach to combine spectral
information, contained in ratio data, with the spatial informa-
tion inherent in the first eigenband. The approach is based on
using two ratio bands, one for each hue and saturation input,
and the first eigenband for the intensity input. The result is
an IHS image where the colors of the image are representative
of the spectral information contained in the ratio data, and
the topographic/structural information is representative of the
spatial information contained in the first eigenband.

We have produced two different versions of IHS imagery. Both have the same saturation and intensity inputs; the only distinction in the generation of the two is a difference in the hue inputs. The saturation and intensity inputs for both versions are the TM 5/TM 7 (1.60 /2.2) and the first eigenband, respectively. For hue inputs, one version uses TM 5/TM 2 (1.60 µ/0.56 µ), and the other uses TM 3/TM 1 (0.66 µ/0.48 µ). For simplicity's sake, we will refer to these as the 5/2 IHS and 3/1 IHS imagery.

The saturation input of TM 5/TM 7 was chosen for both versions because of this ratio's sensitivity to the presence of hydroxyl-bearing surface materials. In the presence of hydroxyl-bearing materials, the strong absorption of incident sunlight in the 2.2 micron wavelength range strongly depresses the TM 7 band. Therefore, the TM 5/TM 7 ratio displays characteristically high values. The presence of hydroxyl-bearing materials correlates well with presence of clay minerals and, especially in the case of Death Valley, gypsum and hydrated salts. It should be noted that water associated with vegetation will also create low TM 7 values; care must be taken in interpreting this ratio in the presence of vegetation.

The selection of the first eigenband as the intensity (i.e., brightness) input requires little explanation. By definition, the first eigenband is along the direction within the TM color space of maximum scene variance. When using only the first four TM bands, this falls along the direction of increasing albedo. Thus, projection of the TM pixels along the

first eigenvector creates a low-noise panchromatic image which contains the majority of the geomorphological, topographic and structural information.

The choice of the hue inputs was determined based on the intended application. Using the GEOMAS interactive image analysis system, the TM 5/TM 2 combination was selected empirically as the ratio combination which demonstrated the greatest variance between the largest number of rock types. Thus, using the TM 5/TM 2 as the hue resulted in an IHS image which was especially useful in discriminating between the various rock types on the basis of their spectral contrasts.

The TM 3/TM 1 hue input was selected specifically to map areas of anomalous concentrations of iron oxides. In the presence of ferric iron, due to absorption of light less than 0.55 microns in wavelength, TM 1 is greatly suppressed with respect to TM 3. Thus, where ferric iron is present, the TM 3/ TM 1 ratio value is anomalously large.

The individual IHS input bands are shown for the Greenwater and Cotton subscenes on plates 1b and 1c, respectively. The final 5/2 IHS and 3/1 IHS color imagery are shown in plates 2c and 2d for the Cotton and Greenwater subscenes, respectively. In both cases, the dynamic range of the hue input gray level values was constrained between output values of 0 to 170; with a value of 0 gray level mapping to blue, 82 gray level to green and 170 gray level to red. Therefore, when comparing the 3/1 ratio of Greenwater or the 5/2 ratio of Cotton with their respective color IHS images, the low gray level values will be bluish, the mid-values greenish, and the

high gray level values will be reddish. For the saturation inputs, low gray level values will be unsaturated (white, grays and pastels) and high gray level values will be fully saturated (bold colors).

5/2 IHS Imagery

We suggest comparison of this image with the 1:250,000 scale Death Valley sheet of the Geologic Map Series of California (Streitz and Stinson, 1974). Through comparison with the geologic map, some interesting examples of the unique information content of the IHS image appear along the northeastern flank of the Panamint Mountains, the eastern Funeral Mountains and the northern portions of the Resting Spring Mountains. The Lower Paleozoic marine section along the northeastern flank of the Panamints is clearly distinguished from the older metasediment section to the west. The small outcrops of Tertiary volcanics overlying the Paleozoic section are also clearly distinguishable. Note, however, that the Paleozoic marine section to the north (Tucki Mountain section) is spectrally "confused" with the Tertiary volcanics. The Tucki Mountain section is distinctly different from the Paleozoic sediments to the south of Black Water Wash (Trail Wash stratigraphic section), however, it is not immediately clear why its 5/2 ratio should be so spectrally similar to that of the Tertiary volcanics.

Along the eastern portions of the Funeral Mountains and within the Resting Spring Range, there are several examples of stratigraphic horizons which are clearly mappable on the 5/2

IHS imagery and have been grouped into the Cambrian marine unit on the 1:250,000 scale geologic map. Although such groupings are obviously necessary during geologic mapping, the ability to map the individual lithologic beds on the IHS imagery signifi- cantly augments the information available on the geologic maps. Note how the detritus eroding from the purple colored marine sections covering the Resting Springs Mountain so closely matches the spectral characteristics of its parent material.

3/1 IHS Imagery

In mineral exploration, the presence of surface iron oxides produced by the weathering of sulfide minerals is an important indicator of the potential for an economic mineral deposit at depth. A key distinction between such gossan deposits and an economically uninteresting sedimentary red bed is the association of the iron oxides with clay minerals produced during the alteration and/or weathering process. The MSS sensors were fairly capable in spectrally detecting the presence of ferric iron, however, they had no ability to detect clay minerals. Taking advantage of the 2.2 micron band (band 7) of the TM system, it is possible to generate ratios (typically 5/7) which are sensitive to the presence of the hydroxyl bonding associated with clay mineralogies.

In order to demonstrate TM's ability to detect gossan deposits, we have generated the 3/1 IHS image of a subscene at the south end of the Greenwater Range just to the east of Death Valley proper. This subscene, like the Cotton subscene, has been subsampled as every other pixel on every other line. The
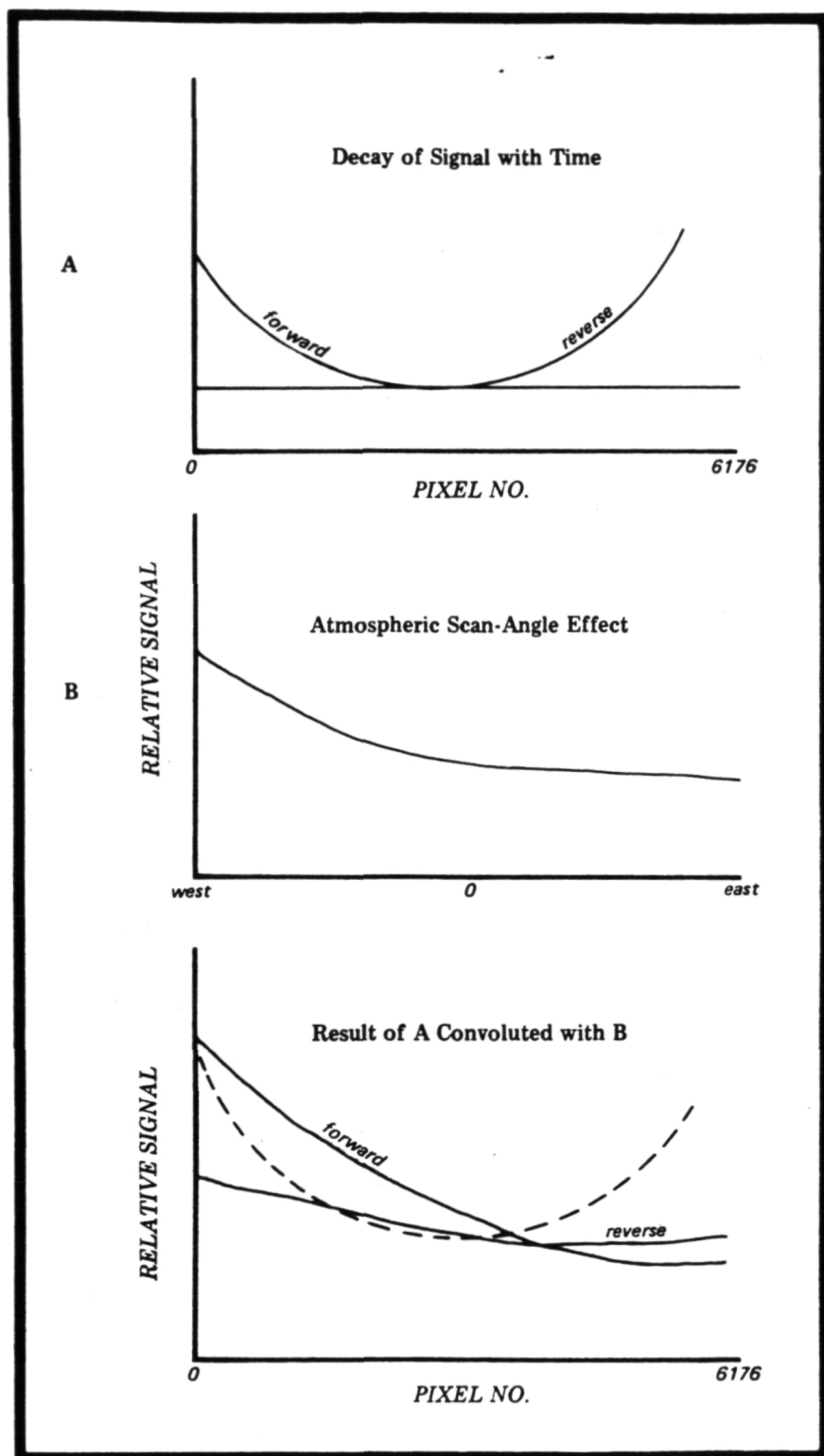
resulting image (labeled Greenwater on Plates 1b and 2d) covers

four times the area of an equal-sized full resolution image

with only a minor loss of spectral information. The individual

hue, saturation and intensity inputs for the 3/1 IHS image of

the Greenwater subscene are presented on Plate 1b. The full-

color Greenwater 3/1 IHS and the corresponding area as a 1,3,4

false-color composite are presented on Plate 2d. The 3/1

ratio, due to the anomalous absorption of band 1 by ferric

iron, will have high values over areas of ferric oxide concen-

tration. The hue input to the 3/1 IHS was set up such that

high ratio values will appear red, medium values green, and low

values blue. The saturation input is such that areas of clay

mineralogy, or other hydroxyl-rich materials, will be displayed

in high saturation. Therefore, gossan areas would be expected

to appear in red colors.

A portion of the southern Greenwater Range appears as

a triangular highland area protruding down from the north

central edge of the Greenwater subscene. The two southern

lobes of bright white rock (appearing identically on both the

3/1 IHS and the TM 1,3,4 false-color composite) have been

mapped on the 1:250,000 scale geologic quad of Death Valley as

Tertiary granitic rocks which have intruded on overlying

Tertiary age volcanic pile. Along the northern contact between

the intrusive and volcanic rocks is a well-defined zone of

bright reddish coloration on the 3/1 IHS imagery. The two

Greenwater zoom-3x subscenes are three times enlargements of

their respective Greenwater image types. In the enlargements,

the zone is clearly seen as a very probable site of an iron-

rich metasomatic mineral deposit associated with the emplacement of the Tertiary intrusive rocks. The red hue is indicative of the presence of ferric iron and the high saturation (bright red pixels) is strong evidence for the presence of associated clay mineralogies. Note how the altered materials are visible in the detritus eroding off to the southeast. In addition, there appears to be a similarly anomalous area just to the west-northwest.

5.0 ENGINEERING EVALUATION

The A-tape engineering study evaluates the potential and desirability of using various image processing techniques on a CCT A-tape in order to enhance the TM data for hydrocarbon exploration purposes. In short is it worth the effort to start with an A-tape rather than a P-tape? The P-tape is a radiometrically and geometrically corrected product, while the A-tape is only radiometrically corrected. Using the A-tape in these studies preserves the radiometric integrity of the data, since geometric corrections of bi-directional sampled data require resampling not only along the scan line, but across scan lines. Although NASA uses a 4 x 4 cubic convolution, one of the best methods available, for their resampling technique, mixing of detector data within a swath (16 detectors in one direction) and across swath boundaries will deteriorate individual detector histograms, compounding problems of applying individual gains and biases to a single detector. Additionally, the mixing of defective and/or dead detector data with good detector data introduces a systematic radiometric deterioration that is impossible to correct. Another possible detrimental contribution to radiometric deterioration is the asymmetric effect of skylight on the forward and reverse swaths. At the end of each swath, preceding the next swath, each detector goes through a direct current (DC) restore cycle, charging a bias capacitor which should have a time constant that is long with respect to the swath time. Previous experimental studies have shown that this time constant may not be long with respect to the swath time. The resulting effect is an asymmetric decay in the DC bias which, when convolved with the asymmetric skylight effects, gives a nonlinear skylight effect in the forward vs reverse swaths. The effect is more pronounced in the west direction. Graphically, this is shown in Figure 1. For this reason, we chose to limit the geometric corrections done to

Decay of Signal with Time

A

forward   reverse

0   6176

PIXEL NO.

Atmospheric Scan-Angle Effect

B

RELATIVE SIGNAL

west   0   east

Result of A Convoluted with B

forward

reverse

RELATIVE SIGNAL

0   6176

PIXEL NO.

GR 5047

Figure 45   DC Bias Decay and Scan Angle Effect

215

the A-tape to simply shifting the reverse scan to bring it into a "best" fit alignment to the forward scan.

5.1 Character of A-tape

No geometric corrections are applied to the CCT A-tape. Radiometric corrections are made using the internal calibrator and/or scene histograms to adjust the estimated gains and offsets. Nominally, these gains and offsets are recomputed several times (typically 4) per scene. However, from the test tape available these values were the same per band through the scene, hence no segmentation was present. The current tape format contains information necessary to perform all radiometric and geometric corrections. Generally, these corrections use gains and offsets per detector per band to produce lookup tables that translate digital counts into pixel grey levels that are proportional to scene radiance. The CCT A-tape available for this evaluation was of an interim format (REV 0) which did not contain these gains and offsets, and as a result, preprocessing corrections by NASA could not be removed. The cumulative histogram matching algorithm developed by Earthsat differs from NASA's histogram normalization in that NASA uses estimated gains and biases calculated from the internal calibrator. These estimates can then be adjusted by an average-scene histogram computed from each of the 16 detectors. Each detector is thus normalized to the average histogram for that band and histogram normalized gains and biases are generated.

The EarthSat algorithm selects a detector to which all other detectors are normalized. In addition, the Earthsat algorithm expands the dynamic range of the data from (0-127) to (0-255). The

geometric correction data present, but not applied to the A-tape, consist of two types. The first type is the relatively constant correction parameters, including:

1. Band and detector offsets

2. Mirror velocity profile coefficients

3. Instrument and spacecraft parameter values

The second type of correction parameters consist of scene dependent constants, including:

1. Nominal World Reference System (WRS) scene location

2. Actual image center

3. Spacecraft heading

4. Earth rotation

5. Benchmark and High Frequency matrices

6. Mirror scan data

7. Nominal pointing vector and scan rate

8. Detector location data including adjustments for detector response times which are unique for each detector and scan direction

5.2 Character of P-tape

Radiometrically, the P-tape and the A-tape have received the same corrections. The difference then is that the P-tape has geometric corrections applied by a 4x4 cubic convolution.

5.3 EarthSat Experimental Program

Our engineering evaluation of A-tapes and P-tapes focused on Band 2 of a Washington-Baltimore scene (ID 40109-15140, 2 November

1982), using the interim revised A-tape format (REV 0). Striping
problems were most apparent in this band and band 1. Previous
investigators have reported band 2 anomalies, including low
frequency noise in detectors and odd/even detector correlation.
Full-scene histograms were generated and three windows were selected
to illustrate the maximum and minimum striping problems encountered
over the scene. A cumulative histogram matching algorithm was
modified to:

1.   Expand the dynamic range of the TM data from 7

     bits (0-127) to 8 bits (0-255)

2.   Normalize all 16 detectors to detector 6

     (see below)

3.   Eliminate detector 14 by averaging detectors 13

     and 15.

The three destriping variations of this algorithm chosen to process
each window were:

1.   Normalize forward swaths to detector 6 in the

     forward swath, and normalize reverse swaths to

     detector 6 in the reverse swath.

     (FWD-FWD,REV-REV)

2.   Normalize the forward swath to detector 6 in the

     reverse swath, and normalize the reverse swath

     to detector 6 in the reverse swath.

     (FWD-REV,REV-REV)

3.   Normalize the forward swath to detector 6 in the

     forward swath, and the reverse swath to detector

     6 in the forward swath.

     (FWD-FWD,REV-FWD)

Original P-tape data for three scene windows appear in Figures 46
through 49. Destriped windows appear in Figures 50-53. Since
contrast stretching accentuates striping effects, the same stretch
was applied to each figure. Striping is prominent in the low albedo
areas that correspond to wooded areas and the Chesapeake Bay. The
striping effect is minimized over small-scale land use activities
and high albedo urban areas. Each destriping technique visually
improved the area over water, while only a marginal improvement, if
any, can be seen elsewhere in the figures. The first cumulative
histogram matching variation (FWD-FWD,REV-REV) produced the most
improved image on a high resolution video monitor; however,
striping is still prominent.

5.4 Conclusions

Image processing using a full-scene cumulative histogram
matching algorithm is scene and band dependent. Band 2 represents
one of the worst cases, if not the worst, and as a result, shows the
greatest improvement. However, residual banding continues to occur
due to the restricted quantization range in band 2, and in other
bands would not appear to improve as much. Since the improvement is
largely cosmetic, that is, no additional radiometric detail has been
obtained, application of the destriping algorithm should include
weighing these considerations:

1. End use of product, such as photointerpretation
    or digital analysis

2. Usefulness of band 2 data for false-color
    composite, ratio, or IHS.
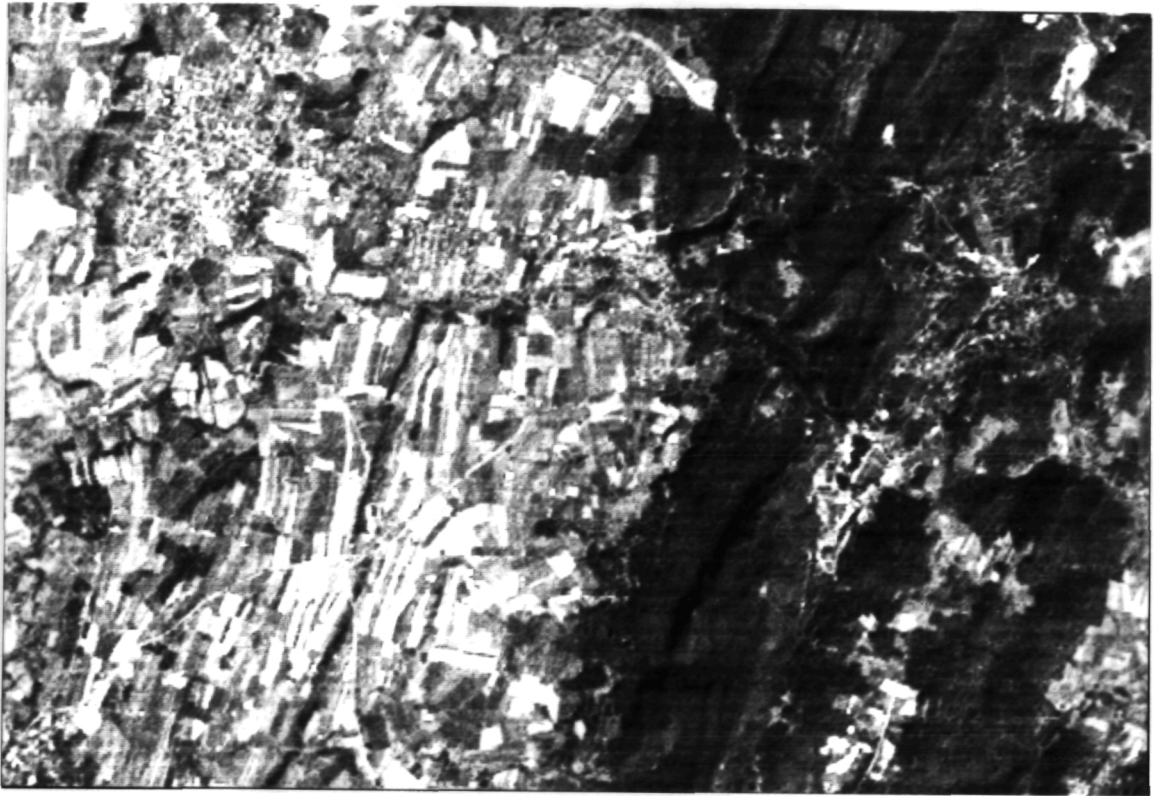
Figure 46   P-tape Window 1 (Contrast .7x)
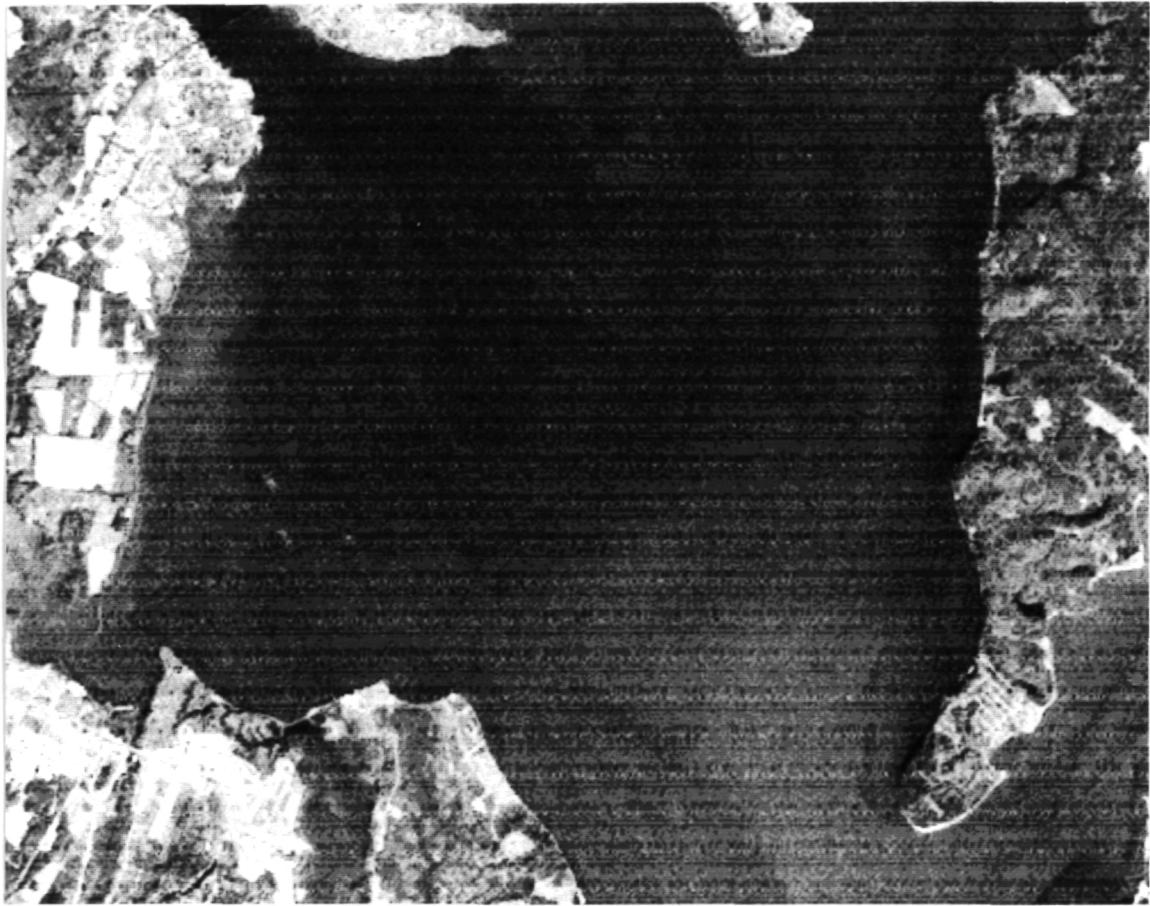
Figure 47   P-tape Window 2 (Contrast .7x)

Figure 48   P-tape Window 3 (Contrast .7x) (Baltimore)
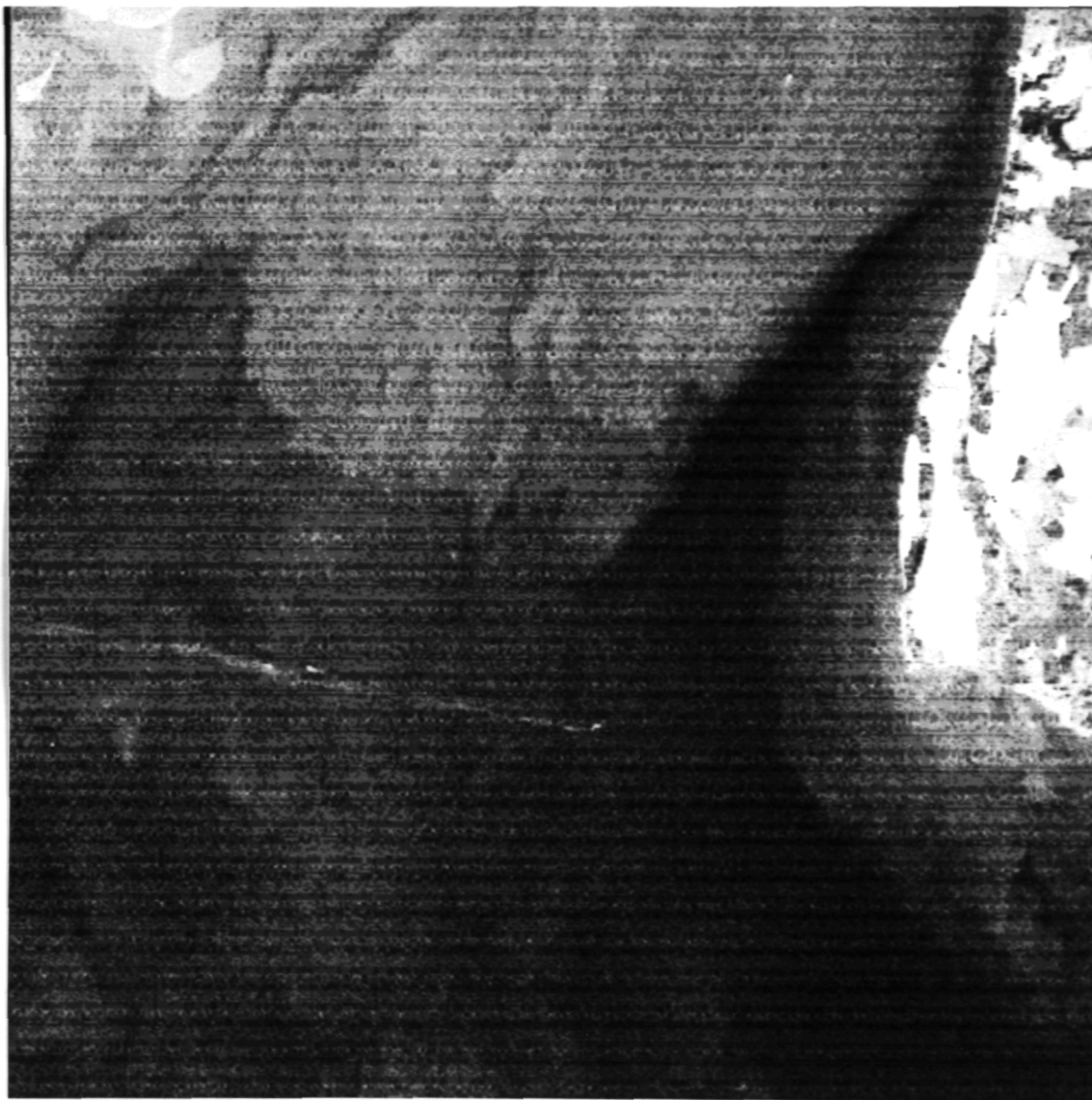
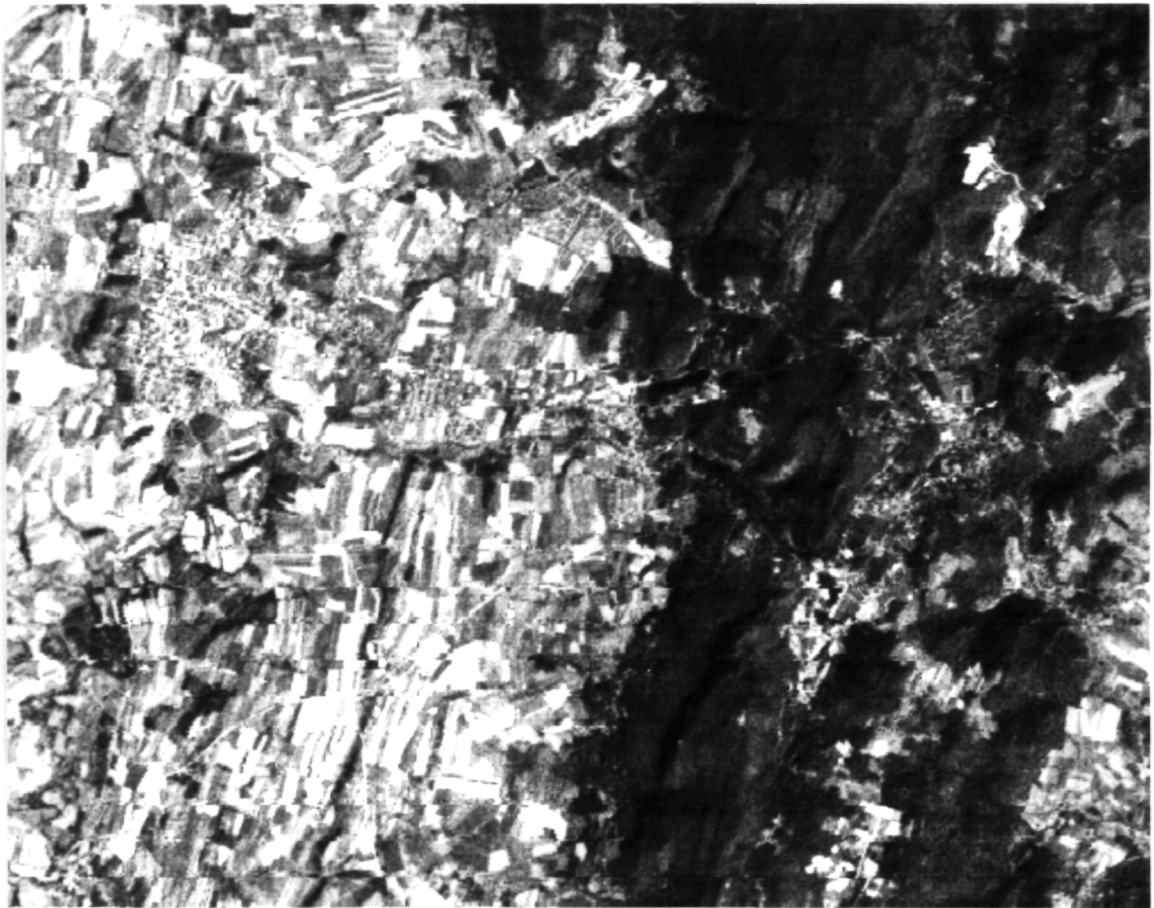Figure 49   P-tape Window 4 (Contrast .7x) (Chesapeake Bay)

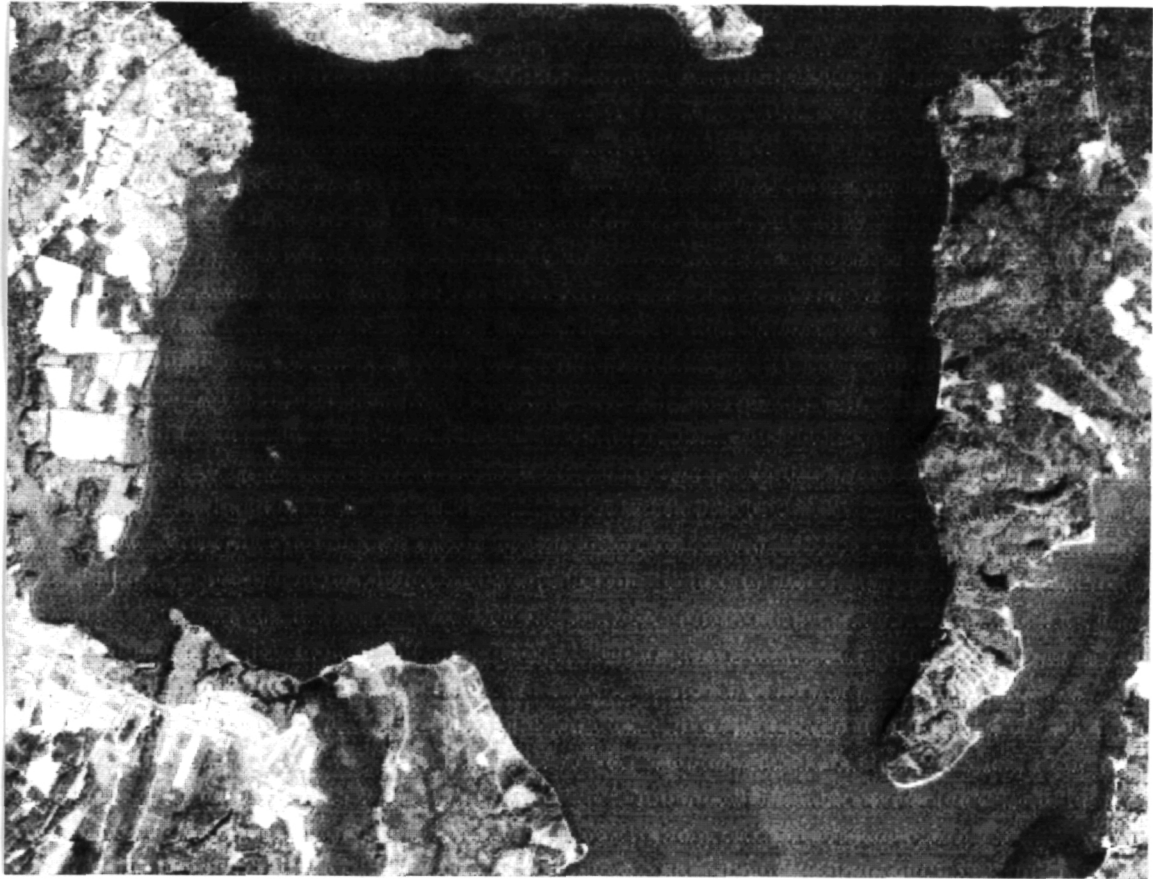Figure 50   A-tape EarthSat Destriped Window 1 (Contrast .7x)

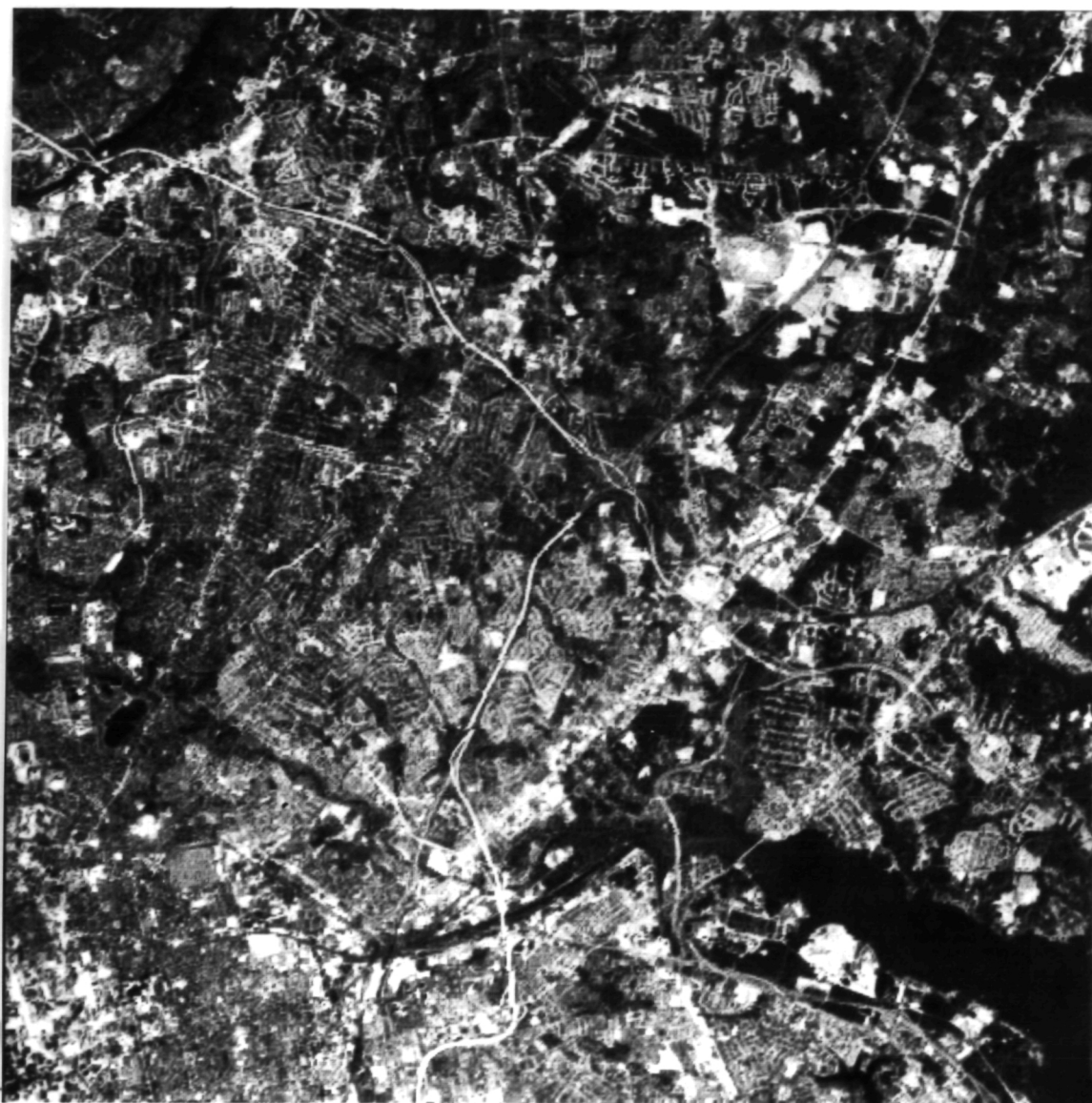Figure 51   A-tape EarthSat Destriped Window 2 (Contrast .7x)

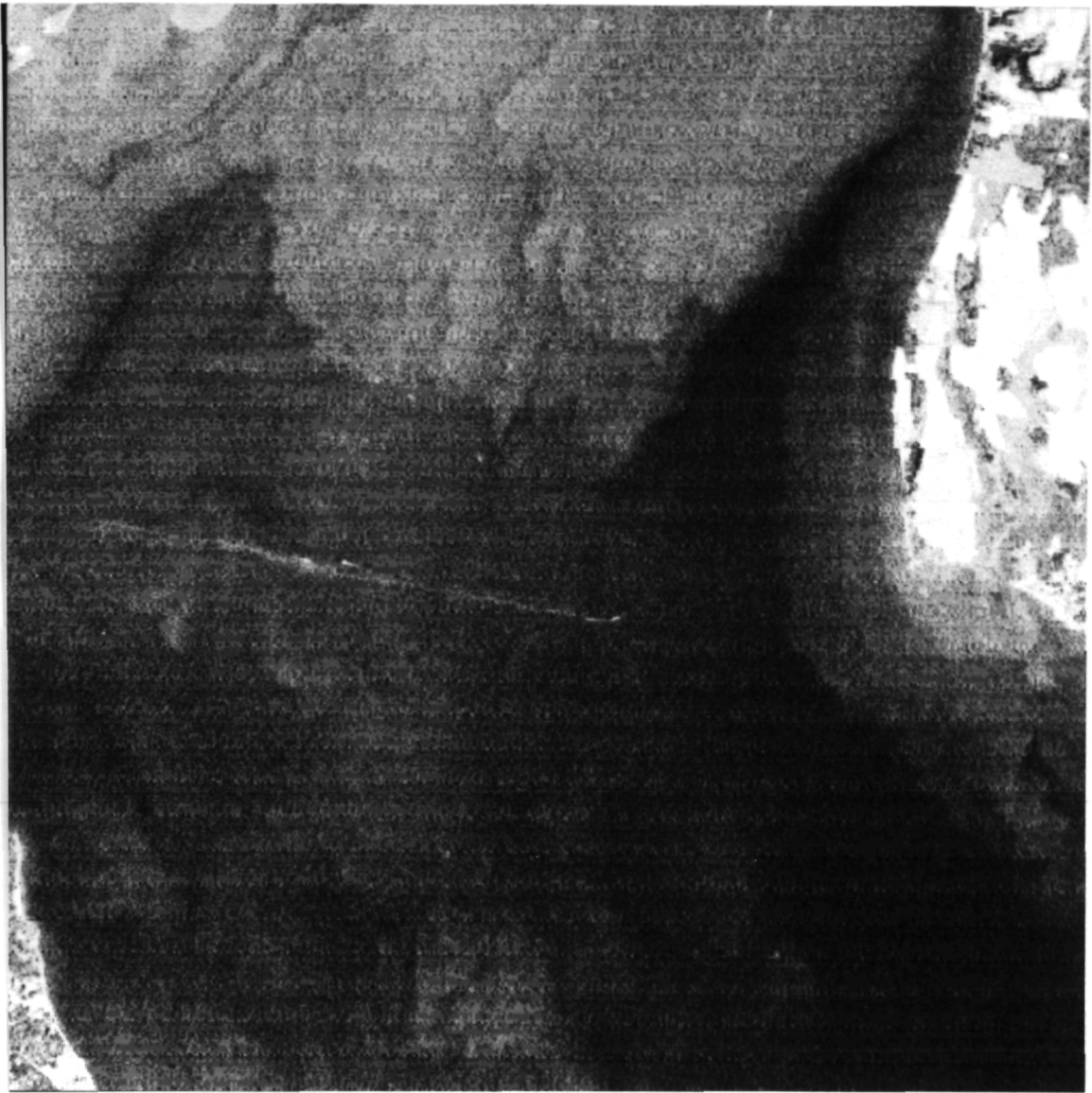Figure 52   A-tape EarthSat Destriped Window 3 (Contrast .7x) (Baltimore)

Figure 53   A-tape EarthSat Destriped Window 4 (Contrast .7x) (Chesapeake Bay)

3. Scene composition and albedo (i.e., the proportion of water to land, land use activity, etc.).

Our overall conclusion is that for almost all, if not all petroleum exploration activities, the data in P-tapes are more than adequate. The radiometric integrity is adequate and the additional time and cost of dealing with A-tapes is not worth the slight cosmetic gain.

6.0 BIBLIOGRAPHY

Al-Shaieb, Z., and Lilburn, R.A., 1982, Geochemistry and isotopic composition of hydrocarbon induced diagenetic aureole (HIDA), southwestern Oklahoma [abs]: Am. Assoc. Petrol. Geol. Bull., v. 66, n. 5, p. 542-543.

Al-Shaieb, Z., Thomas, R.G., Stewart, G.F., 1982, National uranium resource evaluation, Lawton quadrangle, Oklahoma and Texas: U.S. Department of Energy Report GJQ-017 (82), Grand Junction, Colorado, 48 p.

Armstrong, F.E., and Heemstra, R.J., 1973, Radiation halos and hydrocarbon reservoirs; A Review: U.S. Bureau of Mines Information Circular 8579, 51 p.

Axtmann, T.C., 1983, Structural mechanisms and oil accumulation along the Mountain View-Wayne Fault, south-central Oklahoma: Shale Shaker, v. 34, n. 1 and 2, 29 p.

Baars, D.L., 1966, Pre-Pennsylvanian paleotectonics - key to basin evaluation and petroleum occurrences in Paradox Basin, Utah and Colorado: Am. Assoc. Petroleum Geologists Bull., v. 50, p. 2080-2111.

_____, 1976, The Colorado Plateau aulocogen - key to continental scale basement rifting, in Podwysocki, M.H., and Earle, J.L., 1976, eds., Proceedings of the Second International Conference on Basement Tectonics: Basement Tectonics Committee, Contribution no. 15, p. 157-164.

Baker, D.R., Ferguson, W.S., 1965, Stable carbon isotopes in petroleum and sediment hydrocarbons from the Cherokee petroleum province [abs]: Geol. Soc. Am. Special Paper 82, p.7.

Bally, A.W., 1981, Thoughts on the tectonics of folded belts, in McClay, K.R., and Price, N.J., eds., Thrust and nappe tectonics: Geol. Soc. London, Special Publication, n. 9, p. 13-32.

Barazangi, M., and Isacks, B.L., 1976, Spatial distribution of earthquakes and subduction of the Nazca Plate beneath South America: Geology, v. 4, p. 686-692. .

Bower, P., 1983, Geochemical prospecting and value to the oil finder: Oil and Gas Journal, August 22, 1983, p. 163-174.

Bown, T.W., 1982, Geology, paleontology, and correlation of Eocene volcaniclastic rocks, southeast Absaroka Range, Hot Springs County, Wyoming: U.S. Geol. Survey Prof. Paper 1201-A, 75 p.

Brewer, J.A., Smithson, S.B., Oliver, J.E., Kaufman, S., Brown, L.D., 1980, The Laramide orogeny: Evidence from COCORP deep

crustal seismic profiles in the Wind River Mountains, Wyoming: Tectonophysics, v. 62, p. 165-189.

Burchfiel, B.C., and Davis, G.A., 1975, Nature and controls of Cordilleran orogenesis, western United States: Expansions of an earlier synthesis: Am. Jour. Sci., (Rogers Volume), v. 275-A, p. 363-396.

Burchfiel, B.C., and Stewart, J.H., 1966, Pull-apart origin of the central segment of Death Valley, California: Geol. Soc. America Bull., v. 77, p. 439-442.

Chapin, C.E., and Cather, S.M., 1981, Eocene tectonics and sedimentation in the Colorado Plateau - Rocky Mountain area, in Dickinson, W.R., and Payne, M.D., eds., Relations of tectonics to ore deposits in the southern Cordillera: Arizona Geol. Soc. Digest, v. 14, p. 173-198.

Clayton, J., and Swetland, P., 1977, Preliminary Report: Petroleum geochemistry of the Denver Basin, in Veal, H.K., ed., Symposium on exploration frontiers of the central and southern Rockies: Rocky Mtn. Assoc. Geol., p. 223-233.

Conel, J.E., and Niesen, P.L., 1981, Remote sensing and uranium exploration at Lisbon Valley, Utah: IEEE, International Geoscience and Remote Sensing Symposium, v. 1, p. 318-324.

Coney, P.J., 1972, Cordilleran tectonics and North America plate motion: Am. Jour. Sci., v. 272, p. 603-628.

_____, 1976, Plate tectonics and the Laramide orogeny, in Woodward, L.A., and Northrop, S.A., eds., Tectonics and mineral resources of southwestern North America: New Mexico Geol. Soc. Spec. Pub., n. 6, p. 5-10.

_____, 1978, Mesozoic-Cenozoic Cordilleran plate tectonics, in Smith, R.B., and Eaton, G.P., eds., Cenozoic tectonics and regional geophysics of the western Cordillera: Geol. Soc. Am. Mem. 152, p. 33-50.

Coney, P.J., and Reynolds, S.J., 1977, Cordilleran Benioff zones: Nature, v. 270, p. 403-406.

Cook, R.A., 1978, A relationship between strike-slip faults and the process of drape folding of layered rocks, in Matthews, V., ed., Laramide folding associated with basement block faulting in the western United States, Geol. Soc. Am. Mem. 151: p. 197-214.

Cross, T.A., and Pilger, R.H., Jr., 1978, Constraints on absolute motion and plate interaction inferred from Cenozoic igneous activity in the western United States: Am. Jour. Sci., v. 278, p. 865-902.

_____, 1982, Controls of subduction geometry, location of magmatic arcs, and tectonics of arc and back-arc regions: Geol. Soc. Am. Bull., v. 93, p. 545-562.

Dalziel, M.C., and Donovan, T.J., 1980, Biogeochemical evidence for subsurface hydrocarbon occurrence, Recluse Oil Field, Wyoming: Preliminary Results: U.S. Geol. Survey Circular 837, 11 p.

Davidson, M.J., 1982, Toward a general theory of vertical migration: Oil and Gas Journal, June 21, 1982, p. 288-300.

Davis, T.L., and Weimer, R.J., 1976, Late Cretaceous growth faulting, Denver Basin, Colorado, in Epis, R.C., and Weimer, R.J., eds., Professional Contributions of Colorado School of Mines No. 8, p. 280-300.

Dickinson, W.R., and Snyder, W.S., 1977, Paleozoic plate tectonics and the evolution of the Cordilleran continental margin, in Stewart, J. et al., eds., Paleozoic Paleogeography of the Western United States, Pacific Coast Paleogeography Symposium 1, p. 137-155.

_____, 1978, Plate tectonics of the Laramide orogeny, in Matthews, V., ed., Laramide folding associated with basement block faulting in the western United States: Geol. Soc. Am. Mem. 151, p. 355-366.

Donovan, T.J., 1972, Surface mineralogical and chemical evidence of buried hydrocarbons and the vertical migration of oil and gas, Cement Field, Oklahoma [abs]: Oklahoma Geol. Notes, v. 32, n. 11, p. 18-19.

_____, 1974, Petroleum microseepage at Cement, Oklahoma Evidence and mechanism: Am. Assoc. Petrol. Geol. Bull., v. 58, p. 429-446.

Donovan, T.J., Friedman, I., and Gleason, J.D., 1974, Recognition of petroleum bearing traps by unusual isotopic compositions of carbonate cemented surface rocks: Geology, v. 2, n. 7, p. 351-354.

Donovan, T.J., Nobel, R.L., Friedman, I., and Gleason, J.D., 1975, A possible petroleum-related geochemical anomaly in surface rocks, Boulder and Weld Counties, Colorado: U.S. Geol. Survey Open-File Report 75-47, 11 p.

Donovan, T.J., and Dalziel, M.C., 1977, Late diagenetic indicators of buried oil and gas: U.S. Geol. Survey Open-File Report 77-817, 44 p.

Donovan, T.J., Forgey, R.L., and Roberts, A.A., 1979a, Aeromagnetic detection of diagenetic magnetite over oil fields [abs]: U.S. Geol. Survey Prof. Paper 1150, p. 33-34.

_____, 1979b, Aeromagnetic detection of diagenetic magnetite over oil fields: Am. Assoc. Petrol. Geol. Bull., v. 63, n. 2, p. 245-248.

Donovan, T.J., Termain, P.A., and Henry, M. F., 1979c, Late diagenetic indicators of buried oil and gas; Direct detection experiment at Cement and Garza oil fields, Oklahoma and Texas, using enhanced Landsat-1 and -2 images: U.S. Geol. Survey Open File-Report, II, n. 79-243, 49 p.

Donovan, T.J., 1981, Geochemical prospecting for oil and gas from orbital and suborbital altitudes, in Gottlieb, B.M., ed., Unconventional methods in exploration for petroleum and natural gas: Symposium II, Southern Methodist University Press, Dallas, p. 96-115.

Donovan, T.J., Roberts, A.A., and Dalziel, M.C., 1981, Epigenetic zoning in surface and near-surface rocks resulting from seepage induced redox gradients: Velma Oil Field, Oklahoma: Shale Shaker, v. 27, n. 11, p. 1-7.

Duchscherer, W., Jr., 1980, Geochemical methods of prospecting for hydrocarbons: Oil and Gas Journal, December 1, 1980, p. 194-208.

_____, 1982, Geochemical exploration for hydrocarbons - no new tricks - but an old dog: Oil and Gas Journal, July 5, 1982, p. 163-176.

Elias, G.K., 1963, Habitat of Pennsylvanian algal bioherms, Four Corners Area, in Shelf Carbonates of the Paradox Basin, A Symposium Fourth Field Conference 1963: Four Corners Geological Soc., P. 185-202.

Engebretson, D., 1983, Relative motions between oceanic and continental plates in the Pacific basin: Ph.D. Dissertation, Stanford University, Palo Alto, CA, 211 p.

Fassett, J.E., ed., 1978, Oil and gas fields of the Four Corners Area: Four Corners Geological Society, v. 1 and 2, 727 p.

Fentress, G.H., 1955, Little Beaver Field, Colorado, a stratigraphic, structural, and sedimentation problem: Am. Assoc. Petrol. Geol. Bull., v. 39, p. 155-188.

Ferguson, J.D., 1979, The subsurface alteration and mineralization of Permian red beds overlying several oil fields in southern Oklahoma (Part 1): Shale Shaker, v. 29, n. 8, p. 172-208.

_____, 1979, The subsurface alteration and mineralization of Permian red beds overlying several oil fields in southern Oklahoma, (Part 2): Shale Shaker, v. 29, n. 9, p. 200-208.

Gries, R., 1981, Oil and gas prospecting beneath the Precambrian foreland thrust plates in the Rocky Mountains: The Mountain Geologist, v. 18, p. 1-18.

_____, 1983a, Oil and gas prospecting beneath the Precambrian of foreland thrust plates in the Rocky Mountains: Am. Assoc. Petroleum Geologists, Bull., v. 67, p. 1-26.

_____, 1983b, North-south compression of Rocky Mountain foreland structures, in Lowell, J.D., ed., Rocky Mountain foreland basins and uplifts: Rocky Mtn. Assoc. Geol., Denver, CO, p. 9-32.

Hamilton, W., 1978, Mesozoic tectonics of the western United States: Mesozoic Paleogeography of the western United States: Pacific Coast Paleogeography Symposium 2, Society of Economic Paleontologists and Mineralogists, p. 33-70.

_____, 1981, Plate-tectonic mechanism of Laramide deformation, in Boyd, D.W., and Lillegraven, J.A., eds., Rocky Mountain foreland basement tectonics: Univ. Wyoming Contributions to Geology, v. 19, p. 87-92.

Harding, T.P., 1974, Petroleum traps associated with wrench faults: American Association of Petroleum Geologists Bulletin 58, p. 1290-1304.

Harlton, B.H., 1960, Stratigraphy of cement pool and adjacent area, Caddo and Grady Counties, Oklahoma: Am. Assoc. Petrol. Geol. Bull., v. 44, p. 210-226.

Hathaway, J.C., and Degens, E.T., 1968, Methane-derived marine carbonates of Pleistocene Age: Science, v. 165, p. 690-692.

Henry, M.E., and Donovan, T.J., 1978, Isotopic and chemical data from carbonate cements in surface rocks over and near four Oklahoma oil fields: U.S. Geol. Survey, Open-File Report 78-927.

Herrmann, T.A., 1961, Structural geology of Cement-Chickasha area, Caddo and Grady Counties, Oklahoma: Am. Assoc. Petrol. Geol. Bull., v. 45, p. 1971-1993.

Hite, R.J., 1975, An unusual northeast-trending fracture zone and its relations to basement wrench faulting in northern Paradox Basin, Utah and Colorado: Four Corners Geol. Soc., 8th Field Conf. Guidebook, Canyonlands Country, p. 217-233.

Hite, R.J., and Buckner, D.H., 1981, Stratigraphy correlations, facies concepts, and cyclicity in Pennsylvanian rocks of the Paradox Basin, in Geology of the Paradox Basin: Rocky Mtn. Assoc. Geologists, p. 147-159.

Hunt, J.M., 1979, Petroleum geochemistry and geology: W.H. Freeman and Co., San Francisco, 617 p.

Keefer, W.R., 1957, Geology of the Du Noir area, Fremont Co., Wyoming: U.S. Geol. Survey Prof. Paper 294-E, p. 155-221.

Keefer, W.R., and Love, J.D., 1963, Laramide vertical movements in central Wyoming: Univ. Wyoming, Contributions to Geology, v. 2, p. 47-54.

Keefer, W.R., 1965, Stratigraphy and geologic history of the uppermost Cretaceous, Paleocene, and lower Eocene rocks in the Wind River Basin, Wyoming: U.S. Geol. Survey Prof. Paper 495-A, 77 p.

Keith, S.B., 1982, Paleoconvergence rates determined from K_2O/SiO_2 ratios in magmatic rocks and their application to Cretaceous and Tertiary tectonic patterns in southwestern North America: Geol. Soc. Am. Bull., v. 93, p. 524-532.

Kelley, V.C., 1955, Regional tectonics of the Colorado Plateau and relationship to origin and distribuion of uranium: Univ. New Mexico Pubs. Geology No. 5, 120 p.

_____, 1979, Tectonics of the Colorado Plateau and new interpretation of its eastern boundary: Tectonophysics, v. 61, p. 97-102.

Kelley, V.C., and Clinton, N.J., 1960, Fracture systems and tectonic elements the Colorado Plateau: Univ. New Mexico Pubs. Geology No. 6, 104 p.

Kilmer, C., 1983, Radiation lows over productive areas seen as soil geochemical phenomenon: Oil and Gas Journal, July 25, 1983, p. 179-182.

Kirkland, D.W., and Evans, R., 1976, Origin of limestone buttes, Gypsum Plain, Culberson County, Texas: Am. Assoc. Petrol. Geol. Bull., v. 60, p. 2005-2018.

Kiteley, L.W., 1977, Shallow marine deposits in the Upper Cretaceous Pierre Shale of the Northern Denver Basin and their relation to hydrocarbon accumulation, in Veal, H.K., ed., Symposium on Exploration Frontiers of the Central and Southern Rockies: Rocky Mtn. Assoc. Geol., p. 197-211.

Krivanek, C.M., 1981, New fields and exploration drilling, Paradox Basin, Utah and Colorado, in Wiegard, D.L., ed., Geology of the Paradox Basin: Rocky Mtn. Assoc. Geol., p. 77-83.

Levandowski, D.W. et al., 1973, Cementation in Lyons Sandstone and its role in oil accumulation, Denver Basin, Colorado: Am. Assoc. Petrol. Geol. Bull., v. 57, p. 2217-2244.

Levorsen, A.I., 1967, Geology of Petroleum: Second Edition, W.K. Freeman and Co., San Francisco, 724 p.

Lilburn, R.A., and Al-Shaieb, Z., 1983, Geochemistry and isotopic
    composition of hydrocarbon-induced diagenetic aureole (HIDA),
    Cement Field, Oklahoma (Part 1): Shale Shaker, December, 1983,
    p. 40-56.

Livaccari, R.F., Burke, K., and Sengor, A.M.C., 1982, Was the
    Laramide orogeny related to subduction of an oceanic plateau?:
    Nature, v. 289, p. 276-278.

Livaccari, R.F., and Engebretson, D.C., 1983, Mesozoic-early
    Tertiary North American plate motion and development of
    foreland structures: Geol. Soc. Am. Abst. with Programs, v.
    15, p. 271.

Love, J.D., 1978, Cenozoic thrust and normal faulting, and tectonic
    history of the Badwater area, northeastern margin of Wind River
    Basin, Wyoming: Wyoming Geol. Assoc. Guidebook, p. 235-238.

Lowell, J.D., 1972, Spitsbergen Tertiary Orogenic Belt and the
    Spitsbergen Fracture Zone: Geol. Soc. America Bull., v. 83, p.
    3091-3102.

MacElvain, R.C., 1963, What do near-surface signs really mean in oil
    findings: Oil and Gas Journal, February 18, 1963, p. 132-136.

_____, 1969, Mechanics of gaseous ascension through a
    sedimentary column, in Unconventional Methods in Exploration
    for Petroleum and Natural Gas, Symposium I, Southern Methodist
    University Press, Dallas, p.15-28.

MacLachlan, M.E., 1967, Paleotectonic investigations of the Permian
    system in the United States: U.S. Geol. Survey Professional
    Paper 515 - E, p.85-92.

Mallory, W.M., 1977, Oil and gas from fractured shale reservoirs in
    Colorado and northwest New Mexico: Rocky Mtn. Assoc. Geol.
    Special Pub. #1, 38 p.

Marrs, R.W., and Kaminsky, B., 1977, Detection of petroleum-related
    soil anomalies from Landsat, in 29th Annual Field Conference,
    Wyoming Geology Association Guidebook, p. 353-365.

Martin, C.A., 1965, Denver Basin: Am. Assoc. Petrol. Geol. Bull.,
    v. 49, p. 1908-1925.

Martin, G.W., 1981, Patterson Field San Juan County, Utah, in
    Geology of the Paradox Basin: Rocky Mtn. Assoc. Geologists, p.
    61-70.

Masters, J.A., 1979, Deep Basin Gas Trap, Western Canada: Am.
    Assoc. Petrol. Geol. Bull., v. 63, p. 151-181.

Matthews, V., and Work, D.F., 1978, Laramide folding associated with
    basement block faulting along the northeastern flank of the
    Front Range, Colorado, in Matthews, V., ed., Laramide folding

associated with basement block faulting in the western United
States, Geol. Soc. Am. Memoir 151, p. 101-124.

Matuszczak, R.A., 1973, Wattenberg field, Denver basin: The
Mountain Geologist, v. 19, p. 99-105.

Miller, F., 1963, Cretaceous oil in the Denver Basin, in Geology of
Denver Basin and adjacent uplift, Rocky Mtn. Assoc. Geol., p.
211-214.

Monster, J., 1972, Homogeneity of sulfur and carbon isotopes S^{34}/S^{32}
and C^{12}/C^{13} in petroleum: Am. Assoc. Petrol. Geol. Bull., v.
56, n. 5, p. 941-949.

Moredock, D.E., and Williams, S.J., 1976, Upper Cretaceous Terry and
Hygiene sandstones - Singletree, Spindle, and Surrey fields, in
Epis, R.C., and Weimer, R.J., eds., Professional Contributions
of Colorado School of Mines #8, p. 264-274.

Murphy, J.F., Privrasky, N.C., and Moerlein, G.A., 1956, Geology of
Sheldon-Little Dome area, Fremont County, Wyoming: U.S. Geol.
Survey Oil and Gas Inv. Map, OM 181.

NASA, 1982a, Landsat Data Users Notes, Issue No. 23, July.

NASA, 1982b, NASA News Press Kit Release No. 82-100, Project:
Landsat-D.

NASA, 1982c, Landsat Data Users Notes, Issue No. 25, December.

Nisle, R.G., 1941, Considerations on the vertical migration of
gases: Geophysics, v. 6, n. 1, p. 449-454.

NOAA, 1983, NOAA Satellite Programs Briefing, August.

O'Sullivan, R.B., 1965, Geology of the Cedar Mesa-Boundary Butte
area, San Juan County, Utah: U.S. Geol. Survey Bull. 1186, 128
p.

Peace, H.W., 1965, The Springer group of the southeastern Anadarko
basin in Oklahoma: Shale Shaker, v. 15, n. 5, p. 81-99.

Peterson, J.A., 1966, Stratigraphic versus structural controls on
carbonate-mound hydrocarbon accumulation, Aneth area, Paradox
Basin: Am. Assoc. Petroleum Geologists Bull., v. 50, n. 10, p.
2068-2081.

Peterson, J.A., and Hite, R.J., 1969, Pennsylvanian evaporite-
carbonate cycles and their relation to petroleum occurrence,
southern Rocky Mountains: Am. Assoc. Petroleum Geologists
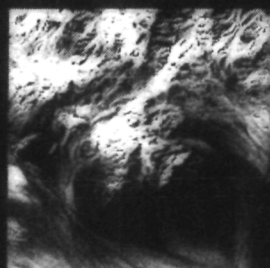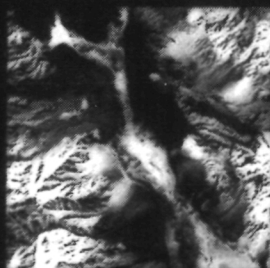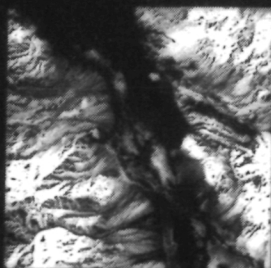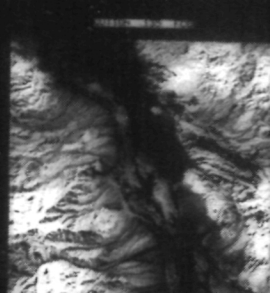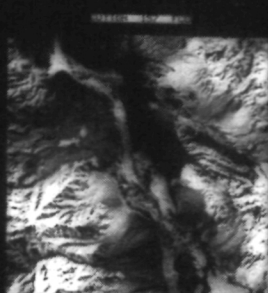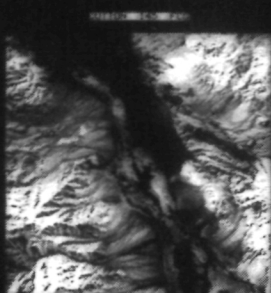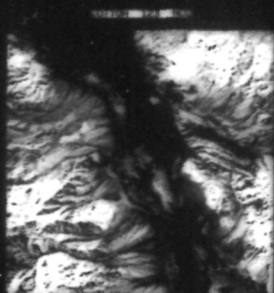Bull., v. 53, n. 4, p. 884-908.

Peterson, J.A., and Ohlen, H.R., 1963, Pennsylvanian shelf
carbonates, Paradox Basin, in Shelf carbonates of the Paradox
Basin: Four Corners Geol. Soc., 4th Field Conf., p. 65-79.

Pruatt, M.A., 1975, The southern Oklahoma aulocogen: a geological and geophysical investigation: unpublished Master's thesis, Univ. Oklahoma.

Pruit, J.D., 1978, Statistical and geological evaluation of oil and gas production from the J sandstone, Denver Basin, in Pruit, J.D., and Coffin, P.E., eds., Energy Resources of the Denver Basin, Rocky Mtn. Assoc. Geol., p. 9-34.

Reeves, F., 1921, Geology of the Cement oil field, Caddo County, Oklahoma: U.S. Geol. Survey Bull. 726-B, 85 p.

Reynolds, M.W.,1978, Late Mesozoic and Cenozoic structural development and its effect on petroleum accumulation, southwest arm of the Wind River Basin, Wyoming: Wyoming Geol. Assoc. Guidebook 30th Ann. Field Conf., p.77-78.

Roberts, A.A., Donovan, T.J., Dalziel, M.C., and Forgey, R.L., 1978, Application of helium surveys to petroleum exploration [abs.]: U.S. Geol. Survey Prof. Paper, n. 1100, p. 24.

Roberts, W.H., 1980, Design and function of oil and gas traps, in Roberts, W.H., and Cordell, R.J., eds., Problems of Petroleum Migration, Amer. Assoc. Petrol. Geol.: Studies in Geology No. 10, p. 207-216.

Rowan, L.C., Wetlaufer, P.H., Goetz, A.F.H., Billingsley, F.C., and Stewart, J.H., 1974, Discrimination of rock types and detection of hydrothermally altered areas in south central Nevada by the use of computer enhanced ERTS images: U.S. Geol. Survey Prof. Paper 883, 35 p.

Rutledge, R.B., 1954, The Velma oil field, Stephens County, Oklahoma: Tulsa Geological Society Digest, v. 22, p. 40-52.

Sales, J.K., 1968, Crustal mechanics of Cordilleran Foreland deformation: A regional and scale model approach: Am. Assoc. Petrol. Geol. Bull., v. 52, n. 10, p. 2016-2044.

Saunders, D.F., 1980, Use of Landsat geomorphic and tonal anomalies in petroleum prospecting: Unconventional Methods in Exploration for Petroleum and Natural Gas, II, Southern Methodist University Press, Dallas, 1980.

Sears, J.D., 1956, Geology of Comb Ridge and vicinity north of San Juan River, San Juan County, Utah: U.S. Geol. Survey Bull. 1021-E, 207 p.

Sheffield, C., 1982, Earth Resources and satellite imaging systems: Interdisciplinary Science Review (England).

Stahl, W., Faber, E., Carey, B.D., and Kirksey, D.L., 1982, Near-surface evidence of migration of natural gas from deep

reservoirs and source rocks: Am. Assoc. Petrol. Geol. Bull., v. 65, n. 9., p. 1543-1550.

Streitz, R., and Stinson, M., 1974, Geologic map of California, Death Valley sheet: Division of Mines and Geology, State of California.

Szabo, E., and Wengerd, S.A., 1975, Stratigraphy and tectogenesis of the Paradox Basin, in Four Corners Geol. Soc., 8th Field Conf. Guidebook, Canyonlands Country, p. 193-210.

Thomas, G.E., 1974, Lineament-block tectonics: Williston-Blood Creek Basin: Am. Assoc. Petrol. Geol. Bull., v. 58, p. 1305-1322.

Tanaka, H.H., and Davis, L.V., 1963, Groundwater resources of the Rush Springs Sandstone in the Caddo County area, Oklahoma: Oklahoma Geol. Survey Circular 61, 63 p.

Thomas, G.E., 1976, Lineament-block tectonics: North America-Cordilleran orogen, in Podwysocki, M., and Earle, J., eds., Proc. Second Intern. Conf. Basement Tectonics, p. 361-370.

Trollinger, W.V., 1968, Surface evidence of deep structures in the Anadarko Basin: Shale Shaker, v. 18, n. 8, p. 162-171.

Warner, L.A., 1978, The Colorado Lineament: A middle Precambrian wrench fault system: Geol. Soc. Am. Bull., v. 89, p. 161-171.

Weart, R.C., and Heimberg, G., 1980, Exploration radiometrics: Post survey drilling results, in Gottlieb, B., ed., Unconventional methods in exploration for petroleum and natural gas: II, Southern Methodist University Press, Dallas, 1980.

Weaver, L.K., and Anderson, K.F., 1966, Oil recovery from gas-cap reservoirs - an engineering evaluation of conservation practices in six reservoirs: U.S. Bureau of Mines, Monograph 13, p. 26-41.

Weimer, R.J., 1973, Guide to uppermost Cretaceous stratigraphy, central Front Range Colorado: Deltaic sedimentation growth faulting and early Laramide crustal movement: The Mountain Geologist, v. 10, n. 3, p. 53-97.

_____, 1978, Influence of transcontinental arch on Cretaceous marine sedimentation: A preliminary report, in Pruit, J.D., and Coffin, P.E., eds., Symposium on Energy Resources of Denver Basin: Rocky Mtn. Assoc. Geol., p. 211-221.

Wengerd, S.A., 1973, Regional stratigraphic control of the search for Pennsylvanian petroleum southern monument upwarp, southeastern Utah: New Mexico Geol. Soc. Guidebook 24th Field Conf., Guidebook of Monument Valley and Vicinity, Arizona and Utah, p. 122-138.

Wilson, J.M., 1978, Permo-Pennsylvanian of the west-central Nebraska panhandle, in Pruit, J.D.. and Coffin, P.E., eds., Symposium on Energy Resources of Denver Basin: Rocky Mtn. Assoc. Geol., p. 129-140.

Winterfeld, G.F., and Conard, J.B., 1983, Laramide tectonics and position, Washakie Range and northwestern Wind River Basin, Wyoming: Lowell, J.D., ed., Rocky Mountain Foreland Basins and Uplifts: Rocky Mtn. Assoc. Geol., p. 137-148.
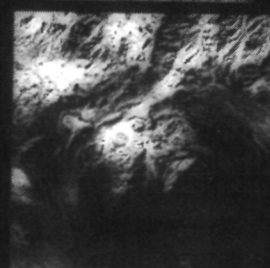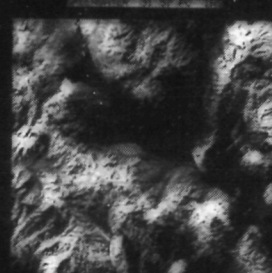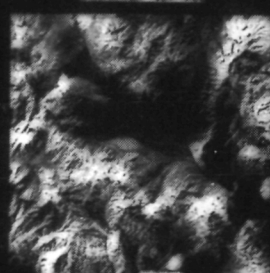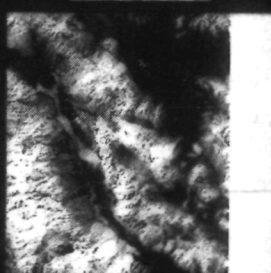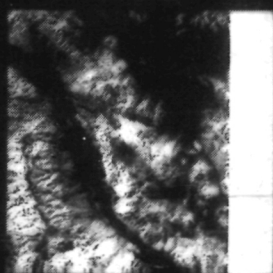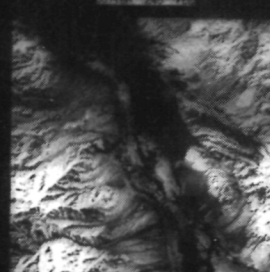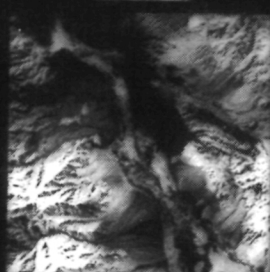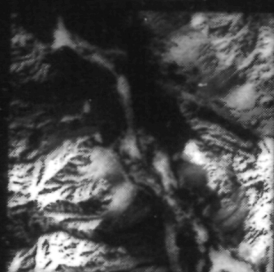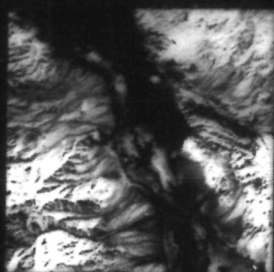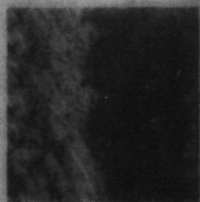
CON # _____ LOCATION _____ FRAME # _____

BAND	1	2	3	4	5	6	7
DX							
DD							

SPOT
| 25 |
| 50 |
| 100 |

OPT. DATE _____

COLOR NEG PROC. DATE	C	M	Y	
DX				
DD				

CONTACT PRINT DATE 7-5-84	C	M	Y
PACK		60	100
EXP			12

SCALE	MAG	2" cm	XH
ORIG.		17.1	

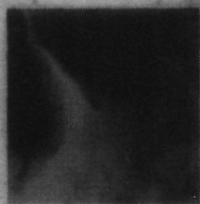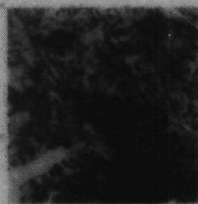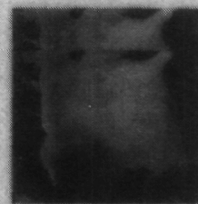|	ENLARGER #1					ENLARGER #2					ENLARGER #3			
DATE	C	M	Y	F/T	DATE	C	M	Y	F/T	DATE	C	M	Y	F/T
										7-5-84		52	40	11/33

PT-W1

AT-W2

AT-W1

PT-W4

PT-W3

PT-W2

AT-W4

AT-W3